Design and Synthesis of Donor–Acceptor Type Small Molecules for High Performance Organic Solar Cells

고성능 유기태양전지를 위한

전자주개-전자받개 형태의

저분자 설계 및 합성

2016년 2월

서울대학교 대학원

재료공학부

최 윤 석

Abstract

Design and Synthesis of Donor–Acceptor Type Small Molecules for High Performance Organic Solar Cells

Yoon Suk Choi

Department of Materials Science and Engineering

The Graduate School

Seoul National University

As a promising alternative to polymer solar cells, small molecular organic solar cells (OSCs) have recently been developed because of their characteristic advantages of well-defined molecular weight, synthetic reproducibility, and simple purification process. However, the photovoltaic performance is still lower than those of polymer solar cells. Thus, further works on designing molecular structure are needed for improving the performance of organic solar cell.

Owing to intensive studies on the ideal donor material in bulk heterojunction OSCs for the past decade, some requirements for high performance OSCs have been established: (1) broad and strong light absorption in the visible region to harvest enough solar light, (2) high hole mobility for fast charge carrier transport to yield high short-circuit current (J_{SC}), (3) suitable energy levels to ensure high open-circuit voltage (V_{OC}) and efficient exciton dissociation, and (4) appropriate compatibility with the

i

fullerene acceptor to form nano-scale bicontinuous interpenetrating networks for efficient exciton dissociation. These properties can offer high values of J_{SC}, V_{OC} and fill factor of the OSCs, and result in high power conversion efficiency (PCE).

In order to satisfy these requirements, reasonable integration of donor and acceptor unit in conjugated small molecule (SM) should be carefully considered in terms of molecular energy levels, crystallinity, and solubility in organic solvent. In this thesis, we designed and synthesized new small molecular donors to examine the effect of structural modification on their photovoltaic properties.

Firstly, a series of simple structured SMs based on diketopyrrolopyrrole (DPP) are synthesized and their photovoltaic properties are investigated in terms of the type of electron donating unit. By introducing a donor unit with different electron-donating power such as thiophene (T) and phenylene (Ph), into A–D–A type SM, the frontier orbital energy levels of SMs can effectively be tuned. The SM with a weak donor unit of Ph, Ph(TDPP)$_2$ exhibits low-lying highest occupied molecular orbital (HOMO) energy level, nanoscale phase separation in blend film with phenyl-C71-butyric acid methyl ester (PC$_{71}$BM). Among DPP-based SMs, Ph(TDPP)$_2$ afforded high V_{OC} of 0.93 V with a PCE of 4.01%.

While the photovoltaic performance with the DPP-based SMs have yielded the promising PCE with high V_{OC}s, the low J_{SC}, around 9.0 mA cm^{-2}, is a main limiting factor for high efficiency OSCs. Generally, close packing of organic materials in solid film leads to high charge carrier mobility. Therefore, we synthesized four different DPP-based SMs with A–D–A type structure, where electron-donating unit was systematically varied with different electron-donating power (thiophene vs. phenylene; thienothiophene vs. naphthalene) and different molecular planarity (bithiophene vs.

thienothiophene; and biphenylene vs. naphthalene). The SMs with weak donating unit (phenylene or naphthalene) have deeper HOMO energy levels than those with strong donating unit (thiophene or thienothiophene), and thus exhibit higher V_{OC}. When the fused aromatic ring (thienothiophene or naphthalene) with planar molecular structure is introduced in SMs, the SMs exhibit high hole mobility and thus afford high J_{SC}. As a result, the introduction of naphthalene (weak donating power and planar structure) enhances both V_{OC} and J_{SC}, resulting in a promising PCE of 4.4%.

Finally, two different thienopyrroledione (TPD)-based SMs with different alkyl substitution positions were synthesized, and their photovoltaic properties are measured and compared to examine the effect of the alkyl substitution position on their optical, electrochemical, and photovoltaic properties. The use of TPD as an electron-accepting unit in conjugated SMs effectively lowers the HOMO energy levels of the conjugated SMs and leads to high V_{OC}. Two SMs with n-hexyl group substituted at different positions exhibit almost identical optical and electrochemical properties in the pristine state. However, the crystallographic and morphological characteristics of DTS(HexTPD2T)$_2$/PC$_{71}$BM blend film yield efficient charge transport. As a consequence, DTS(HexTPD2T)$_2$ exhibits a PCE of 6.0% with a V_{OC} of 0.94 V and a J_{SC} of 11.8 mA cm^{-2}.

Keywords: small molecule, organic solar cell, photovoltaics, bulk heterojunction, diketopyrrolopyrrole, thienopyrroledione.
Student Number: 2011-30788

Contents

List of Tables

List of Schemes

List of Figures

Chapter 1. Introduction

1.1 Organic solar cells

1.1.1 Background

The development of clean and renewable energy sources has become one of the greatest challenges for our present and future society due to the rapidly increasing energy demand and depleting the traditional fossil fuel sources such as coal, oil, and natural gas. The fully renewable source that has capability to meet the large and growing energy demand is solar energy.[1–4] Photovoltaic technologies, which directly convert solar energy to electricity, have achieved tremendous advance in solar cell research and development. At present, the photovoltaic market relies heavily on wafer-based polycrystalline silicon devices, which entail relatively high fabrication cost. Thin film solar cell including amorphous silicon, gallium arsenide, copper-indium-gallium-selenide, and cadmium telluride also provide high efficiencies.[5–8] However, for these materials scarcity of feedstock and issues with toxicity remain the significant problem for world-wide usage.[9–13]

Alternatively, organic solar cells (OSCs) have been rapidly developed as one of the most promising candidates for low-cost solar cells, due to their possibility of fabricating large-scale and flexible solar cells by solution processing.[14–19] The first successful OSCs were reported by Tang in 1986.[20] A

power conversion efficiency (PCE) of about 1% with a high fill factor (FF) was achieved in a bilayer device. Six years later, the Heeger and Wudl groups observed ultrafast electron transfer from the conjugated polymer poly[2-methoxy-5-(2-ethylhexyloxy)]-1,4-phenylenevinylene (MEH-PPV) to fullerene (C$_{60}$),[21,22] which suggested the use of conjugated polymers as electron donors and fullerene derivatives as electron acceptors in OSCs. Concurrently, the concept of the bulk heterojunction (BHJ) was introduced to address the limited exciton (tightly bound electron hole pair) diffusion length in OSCs.[23,24] In a BHJ structure, donor and acceptor materials are mixed together to form a bicontinuous interpenetrating network with large interfacial areas for efficient exciton dissociation. Since then, performance of OSC devices has steadily improved with new materials and/or novel device architectures. Now, both polymer and small molecule (SM)-based OSCs have achieved exceeding 10% of PCE.[25,26] However, the efficiency still needs to be improved for the demand of commercialization.

1.1.2 Device structure and operating mechanism

The most widely utilized device structure of OSCs involves the concept of BHJs in active layer, where a nanoscale phase separated blend of conjugated donor and fullerene derivative acceptor was sandwiched between transparent indium tin oxide (ITO) and a metal electrode.[24] Conventional and inverted device architectures were developed for OSCs, as shown in Figure 1.1. In conventional devices, generally, poly(3,4-ethylenedioxythiophene):

poly(styrenesulfonate) (PEDOT:PSS)-coated ITO and a low work-function metal are used to collect holes and electrons, respectively. PEDOT:PSS is used as a hole transport layer for lowering the contact resistance between anode and active layer, smoothing the ITO surface and promoting the efficient hole transport. Al (work-function –4.3 eV) is commonly used as a cathode, and buffer layer such as Ca and LiF is also deposited under Al layer to lower work function of cathode, which improves electron injection/collecting ability of cathode by forming Ohmic contact with active layer.[27–31] While, for the inverted device, modified ITO with electron transporting layer and a high work-function metal such as Au were used as the electron-collecting and hole-collecting electrode, respectively.
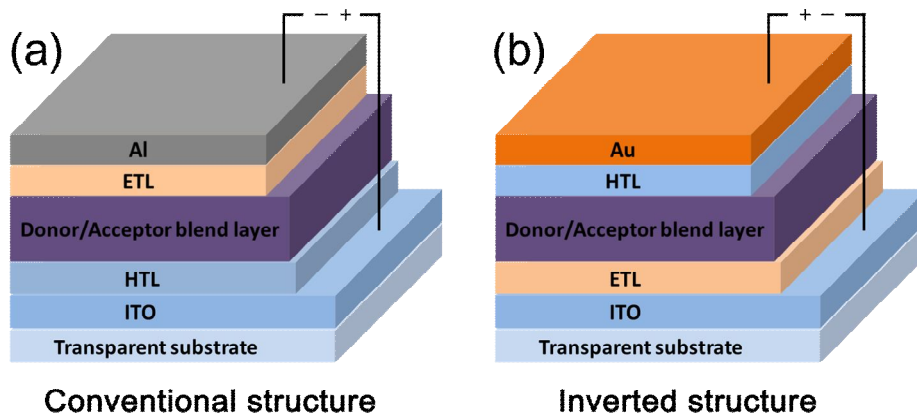
Figure 1.1. Device structure of (a) conventional and (b) inverted structure of BHJ-OSCs

donor/acceptor
interface

LUMO   LUMO

Energy

hv

1   2   3   4   5

cathode

anode

5   4

HOMO   HOMO

donor   acceptor

1. Light absorption
2. Exciton formation and diffusion
3. Exciton dissociation
4. Charge transport
5. Charge collection
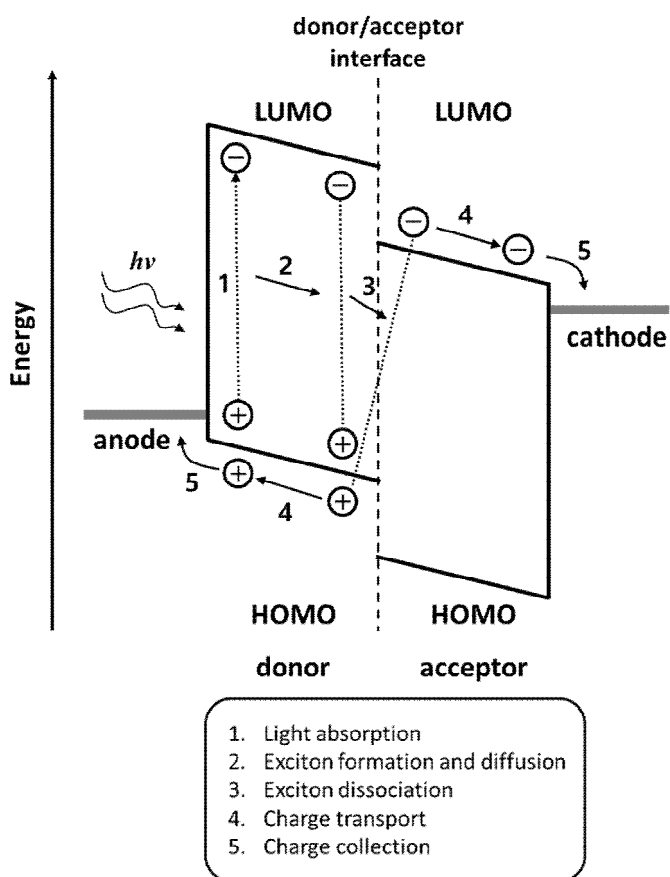
Scheme 1.1. Operating mechanism of BHJ-OSCs.

4
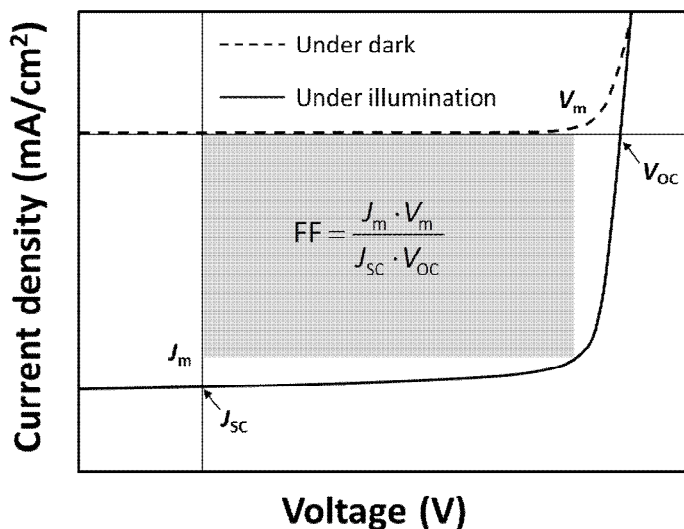
Figure 1.2. *J–V* curves of solar cell under illumination with the parameters.

The fundamental operating principle of BHJ-OSCs is the photo-induced charge transfer between conjugated donor and fullerene derivative acceptors.[21] Operation mechanism of BHJ-OSCs is briefly depicted in Scheme 1.1. Generally, the energy conversion from light energy to electrical energy follows five steps: 1) absorption of photons by conjugated donor materials to generate exciton: Broad absorption spectrum and high absorptivity of active materials are required for maximum exciton generation. 2) Diffusion of exciton to the donor/acceptor interface: Photo-generated excitons are coulombically bound as electron-hole pair and typically diffuse along with conjugated backbone and/or inter-molecules. For the most conjugated organic

5

materials, the exciton diffusion length is in the range of 10–20 nm.[32] Therefore, bicontinous and nanoscale phase separated morphology are necessary for efficient exciton dissociation. 3) Dissociation of the excitons into free charge carriers: Excitons reaching the donor/acceptor interface are separated into free charge carrier. 4) Transportation of the free charge carriers towards corresponding electrodes: In this process, the charge carrier mobility of both electron and hole and their balance (unity is ideal) play an important role in determining device efficiency. 5) Charge collection at electrodes: Finally, hole and electron are collected to corresponding electrodes, cathode and anode, respectively, and pass through the circuit to generate photocurrent.

Current–voltage (J–V) curves represent important and direct characterization method of a solar cell. Figure 1.2 depicts a J–V curve under dark and incident-light illumination. The PCE of a solar cell is determined by the ratio between the open circuit voltage (V_{OC}), the short circuit current (J_{SC}), the FF of the device, and the incident light intensity (P_{in}):

$$PCE = FF \times \frac{V_{OC} \cdot J_{SC}}{P_{in}} \qquad (1.1)$$

$$FF = \frac{J_m \cdot V_m}{J_{SC} \cdot V_{OC}}, \qquad (1.2)$$

The V_{OC} is proportional to the energy difference between the highest occupied molecular orbital (HOMO) energy level of donor component and the lowest unoccupied molecular orbital (LUMO) energy level of acceptor component. Therefore, it can be adjusted up to a certain extent by modifying

the energy levels of the materials.[33–36] The J_{SC} depends on the efficiencies of the light absorption of the active layer, exciton diffusion and dissociation at the interface of donor/acceptor components, charge transportation in active layer, and charge collection on the electrodes. FF is determined by the ratio of the maximum power output ($J_m \times V_m$) of solar cell to the product of its V_{OC} and J_{SC}. The series and parallel resistances significantly influence the FF; lower series resistance and higher parallel resistance result in higher FF values. And P_{in} is the incident light power density. This light intensity is standardized at 100 mW cm^{-2} with a spectral intensity distribution matching the air mass (AM) 1.5G condition.[37]

1.1.3 Active materials for organic solar cells

Organic semiconducting materials feature an ability to transport charge carrier,hole and electron, from one molecule to another. In OSCs, conjugated polymers or SMs and phenyl-C61-butyric acid methyl ester (PC$_{61}$BM) or PC$_{71}$BM are commonly used as the semiconducting donor and acceptor components, respectively. Representative donor and acceptor component are described in Figure 1.3, 1.4 and 1.5.

Polymeric donors. In 1995, soluble polyphenylenevinylene such as MEH-PPV[24] and MDMO-PPV,[38] is applied to active layer of OSCs. The solar cell devices fabricated with PPV derivatives have shown low PCEs of 2–3% because of wide bandgap (> 2.0 eV) and low hole mobility with amorphous nature. Later, the regioregular poly(3-hexylthiophene) (P3HT) had been

focused in field of organic electronics due to excellent optical and electrical properties as well as high crystallinity.[39–45] When blended with $PC_{61}BM$, P3HT-based OSCs have achieved promising PCEs of 4–5% after morphology optimization. However, both PPV derivatives and P3HT have relatively large optical bandgap, which limit the performance of the corresponding devices. Recently, major development in polymer solar cell comes from concept of donor–acceptor (D–A) copolymer, which leads to low bandgap polymers. The PTB7 and PffBT4T-2OD are one of the promising D–A polymer with PCE over 7%.[45,46]

Small molecular donors. In the early 1980s, a single layer of single organic material was applied to conventional OSCs, which adapt a two electrode with different work function.[47] Theses early OSCs showed very poor performance under 0.1%. In 1986, Cupper phthalocyanine (CuPc) was first used as a donor in bilayer heterojunction OSC by Tang, and device showed a PCE of 1%.[20] Bilayer structure was breakthrough in development of OSCs, which is fabricated by vacuum deposition. To reduce the fabrication cost of vacuum process and overcome the disadvantage of bilayer devices, which is limited interfacial area between donor and acceptor components, solution processed SMs were developed. Dicyanovinyl substituted oligothiophene (DCV5T) was synthesized and applied in solution processed OSCs.[48] Due to low HOMO level and red-shifted absorption of DCV5T, these OSCs afforded PCEs of 3.4% with high V_{OC} of 0.98 V. Recently, Chen *et. al.* reported oligothiophene with A–D–A type, where donor are thiophene and benzodithiophene and acceptor is electron-deficient unit such as rhodanine

8

and dicyanovinyl, which achieved deep HOMO energy level and higher absorption derived from introduction of terminal acceptor, and showed PCE over 6%.[49,50] At the same time, Bazan *et. al.* also reported D–A type SMs such as DTS(PTTh2)$_2$ and *p*-DTS(FBTTh2)$_2$. Through device optimization, the PCE has been improved up to 8%[51,52]

Small molecular acceptor. Fullerene and their derivatives have been widely used in bilayer heterojunction and BHJ-OSCs largely due to their strong tendency to accept electrons from donor semiconducting materials and high electron mobilities in the films even in composite form.[53,54] Additionally, fullerene derivatives readily form favorable nanoscale morphological network with donors, which could improve BHJ-OSC performance. Figure 1.5 provides the chemical structures of fullerene and their representative derivatives. Generally, C$_{60}$ were mainly used in vacuum deposited OSCs, while their soluble derivative PCBM were used in solution processed OSCs. The spherical shape of C$_{60}$ renders it a good acceptor in any directions, and this isotropy toward electron transfer is advantageous in bilayer heterojunction OSCs. PC$_{61}$BM has much better solubility in organic solvents than its parent compound C$_{60}$, and therefore, it has been facilitated as an acceptor instead of C$_{60}$ for solution processed OSCs. Currently, in order to increase LUMO energy levels of electron acceptors for high V_{OC}, C$_{60}$-bisadducts such as bis-PCBM and ICBA have also been proposed.[34, 55–57]
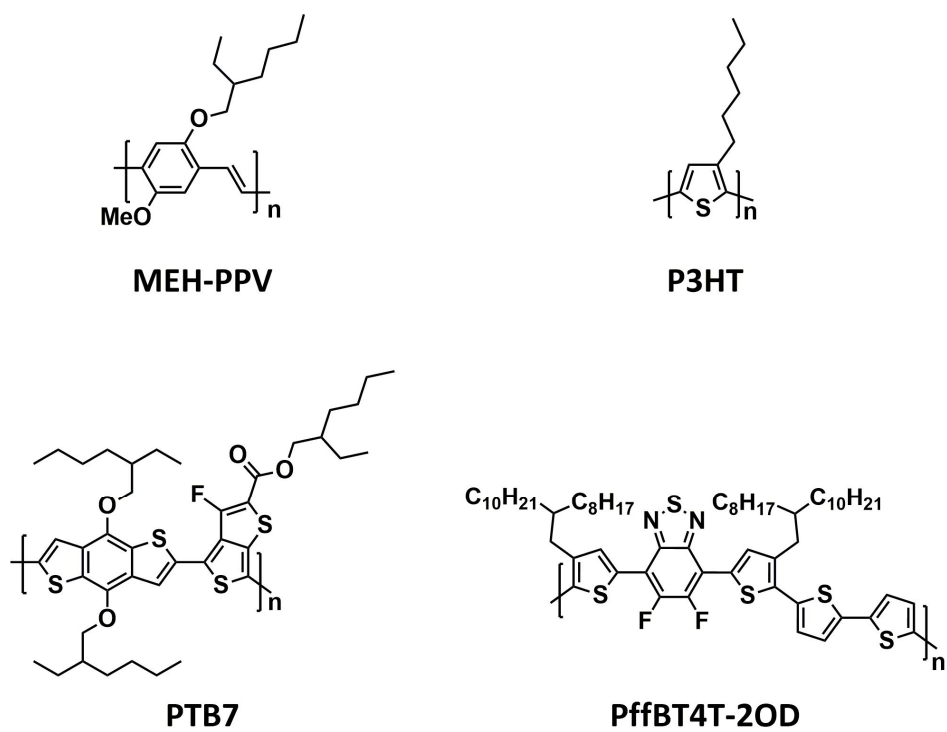
Figure 1.3. Chemical structures of polymers used as electron donors in active layers of OSCs.
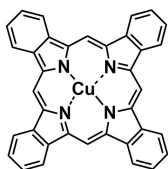
CuPc
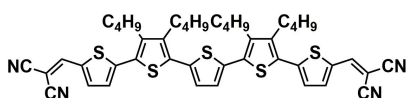
DCV5T
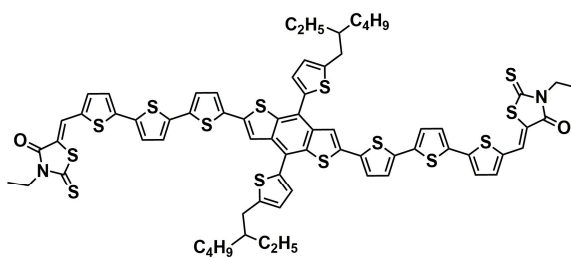
DR3TBDTT
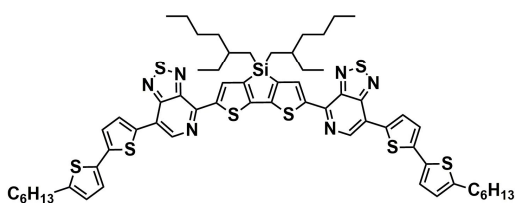
DTS(PTTh2)$_2$

Figure 1.4. Chemical structures of small molecules used as electron donors in active layers of OSCs.

C₆₀ **PCBM**

bis-PCBM **ICBA**
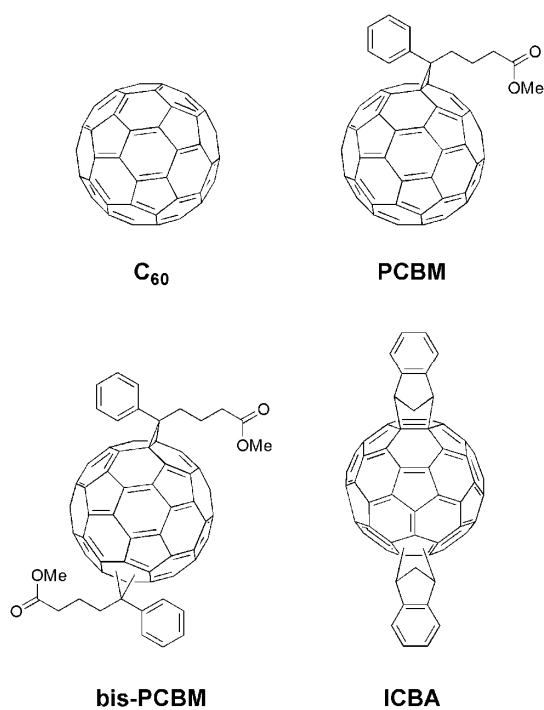
Figure 1.5. Chemical structures of *n*-type materials used as electron acceptors in active layers of OSCs.

1.2 Donor−acceptor type conjugated molecules

1.2.1 Energy levels of D−A type conjugated materials

For the last few years, the conjugated material has been considerably studied for OSC devices. In the past, the polymers used in field of organic light emitting diode and field-effect transistor, such as MEH-PPV and P3HT, were utilized. Recently, however, carefully designed polymers with D−A structure have been developed to finely tune the energy level, solubility and planarity,[58−63] and achieved PCEs over 9% for single junction[64-67] and over 11% for tandem junction OSCs.[68,69] Inspired by the successful development of D−A type low bandgap polymers, SMs with different types of electron D−A structure have been developed.[70−75]

Integration of donor and acceptor units in conjugated materials is one of the effective ways to tune the energy levels of conjugated donor components. These D−A type conjugated materials feature intra-molecular charge transfer (ICT) from donor to acceptor unit which leads to reduction of optical bandgap, as shown in Scheme 1.2. Thus, optical, electrochemical and photophysical properties of conjugated materials can be tuned by a proper combination of donor and acceptor units. Especially, because the HOMO and LUMO levels of D−A structured materials are mainly governed by donor and acceptor units, respectively, the suitable energy levels of D−A conjugated materials for efficient OSCs can be achieved by modifying each of donor and acceptor building blocks.[76,77]
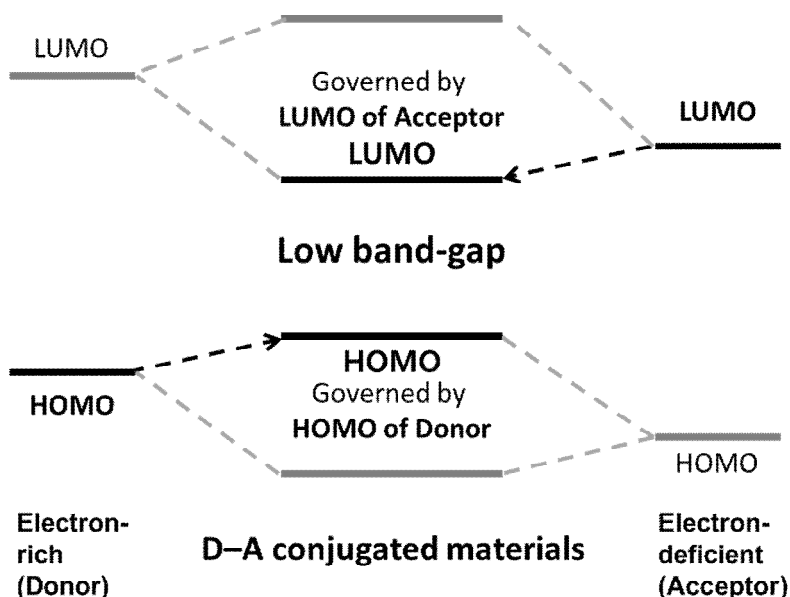
Scheme 1.2. Energy level diagram of the orbital hybridized HOMO and LUMO of D–A conjugated materials.

The bandgap governed by donor and acceptor units determined an amount of absorption of photon flux emitted from the sun. (Figure 1.6) For example, a semiconducting material with a bandgap of 1.1 eV can absorb at most 77% of solar energy, while if bandgap exceeds 2 eV, only about 30% of the solar energy can be absorbed at most.[78] Therefore, selection of donor and acceptor units in conjugated donor materials and corresponding bandgap is important for attaining high J_{SC}. Brabec *et. al.* showed that to achieve a PCE over 10%, the bandgap of donor materials should be around 1.35–1.65 eV.[79]

Meanwhile, narrowing the bandgap of a donor component will lead to a decrease in V_{OC} because it is proportional to the difference the HOMO energy

level of donor component and the LUMO energy level of acceptor component. Most importantly, the LUMO of the donor component should be higher than the LUMO of the corresponding acceptor component at least 0.3 eV to provide enough driving force to break the exciton binding energy and lead to charge separation.[80]

Consequently, energy levels of donor material influence photovoltaic properties including light absorption, exciton dissociation and charge extraction. Therefore, energy levels of donor materials should be controlled carefully for achieving high performance. The ideal energy level of a donor material is suggested in Scheme 1.3. When $PC_{61}BM$ (LUMO = −4.3 eV) is used as an electron acceptor in OSCs, ideal HOMO and LUMO energy level of conjugated materials are around −5.4 and −3.9 eV, respectively.[60]
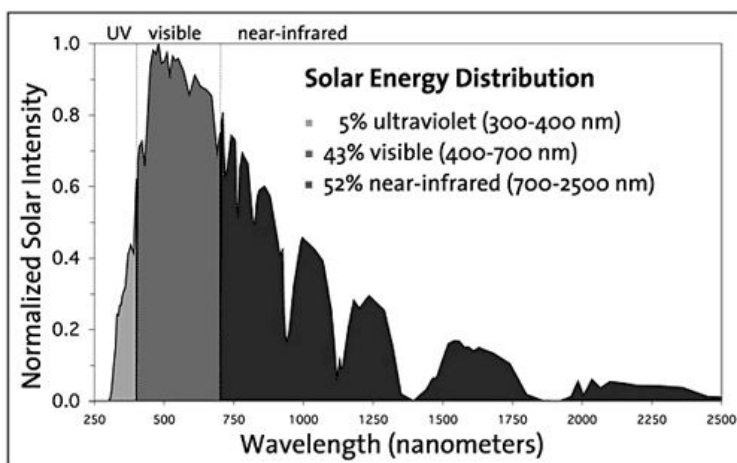
Figure 1.6. Solar energy distribution reached the earth under AM1.5G.
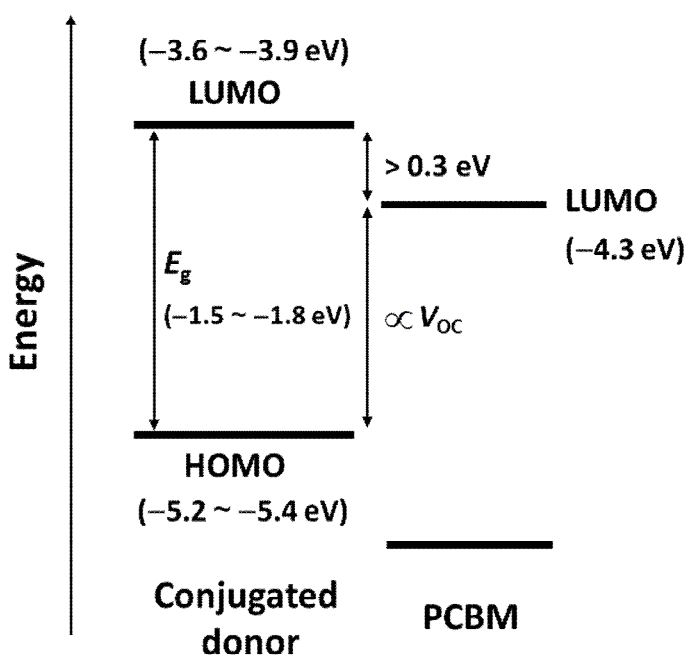
Scheme 1.3. Optimum energy levels of conjugated donor for high performance OSCs.

1.2.2 Donor units in D–A type conjugated molecules

Donor unit refers to an electron-rich unit, which has a large impact on the HOMO level and the band gap of conjugated materials. Thiophene and benzene are the two most basic donor units, and they are also the main fundamental blocks to construct new conjugated donor units. Since an appropriate fusion of a few single aromatic units can not only tune the electronic properties but also impact the charge mobility and intermolecular interactions of related conjugated materials, fused aromatic units are generally employed as donor units. The chemical properties of benzene and thiophene are compared in Figure. 1.7. Basically, benzene has higher aromatic resonance stabilization energy than thiophene. Therefore, for the donor molecules containing benzene ring, π-electrons are relatively located within the benzene ring and thus which can be classified as weak electron-donating units. When
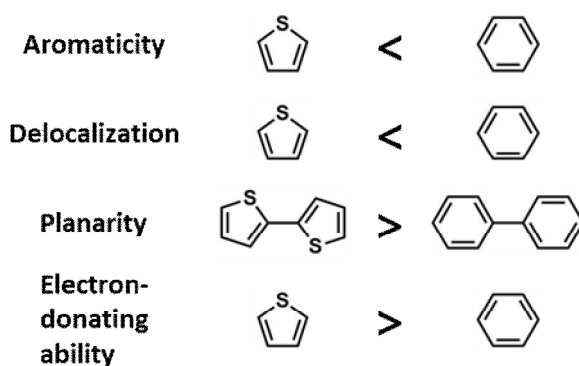
Figure 1.7. Comparisons of chemical properties between thiophene and benzene.

the weak electron-donating unit is used as a building block for conjugated molecules, the molecule is expected to have a deep HOMO energy level and thus afford high V_{OC} in OSCs. On the other hand, a hetero-aromatic ring, thiophene, has less aromatic resonance stabilization energy; thus, π-electrons are delocalized along the conjugated backbone. As a result, the molecular units containing thiophene raise the HOMO energy level as compared to those containing benzene. Donor units derived from benzene and thiophene are described in Figure 1.8. Fluorene,[81,82] dibenzosilole,[83] carbazole[84,85] and naphthalene[86,87] including benzene ring are one of the examples regarded as the week donating unit. Meanwhile, corresponding fused thiophene derivatives such as cyclopenta[2,1-b;3,4-b']dithiophene,[88,89] dithieno[2,3-*b*;2',3'-*d*']silole,[90,91] dithieno[3,2-*b*:2',3'-*d*]pyrrole[92,93] and thieno[3,2-b]thiophene[94,95] are represented as strong donating units.

1.2.3 Acceptor units in D–A conjugated molecules

Acceptor unit refers to electron-deficient building block. Almost each acceptor unit contains the electron-withdrawing groups such as imine (C=N) (e.g., 2,1,3-benzothiadiazole (BT)[96–98] and quinoxaline (Qx)[99,100]) or carbonyl groups (C=O). (e.g., DPP,[101,102] isoindigo[103–105] and thieno[3,4-c]pyrrole-4,6-dione (TPD)[106–110]) Chemical structures of these acceptor units are shown in Figure.1.9.

The BT unit is the most commonly employed acceptor unit because of its
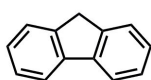
Fluorene
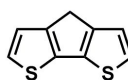
Cyclopentadithiophene
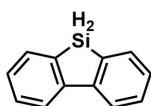
Dibenzosilole
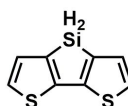
Dithienosilole
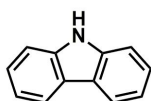
Carbazole
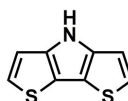
Dithienopyrrole
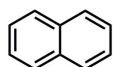
Naphthalene

Thienothiophene

Figure 1.8. Chemical structures of donor units widely used in D−A type conjugated donor components.
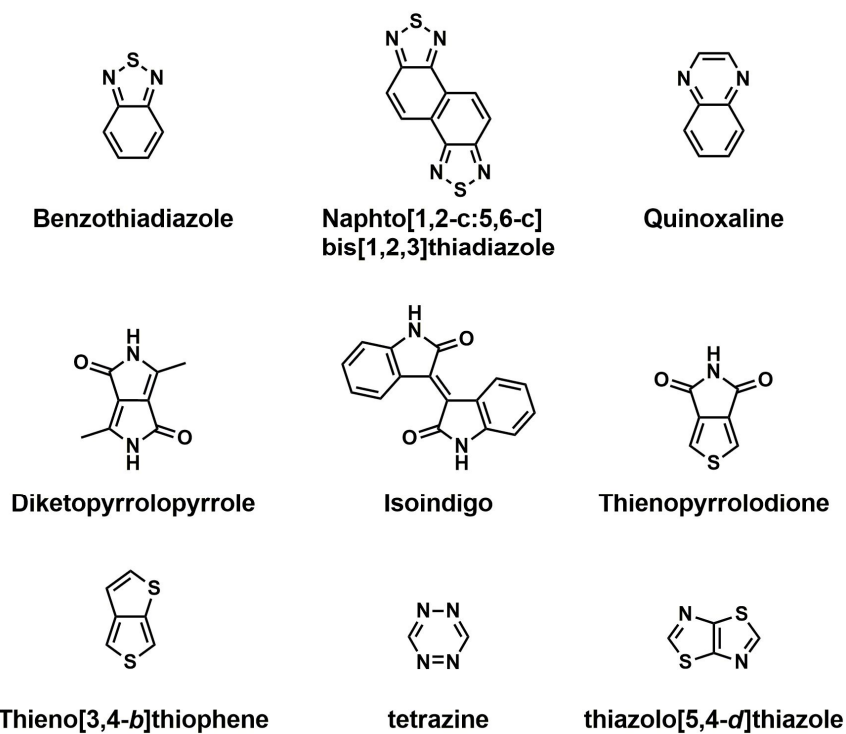
Figure 1.9. Chemical structures of acceptor units widely used in D−A conjugated donor components.

strong electron-accepting ability. Moreover, these two N atoms in the thiadiazole ring could possibly form hydrogen bonding with adjacent units (e.g., the hydrogen atom on the thiophene ring), leading to a more planar backbone.

The DPP unit has a well conjugated and highly planar structure with strong π–π interactions which result in efficient charge transport. Especially, the electron deficiency of the DPP due to imide groups provides the potential use of electron-accepting unit for D–A type conjugated materials. The relatively low lying HOMO and LUMO levels also make the DPP unit a promising candidate for application in OSCs.

The TPD unit is recently intensively explored. Similar to DPP and isoindigo, symmetric, rigidly fused, coplanar structure and strong electron-withdrawing properties of TPD are beneficial for intra- or intermolecular interaction and lowering HOMO energy levels when incorporated into conjugated backbone. Furthermore, lastly, S–O interactions involving proximate imide C=O groups and thienyl S atoms can serve as conformational "locks" to enhance π-conjugated planarity.[111–114]

Fundamentally, the electron-accepting ability can adjust the LUMO energy level of the conjugated donor unit: the stronger the electron-accepting ability, the lower the LUMO energy level. However, the offset of LUMO energy levels between donor and acceptor components in active materials of OSCs should maintain at least higher than 0.3 eV for efficient exciton dissociation.[115–117]

1.2.4 D–A type conjugated small molecules

Conjugated SMs have drawn attention such as well-defined structures and thus less batch-to-batch variation, versatile chemical structure, and thus easier energy level control.[118–121] Especially, D–A type conjugated SMs have been intensively examined, because selection and integration of donor and acceptor unit in conjugated backbone determine their energy level, planarity, light absorptivity, charge carrier mobility, and morphology. As a result, promising performance over 8% has been reported by various research groups.

Chemical structures of D–A type SMs can be classified generally as A–D–A, D–A–D, and D_2–A–D_1–A–D_2 structure, which are shown in Figure 1.10. The SMDPPEH, composed of DPP and thiophene, are representative one of A–D–A type small molecular donors.[122] The HOMO energy level of SMDPPEH determined by ultraviolet photoelectron spectroscopy was −5.2 eV. Photovoltaic properties afforded corresponding high V_{OC} of 0.75 V and a PCE of 3.0%. The OPV performance of DPP-based materials was further improved by replacing hexylbithiophene end group of SMDPPEH with benzofuran. The DPP(TBFu)$_2$ yielded a PCE of 4.4% after thermal annealing leading to suitable phase separation.[123]

Chen *et. al.* have concentrated on the structural evolution of A–D–A type oligothiophene featured with electro-withdrawing terminal units. DCN7T was designed for the goal of solution processed oligothiophene and afforded a PCE of 3.7% when it blended with PC$_{61}$BM.[124] In order to improve the solubility and film forming quality, oligothiophene derivatives substituted by
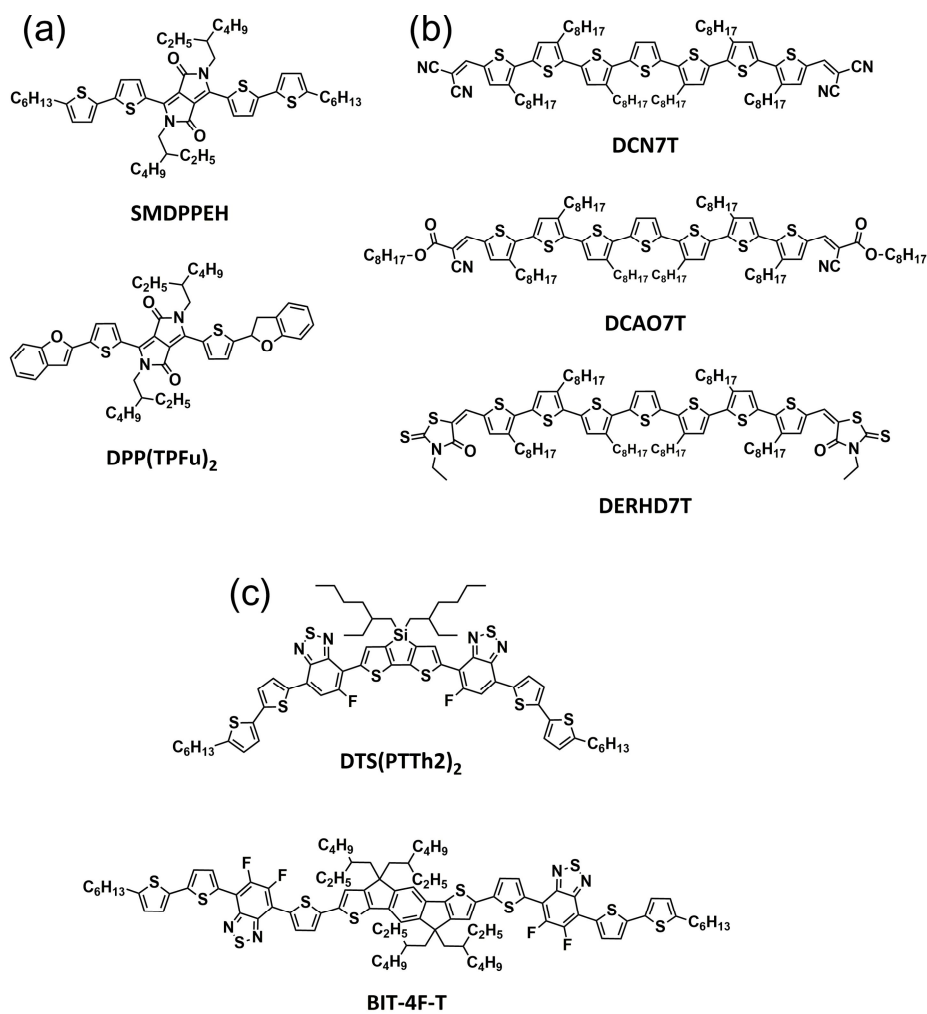
Figure 1.10. Chemical structures of (a) D–A–D, (b) A–D–A, and (c) D_1–A–D_2–A–D_1 type conjugated small molecules.

alkyl cyanoacetate group as the terminal unit was developed and exhibited higher PCE of 5.08%.[125] Recently, further structural development with electro-withdrawing dye as terminal units was accomplished for efficient light absorption. By introducing a 3-ethylrhodamine, the absorption band of DERHD7T showed red-shift of about 100 nm compared to that of DCAO7T, which improved the value of J_{SC}. The device based on DERHD7T:$PC_{61}BM$ showed a PCE of 6.10% with a J_{SC} of 13.98 mA cm^{-2}.[49]

Bazan *et. al.* have designed and synthesized a series of D_1–A–D_2–A–D_1 structure SMs.[51,74,126] Among D_1–A–D_2–A–D_1 type SMs, *p*-DTS(FBTTh2)$_2$ showed the highest performance with a PCE of 9.02%.[127] And Cao and co-workers synthesized D_1–A–D_2–A–D_1 type SMs based on indacenodithiophene and difluorobenzothiadiazole. A high PCE of 8.1% for BIT-4T-T was achieved after morphology optimization by solvent vapor annealing.

Consequently, structural development of SMs has accomplished the high performance OSCs. However, because there are still rooms for improvement of PCE to be commercialized, research about new material should continually be carried out.

1.3 Objectives of this study

OSCs are a promising cost-effective alternative to silicon-based solar cells, and possess light-weight, low-cost, and flexibility advantages. Significant progress has been achieved in the development of novel photovoltaic materials and device structures in the last decade. Nowadays small molecular

semiconductors for OPVs have attracted considerable attention, due to their advantages over their polymer counterparts, including well-defined molecular structure, definite molecular weight, and high purity without batch to batch variations. For developing high efficiency SM-OSCs, understanding of the relation between chemical structure and photovoltaic property of semiconducting conjugated donor is essential.

Basically, broad absorption is requisite for efficient solar cells. Alternative integration of proper donor and acceptor in conjugated backbone is one of the effective strategies to broaden light absorption, where HOMO and LUMO energy levels of D–A type molecules become higher and lower than those of donor and acceptor molecules, respectively. On the other hands, raising the HOMO energy level for lowering the gap leads to decrease in V_{OC}, because the V_{OC} is proportional to the difference between the HOMO energy level of donor and the LUMO energy level of acceptor. Hence, the lowering of bandgap may sacrifice the V_{OC}. As a consequence, a new strategy to overcome this trade-off behavior should be developed for high performance solar cells.

First, we have postulated that the introduction of electron-donating units with different aromatic resonance stabilization energy into the A–D–A type SM, where acceptor is thiophene-capped diketoppyrolopyrrole (TDPP) and donor is an electron-donating unit such as thiophene (T) and phenylene (Ph), would precisely control the HOMO energy levels of the SMs for efficient OPVs. For this approach to be realized, a series of TDPP-based SMs, $(TDPP)_2$, $T(TDPP)_2$, and $Ph(TDPP)_2$, were synthesize and their optical, electrochemical and photovoltaic properties were investigated. Consequently, the solar cell

based on Ph(TDPP)$_2$ achieved a V_{OC} of 0.93 V with a PCE of 4.01%.

And then, we further examined the effects of fused donor units incorporated in similar A–D–A type SMs on their optical, electrochemical and photovoltaic properties. Acceptor is same TDPP and donor is electron-donating unit such as bithiophene (T2), biphenylene (Ph2), thienothiophene (TT) and naphthalene (NPT), where TT and NPT are the corresponding fused aromatic rings of T2 and Ph2, respectively. Four different SMs are denoted as T2(TDPP)$_2$, Ph2(TDPP)$_2$, TT(TDPP)$_2$, and NPT(TDPP)$_2$. Here, it is expected that the use of weak donor increases V_{OC} while the introduction of fused aromatic ring increases J_{SC} as well. Since the electron-donating capability of Ph2 and NPT are weaker than T2 and TT, respectively, Ph2(TDPP)$_2$ and NPT(TDPP)$_2$ exhibit deeper HOMO energy levels than T2(TDPP)$_2$ and TT(TDPP)$_2$ and thus larger V_{OC}, while the introduction of fused aromatic rings (TT and NPT) instead of T2 and Ph2 increases J_{SC} due to planarity of SMs. Consequently, NPT(TDPP)$_2$ with weak electron-donating and fused aromatic ring exhibits a PCE of 4.4% with the highest V_{OC} of 0.87 V and the highest J_{SC} of 9.5 mA cm^{-2} when blended with PC$_{71}$BM as active layer in BHJ solar cells.

Finally, two different thienopyrroledione (TPD)-based SMs with different alkyl substitution positions were synthesized, and their photovoltaic properties are measured and compared to examine the effect of the alkyl substitution position on their optical, electrochemical, and photovoltaic properties. Although it is generally accepted that the HOMO and LUMO energy level of D–A type conjugated molecules are governed mainly by the electronic properties of donor and acceptor units, respectively, exceptional but

interesting results have been reported when a TPD unit is used as an acceptor unit in D–A type conjugated backbone: Both HOMO and LUMO levels are lowered when TPD is used as an acceptor unit in D–A type conjugated molecules. The use of TPD as an electron-accepting unit in conjugated SMs effectively lowers the HOMO energy levels of the conjugated SMs and leads to high V_{OC} of 0.94 V. While the two SMs with n-hexyl group substituted at different positions exhibit almost identical optical and electrochemical properties in the pristine state, their photovoltaic properties were significantly different. We systematically clarified the difference by crystallographic and morphological analysis.

Chapter 2. Diketopyrrolopyrrole-based small molecules for high V_{OC} organic photovoltaics

2.1 Introduction

In developing new conjugated organic materials for BHJ solar cells, a well-known architecture, alternatively composed of weak electron-donating and strong electron-accepting units, has been utilized to manipulate their electronic properties for high V_{OC} and efficient charge separation.[128] Among the electron donating units, phenylene and thiophene rings are considered as basic donor units. Since phenylene has high aromatic resonance stabilization energy, π-electrons are relatively localized within the phenylene ring in the molecule. Thus, molecular units containing phenylenes can be classified as weak electron-donating units. On the other hand, a hetero-aromatic ring such as thiophene has less aromatic resonance stabilization energy; thus, π-electrons are delocalized along the conjugated backbone. As a result, the molecular units containing thiophene raise the HOMO energy level as compared to those containing phenylene. Such synthetic strategy can effectively be used to tune the frontier molecular orbital energy levels for high efficiency OPV solar cells.

Among several moieties for D–A type SMs, diketopyrrolo[3,4-c]pyrrole (DPP) has emerged as an effective electron-deficient building block of low bandgap conjugated organic molecules for OSCs. The planarity of DPP,
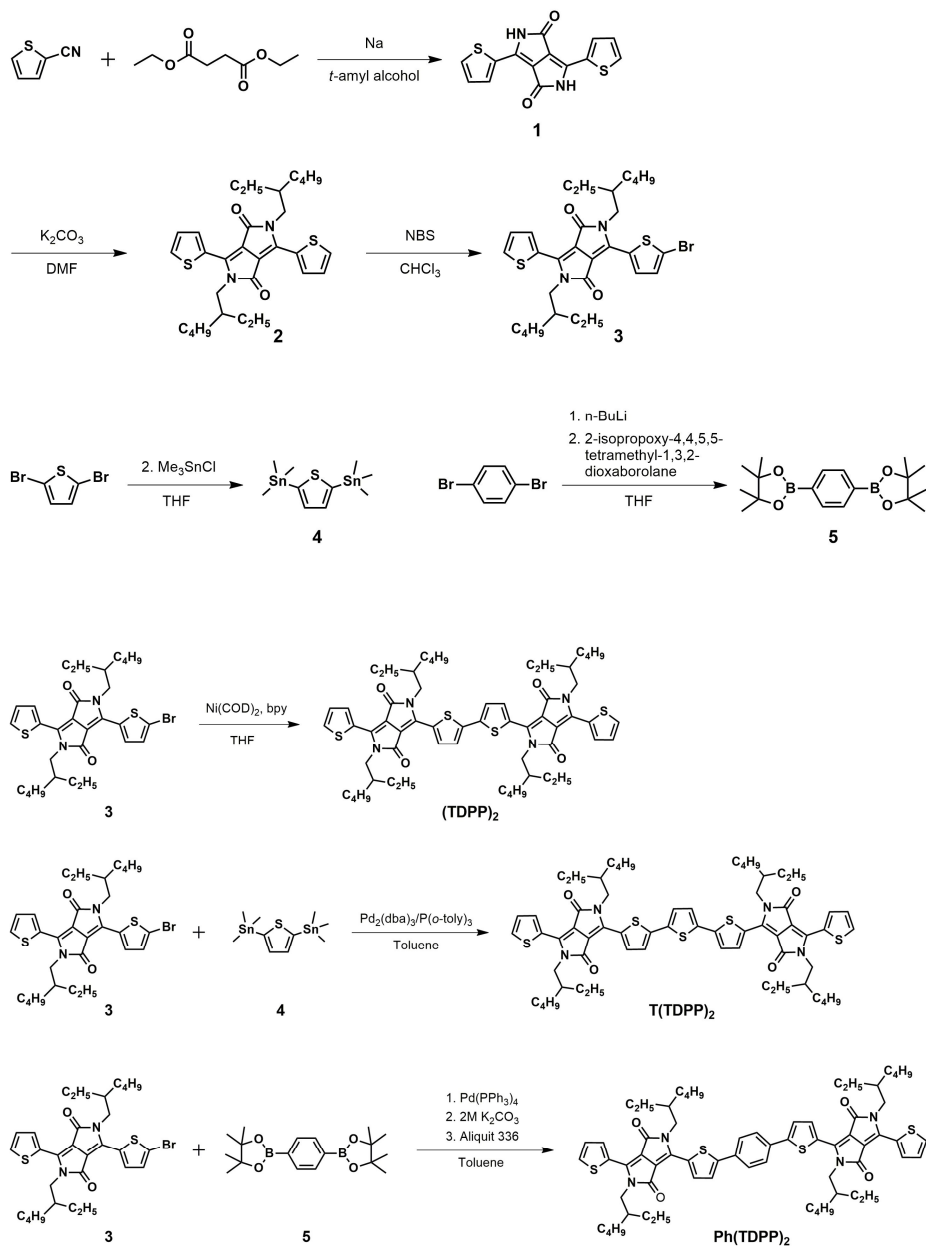
Scheme 2.1. Synthetic scheme of DPP-based small molecules with simple donor units.

strong absorption in near-infrared region and its high optical density render the DPP unit suitable for high performance photovoltaics.[129,130]

In this works, A–D–A type SMs were designed in terms of different aromatic resonance stabilization energy of electron donor units, where A is thiophene-capped DPP (TDPP) and D is an electron-donating unit such as thiophene (T) and phenylene (Ph). The HOMO energy levels of the SMs are efficiently tuned for high V_{OC}. For this approach to be realized, a series of TDPP-based SMs, (TDPP)$_2$, T(TDPP)$_2$, and Ph(TDPP)$_2$, were synthesized and illustrated in Scheme. 2.1. As expected, the HOMO energy level of T(TDPP)$_2$ is slightly higher than that of (TDPP)$_2$ due to a strong electron-donating thiophene bridge, while the HOMO energy level of Ph(TDPP)$_2$ is deeper than that of (TDPP)$_2$ due to the introduction of weak electron-donating phenylene bridge between two TDPPs. The molecular energy level of these DPP-based SMs highly affects the V_{OC}s in OSCs. We systematically examined these relationships.

2.2 Experimental section

2.2.1 Synthesis and characterization

2.2.1.1 Materials

Tetrahydrofuran (THF) (Daejung Chemicals & Metals) was dried over sodium/benzophenone under nitrogen and freshly distilled prior to use. All

reagents were purchased from Sigma-Aldrich, Alfa-Aesar, TCI chemicals, and Acros Organics unless specified and used as received.

2.2.1.2 Small molecules composed of diketopyrrolopyrrole and thiophene and benzene.

3,6-Di(thien-2-yl)pyrrolo[3,4-*c*]pyrrole-1,4(2H,5H)-dione (1): To t-amyl alcohol (250 mL), sodium metal pieces (2.56 g, 108 mmol) were slowly added to the reaction mixture over 1.5 h and the temperature of solution was increased to 120 °C. After all the sodium metal pieces were dissolved, thiophene-2-carbonitrile (11.9 g, 108 mmol) and dimethyl succinate (5.29 g, 36.2 mmol) was added to the solution. The reaction mixture was stirred overnight at 120 °C and then poured into acidic MeOH (400 mL MeOH and 20 mL conc. HCl). Filtration of the suspension yielded the product as a dark red solid. This product was used in next reactions without further purification (6 g, 47%). ^{1}H NMR (300 MHz, CDCl$_3$): δ (ppm) 11.19 (s, 2H), 8.13 (d, 2H), 7.90 (d, 2H), 7.23 (d, 2H).

3,6-Bis-(thiophen-2-yl)-*N*,*N'*-bis(2-ethylhexyl)-1,4-dioxo-pyrrolo[3,4-*c*]pyr role (2): To the compound **1** (5.0 g, 16.6 mmol) in DMF (150 mL), anhydrous K$_2$CO$_3$ (6.43 g, 49.9 mmol) were added and stirred at 120 °C for 1 h. And then the 2-ethylhexyl bromide (7.1 g, 36.6 mmol) was added dropwise, and the reaction mixture was further stirred overnight at 130 °C. After being cooled to room temperature, the solution was poured into water, and stirred

for 30 min. The product was extracted with chloroform, then washed with water, and dried over MgSO$_4$. The product was purified by column chromatography on silica gel (toluene as eluent) to yield the compound **2** (3.9 g, 45%). ^{1}H NMR (300 MHz, CDCl$_3$): δ (ppm) 8.90 (d, 2H), 7.63 (d, 2H), 7.27 (d, 2H), 4.03 (d, 4H), 1.86 (m, 2), 1.35–0.85 (m, 28H).

3-(5-bromothiophen-2-yl)-2,5-bis(2-ethylhexyl)-6-(thiophen-2-yl)pyrrolo [3,4-c]pyrrole-1,4(2H,5H)-dione (3): To the compound **2** (3 g, 5.71 mmol) in CHCl$_3$ (50 mL), NBS (1.01 g, 5.71 mmol) was added slowly in the dark and stirred overnight at room temperature. After pouring into water, the product was extracted with CHCl$_3$ and dried over MgSO$_4$. The solvent was evaporated under reduced pressure and the product was purified by column chromatography on silica gel (toluene as eluent) and recrystallization from acetone yield the compound **3** (2.0 g, 58%). ^{1}H NMR (300 MHz, CDCl$_3$): δ (ppm) 8.90 (d, 1H), 8.63 (d, 1H), 7.64 (d, 1H), 7.27 (d, 1H), 7.21 (d, 1H), 4.01 (m, 2H), 3.94 (m, 2H), 1.84 (m, 2H), 1.37–0.85 (m, 28H).

2,5-bis(trimethylstannyl)thiophene (4): To 2,5-dibromothiophene (1 g, 4.13 mmol) in anhydrous THF (15 mL), 2.5 M of *n*-BuLi in hexane (3.4 mL, 8.5 mmol) was added dropwise at 78 °C. After stirring for 60 min, the solution was further stirred for 30 min at room temperature. The solution was then cooled to 78 °C again before 1 M of trimethyltin chloride in hexane (8.6 mL, 8.6 mmol) was added. After warming up to room temperature and stirring overnight, the resulting mixture was poured into water and extracted with

diethyl ether. The organic phase was collected and dried over MgSO$_4$. Recrystallization from methanol yielded the compound **4** (1.35 g, 80%). ^{1}H NMR (300 MHz, CDCl$_3$): δ (ppm) 7.37 (s, 2H), 0.36 (s, 18H).

1,4-bis(4,4,5,5-tetramethyl-1,3,2-dioxaborolan-2-yl)benzene (5): To 1,4-dibromobenzene (1 g, 4.23 mmol) in anhydrous THF (15 mL), 2.5 M of *n*-BuLi in hexane (3.6 mL, 8.9 mmol) was added dropwise at -78 °C. After stirring for 60 min, the solution was further stirred for 30 min at room temperature. The solution was then cooled to -78 °C again before 2-isopropoxy-4,4,5,5-tetramethyl-1,3,2-dioxaborolane (1.7 g, 9.3 mmol) was added. After warming up to room temperature and stirring overnight, the resulting mixture was poured into water and extracted with diethyl ether. The organic phase was collected and dried over MgSO$_4$. Recrystallization from methanol yielded the compound **4** (1.20 g, 86%). ^{1}H NMR (300 MHz, CDCl$_3$): δ (ppm) 7.80 (s, 4H), 1.35 (s, 24H).

Synthesis of (TDPP)$_2$: (TDPP)$_2$ was synthesized by the Yamamoto coupling. The compound **3** (0.30 g, 0.33 mmol), 2,2'-bipyridiyl (0.12 g, 0.79 mmol) and Ni(COD)$_2$ (0.21 g, 0.79 mmol) were dissolved in THF (10 mL) and the solution was flushed with N$_2$ for 20 min. The reaction mixture was stirred at 150 °C for 3 h in a microwave reactor. After being cooled to room temperature, the mixture was poured into acidic methanol (200 mL methanol and 10 mL HCl) and stirred 1 h to remove nickel catalyst. The crude product was obtained by vacuum filtration and purified by column chromatography on

33

silica gel (100% dichloromethane as eluent) to afford (TDPP)$_2$ as a deep blue solid (0.22 g, 87%). ^{1}H NMR (300 MHz, CDCl$_3$): d (ppm) 8.96 (d, 2H), 8.93 (d, 2H), 7.65 (d, 2H), 7.44 (d, 2H), 7.29 (d, 2H), 4.02-3.88 (m, 8H), 1.84 (m, 4H), 1.37-1.23 (m, 32H), 0.90–0.85 (m, 24H).

Synthesis of T(TDPP)$_2$: T(TDPP)$_2$ was synthesized by the Stille coupling. The compound **3** (0.30 g, 0.33 mmol) and **4** (0.06 g, 0.15 mmol) were dissolved in toluene (8 mL). After the solution was flushed with N$_2$ for 20 min, 10 mg of Pd(PPh$_3$)$_4$ was added. The reaction mixture was stirred at 150 °C for 3 h in a microwave reactor. After being cooled to room temperature, the solvent was evaporated under vacuum. The residue was purified by column chromatography on silica gel (100% dichloromethane as eluent). The product T(TDPP)$_2$ was obtained as a deep blue solid (0.12 mmol, 80%). ^{1}H NMR (300 MHz, CDCl$_3$): d (ppm) 8.93 (d, 2H), 8.90 (d, 2H), 7.62 (d, 2H), 7.34 (d, 2H), 7.28 (d, 4H), 4.11–4.04 (m, 8H), 1.90 (m, 4H), 1.37-1.23 (m, 32H), 0.95–0.85 (m, 24H).

Synthesis of Ph(TDPP)$_2$: Ph(TDPP)$_2$ was synthesized by the Suzuki coupling. The compounds **3** (0.30 g, 0.33 mmol) and **5** (0.05 g, 0.15 mmol) were dissolved in a mixture of aqueous K$_2$CO$_3$ solution (2 M, 2 mL) and THF (8 mL). After the solution was flushed with N$_2$ for 20 min, 10 mg of Pd(PPh$_3$)$_4$ was added. The reaction mixture was stirred at 150 °C for 3 h in a microwave reactor. The residue was purified by column chromatography on silica gel (100% dichloromethane as eluent). The product Ph(TDPP)$_2$ was obtained as a

reddish blue solid (0.12 g, 73%). ^{1}H NMR (300 MHz, CDCl$_3$): d (ppm) 8.97 (d, 2H), 8.91 (d, 2H), 7.72 (s, 4H), 7.63 (d, 2H), 7.53 (d, 2H), 7.29 (d, 2H), 4.14–3.98 (m, 8H), 1.94–1.88 (m, 4H), 1.42–1.27 (m, 32H), 0.95-0.88 (m, 24H).

2.2.1.3 Characterization methods

The chemical structures of compounds were identified by ^{1}H NMR and ^{13}C NMR (Avance DPX-300). Molar masses of compounds were measured matrix-assisted laser desorption/ionization time-of-flight (MALDI-TOF) mass spectrometer (Voyager-DE STR Biospectrometry Workstation, Applied Biosystem Inc) with dithranol as a matrix. The optical absorption spectra were obtained by a UV–vis spectrophotometer (Shimadzu UV-3600 and Lambda 25, Perkin Elmer). Cyclic voltammetry was conducted on a potentiostat/galvanostat (VMP 3, Biologic) in an electrolyte solution of 0.1 M tetrabutylammonium hexafluorophosphate in dichloromethane. Pt wires (Bioanalytical System Inc.) were used as both counter and working electrodes, and silver/silver ion (Ag in 0.1 M AgNO$_3$ solution, Bioanalytical System Inc.) was used as a reference electrode. The HOMO energy levels of polymers were calculated by using the flowing relation: HOMO (eV) = $-[E_{ox} - E_{1/2}$(ferrocene) + 4.8], where E_{ox} is the onset oxidation potential of the polymer and $E_{1/2}$(ferrocene) is the onset oxidation potential of ferrocene vs. Ag/Ag$^+$. Density functional theory (DFT) calculations were carried out at the B3LYP/6-31G(d,p) level on Gaussian 03 and 09.

2.2.2 Device fabrication and measurements

2.2.2.1 Materials

ITO-patterned glass is used as an anode in OSC device. The sheet resistance of the ITO is lower than 15 Ω/sq. PEDOT:PSS (Clevios P VP AI 4083) was purchased from H.C. Stark and passed through a 0.45 μm PVDF syringe filter before spin-coating. $PC_{71}BM$ was obtained from Nano-C. Al and Au were purchased from TCI chemicals and iTASCO, respectively.

2.2.2.2 Solar cell device fabrication

The OSCs were fabricated with a standard device configuration of ITO/PEDOT:PSS/SM:$PC_{71}BM$/Ca/Al. Prior to device fabrication, the ITO-coated glass was cleaned with acetone and then isopropyl alcohol for 15 min. After complete drying at 120 ºC for 30 min, the ITO-coated glass was treated with UV-ozone for 10 min. PEDOT:PSS was spin-coated on the ITO glass at 3000 rpm for 40 s and annealed at 150 ºC for 30 min to yield a 40 nm thick film. The devices were transfered into a glove-box filled with N_2. The SM and $PC_{71}BM$ blended in proper organic solvent were stirred at 40 ºC for 1 h and then spin-coated on the top of PEDOT:PSS. The thickness of resulting film is ca. 70–90 nm. Finally calcium (15–20 nm) and then aluminium (100 nm) were thermally evaporated on the top of the active layer under vacuum ($<10^{-6}$ Torr). The effective area of the cell is 0.1 cm^2.

2.2.2.3 Solar cell performance measurements

The J–V characteristics were measured with a Keithley 4200 source-meter under AM 1.5G (100 mW/cm^2) simulated by a Newport-Oriel solar simulator. The light intensity was calibrated using a NREL-certified photodiode prior to each measurement. The external quantum efficiency (EQE) was measured using a lock-in amplifier with a current preamplifier (K3100, Mac Science Co.) under short circuit current state with illumination of monochromatic light. The space charge limited current (SCLC) J–V curves were obtained in the dark using hole-only devices (ITO/PEDOT:PSS/SM:PC$_{71}$BM/Au), and hole mobilities were calculated using the Mott-Gurney square law, $J = (9/8)\varepsilon_0\varepsilon_r\mu(V^2/L^3)$, where ε_0 is vacuum permittivity, ε_r is the dielectric constant of SM, μ is the charge carrier mobility, V is the effective applied voltage, and L is the thickness of the film. Grazing incidence X-ray diffraction (GIXD) experiments were performed at PLS-II 9A U-SAXS beamline of Pohang Accelerator Laboratory (Korea). The X-rays coming from the in-vacuum undulator are monochromated (wavelength λ = 1.116 Å) using a double crystal monochromator and focused both horizontally and vertically (300 (H) × 30 (V) μm^2 in FWHM @ sample position) using K-B type mirrors. The GIXD sample state is equipped with a 7-axis motorized stage for accurate alignment, and the incidence angle of X-ray beam was set to 0.11° in this study. GIXD patterns were recorded with a 2D CCD detector (Raynoix SX165, USA) and X-ray irradiation time was 5–100 seconds dependent on the saturation level of detector. Diffraction angles were calibrated by a pre-

calibrated sucrose (Monoclinic, P_{21}, a = 10.8631 Å, b = 8.7044 Å, c = 7.7624 Å, b = 102.938°), and the smaple-to-detector distance was about 230 mm. The morphology of active layer films was observed by TEM (JEM-1010, JEOL) with an accelerating voltage of 80 kV. Thickness of the active layers was measured by atomic force microscopy (Nano Xpert2).

2.3 Results and discussion

2.3.1 Synthesis and characterization

3-(5-Bromo-thiophene-2-yl)-2,5-bis-(2-ethyl-hexyl)-6-thiophene-2-yl-2,5-dihydro-yrrole-1,4-dion (compound **3**) and 2,5-bis-trimethylstannanyl-thiophene (compound **2**) were synthesized following the same procedure as reported in the literature.[114] A series of TDPP-based SMs, $(TDPP)_2$, $T(TDPP)_2$, and $Ph(TDPP)_2$, were synthesized by Yamamoto, Stille, and Suzuki cross coupling. Ethyl hexyl side chains ensure the solubility in organic solvent such as chloroform, chlorobenzene and o-dichlorobenzene. The products in each step were assigned by ^1H NMR.

2.3.2 Optical and electrochemical properties

The UV–vis absorptions of three SMs are shown in Figure. 2.9. The maximum absorption wavelength (λ_{max}) and the absorption edge of $(TDPP)_2$ are redshifted as compared to $T(TDPP)_2$ and $Ph(TDPP)_2$ in solution.
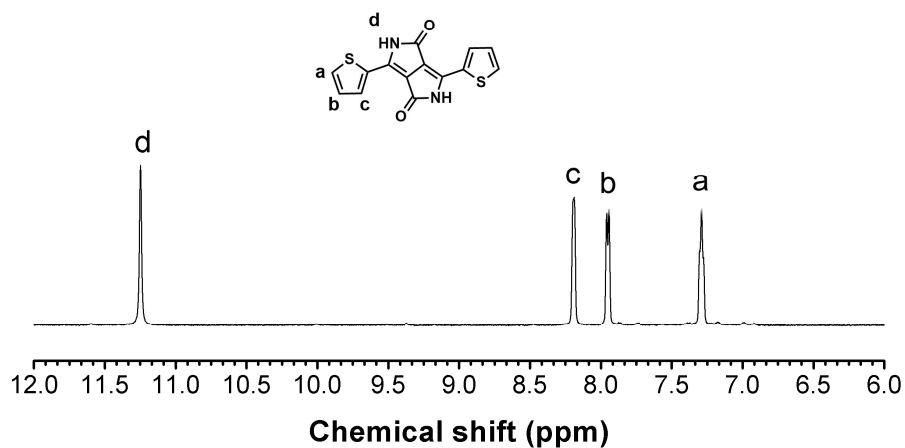
Figure 2.1. ^{1}H NMR spectrum of compound **1** in Scheme 2.1.
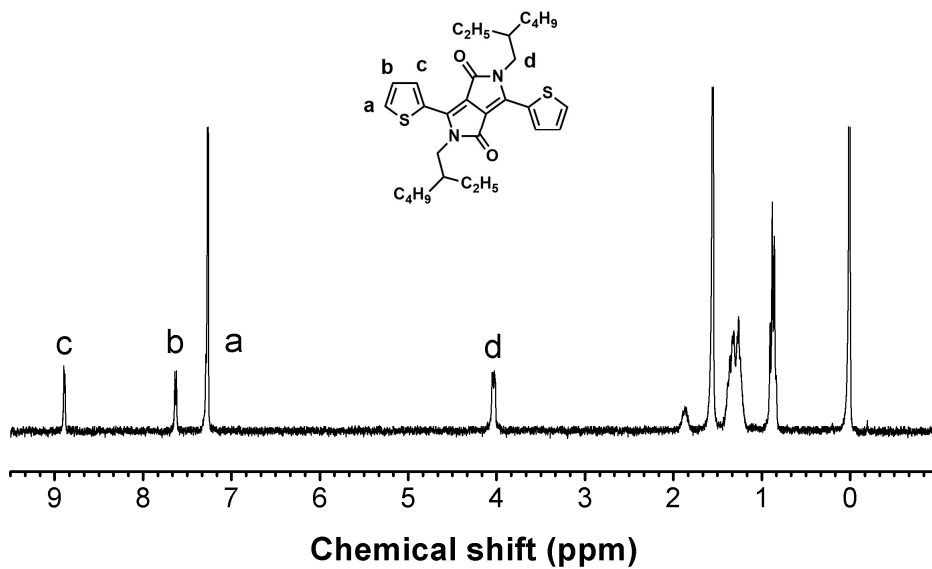
Figure 2.2. ^{1}H NMR spectrum of compound **2** in Scheme 2.1.
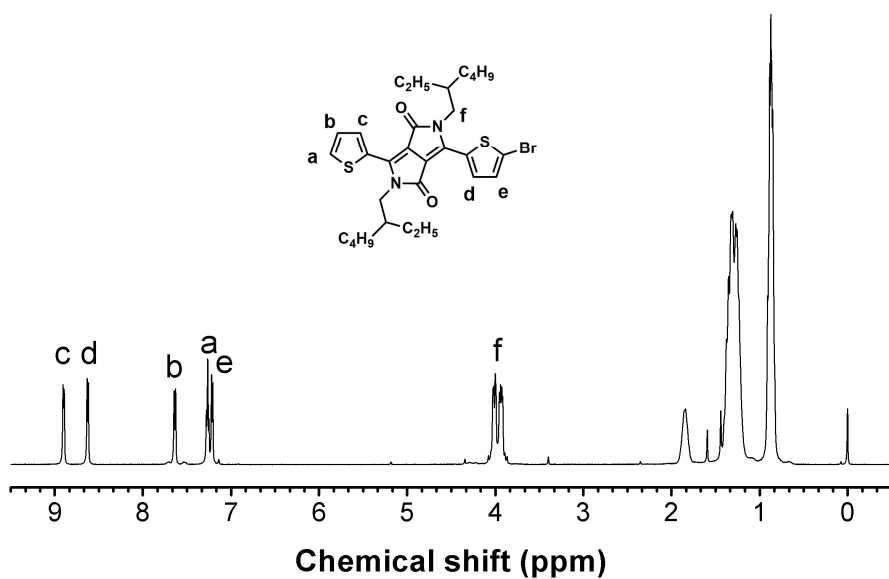
Figure 2.3. ^{1}H NMR spectrum of compound **3** in Scheme 2.1.
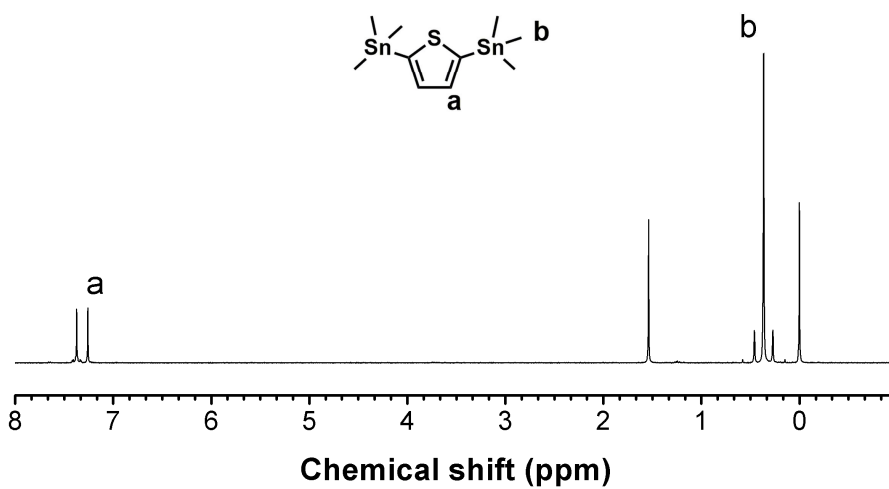
Figure 2.4. ^{1}H NMR spectrum of compound **4** in Scheme 2.1.

40
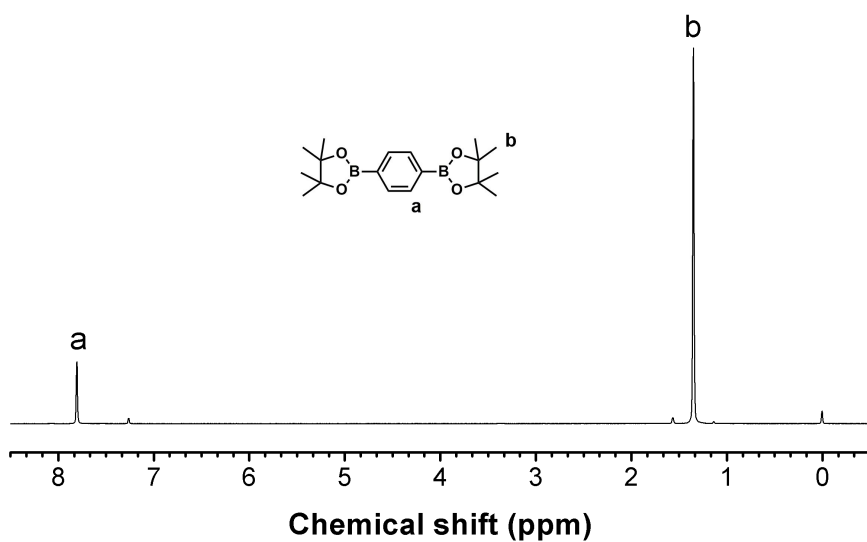
Figure 2.5. ^{1}H NMR spectrum of compound **5** in Scheme 2.1.
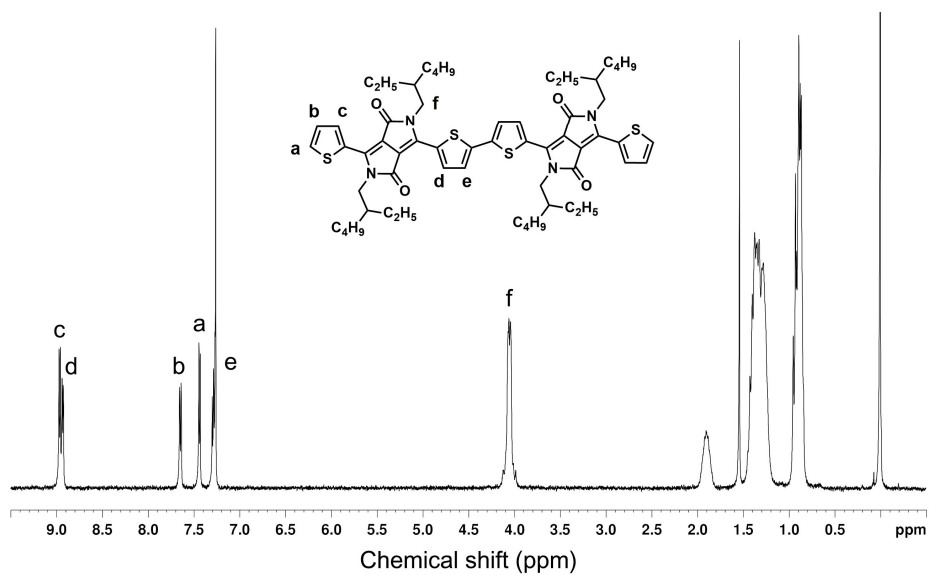
Figure 2.6. ^{1}H NMR spectrum of compound **(TDPP)₂** in Scheme 2.1.

41
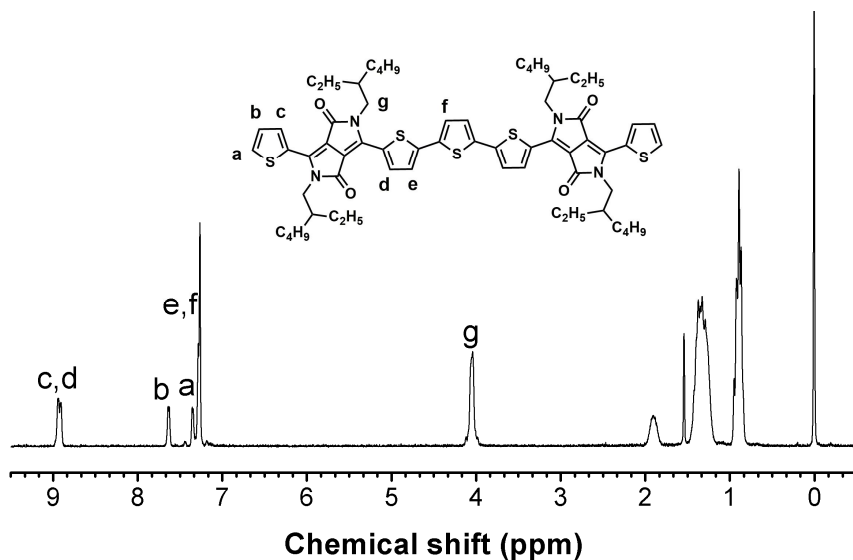
Figure 2.7. ^{1}H NMR spectrum of compound **T(TDPP)₂** in Scheme 2.1.
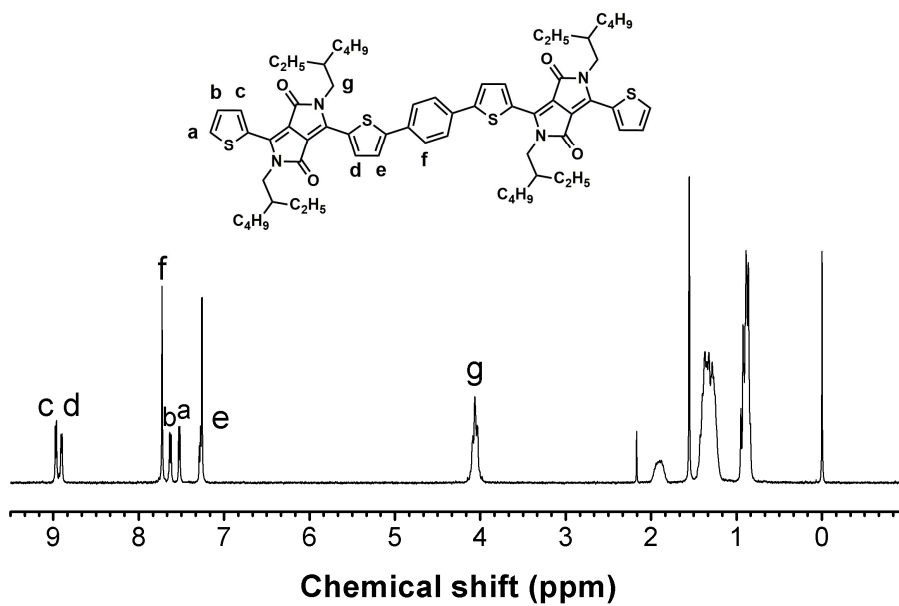
Figure 2.8. ^{1}H NMR spectrum of compound **Ph(TDPP)₂** in Scheme 2.1.

Particularly, (TDPP)$_2$ exhibited a discernible vibronic shoulder in solution, indicating that (TDPP)$_2$ is partially aggregated in solution state. The red-shift in film state of all SMs as compared to the solution state suggests that π–π stacking due to the intermolecular interaction in solid state is more favorable than in the solution. When the optical bandgaps (E_g^{opt}) of the SMs are estimated from the absorption edges of thin films, the bandgaps of (TDPP)$_2$, T(TDPP)$_2$ and Ph(TDPP)$_2$ are 1.51 eV, 1.51 eV and 1.66 eV, respectively. Particularly, the E_g^{opt} of Ph(TDPP)$_2$ is significantly larger than those of (TDPP)$_2$ and T(TDPP)$_2$. In D–A type SMs based on push–pull structure, the LUMO energy level is controlled by electron accepting (deficient) unit, while the HOMO energy level is governed by electron rich (donating) unit. Since (TDPP)$_2$, T(TDPP)$_2$ and Ph(TDPP)$_2$ have the same electron accepting unit (DPP), it is expected that the LUMO energy levels of three SMs are almost the same, whereas the HOMO energy levels are different because of different electron-donating unit in conjugated SMs. Ph(TDPP)$_2$ has deeper HOMO energy level and thus larger bandgap than (TDPP)$_2$ and T(TDPP)$_2$, because the electron-donating power of phenylene is weaker than thiophene.

Electrochemical properties of three SMs are measured by cyclic voltammetry (CV) (Figure. 2.10). The HOMO and LUMO energy levels are determined from CV, and the results are summarized in Table 2.1. Since the electron-donating power of phenylene is weaker than thiophene in A–D–A type conjugated SMs, the HOMO energy levels of these three SMs are deeper in the order of Ph(TDPP)$_2$ (−5.31 eV), (TDPP)$_2$ (−5.19 eV) and T(TDPP)$_2$ (−5.17 eV). While the HOMO energy levels are different, the
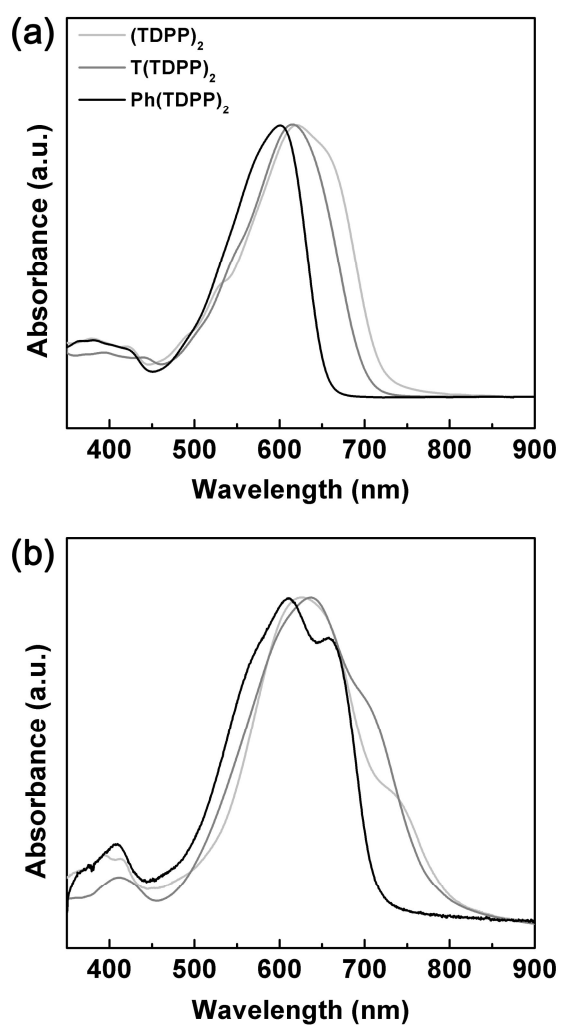
Figure 2.9. UV−vis absorption spectra of SMs in (a) CHCl₃ solution and (b) film state.
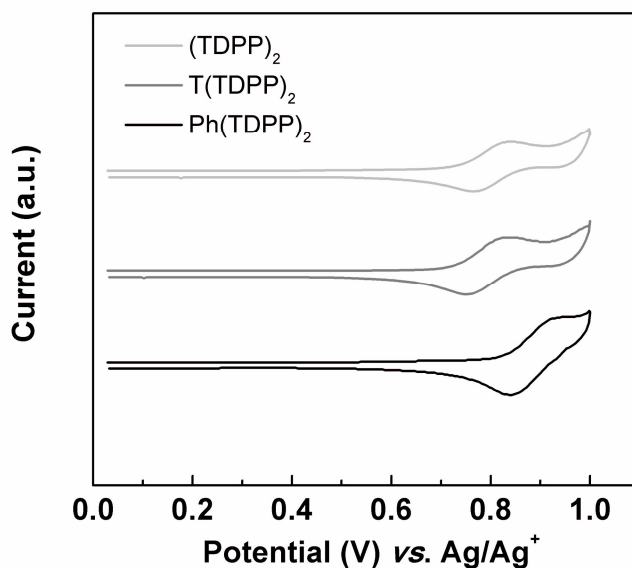
Figure 2.10. Cyclic voltammograms of DPP-based small molecules.

Table 2.1. Optical and electrochemical properties of DPP-based small molecules.

SMs	UV−vis absorption		$E_{g,opt}{}^{a}$ (eV)	HOMO (eV)	LUMO[b] (eV)
	$\lambda_{max, CHCl3}$ (nm)	$\lambda_{max, film}$ (nm)			
(TDPP)₂	625	628	1.51	−5.19	−3.68
T(TDPP)₂	615	638	1.51	−5.17	−3.66
Ph(TDPP)₂	601	612	1.66	−5.31	−3.65

[a] Determined from the onset of UV−vis absorption spectra.

[b] $E_{g}{}^{opt}$ + HOMO.

LUMO energy levels of (TDPP)$_2$, T(TDPP)$_2$ and Ph(TDPP)$_2$ are almost the same (around -3.70 eV) because they have the same electron-accepting unit.
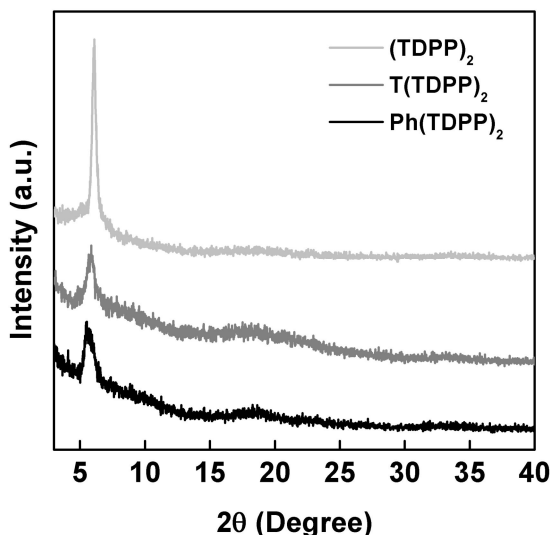
Figure 2.11. X-ray diffractograms of DPP-based small molecules.

2.3.3 Crystallinity

When the crystallinities of the conjugated SMs are examined by differential scanning calorimetry (DSC), (TDPP)$_2$ exhibits the highest melting temperature (265 °C) with the largest enthalpy of melting while T(TDPP)$_2$ does the lowest melting temperature (178 °C) with the smallest enthalpy of melting (Figure 2.12), indicating that (TDPP)$_2$ has the highest degree of crystallinity. All the three SMs exhibit a strong X-ray diffraction peak at $2\theta =$
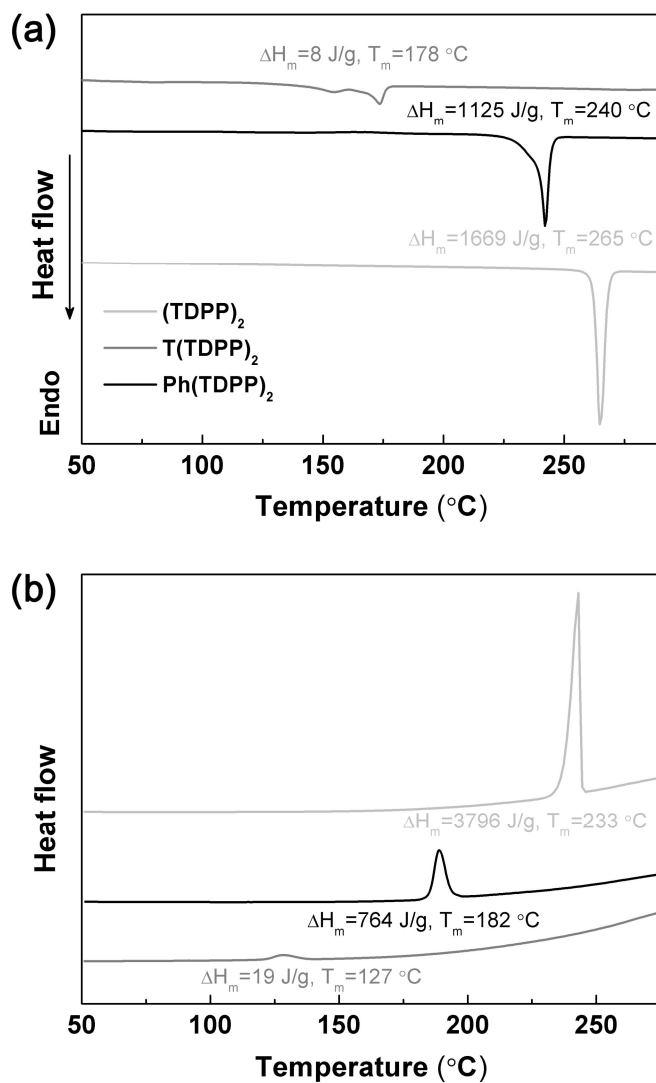
Figure 2.12. DSC thermograms of DPP-based small molecules.

47

6.10°, corresponding to the (100) diffraction with an interlayer spacing of 14.4 Å, as shown in Figure. 2.11.

2.3.4 Photovoltaic properties

The photovoltaic properties of the SMs were measured at least 8 times with the standard device configuration of ITO/PEDOT:PSS/SM:PC$_{71}$BM/Al under AM 1.5G simulated light. The devices were optimized by varying processing conditions, such as the blend ratio and thermal annealing. The J–V curves of the devices of optimized blend ratio between SMs and PC$_{71}$BM before and after thermal annealing are shown in Figure 2.13 and the photovoltaic properties are listed in Table 2.2. After thermal annealing, the J_{SC} and FF values were enhanced at optimum blend ratio of respective SMs. The tendency of V_{OC}s is same regardless of thermal condition. Since Ph(TDPP)$_2$ has deeper HOMO energy level than others, Ph(TDPP)$_2$ exhibits the highest V_{OC} of 0.93 V, and as a consequence a high PCE of 4.01% after thermal annealing at 120 °C for 10 min.

2.3.5 Morphologies of active layer

The length scale of phase separation is critically important for exciton dissociation and charge transport. If the length scale is too large, excitons may recombine before reaching the interface between donor and acceptor phases, while too small phase separation length scale may also block the efficient
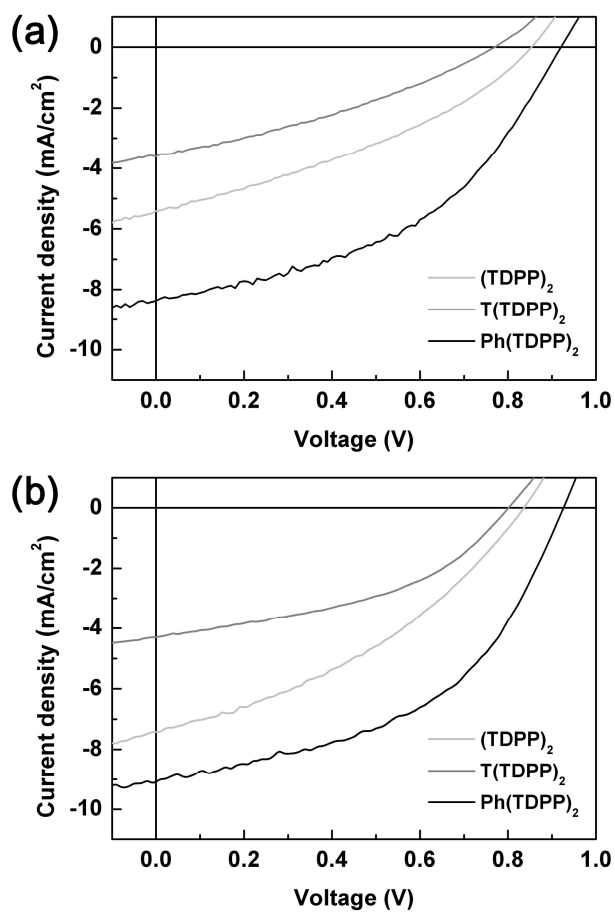
Figure 2.13. *J–V* curves of SMs/PC$_{71}$BM BHJ-OSCs (a) before and (b) after annealing 120 °C for 10 min.

Table 2.2. Photovoltaic properties of devices with DPP-based small molecules under standard AM 1.5G illumination.

	Small molecules	SM: PC$_{71}$BM (w/w)	V_{OC} (V)	J_{SC} (mA/cm^2)	FF (%)	PCE (%)
As cast	(TDPP)$_2$	1:1	0.85	5.41	0.34	1.59
	T(TDPP)$_2$	1:1	0.77	3.60	0.32	0.89
	Ph (TDPP)$_2$	1:0.8	0.92	8.36	0.45	3.47
Annealed	(TDPP)$_2$	1:1	0.84	7.4	0.37	2.31
	T(TDPP)$_2$	1:1	0.80	4.0	0.43	1.49
	Ph (TDPP)$_2$	1:0.8	0.93	9.09	0.47	4.01
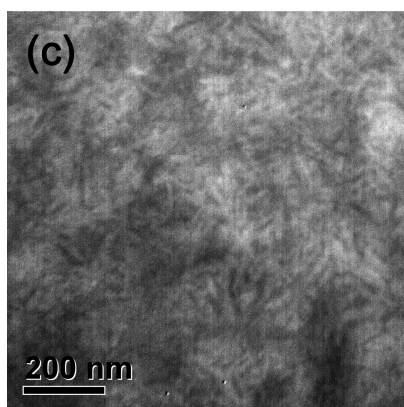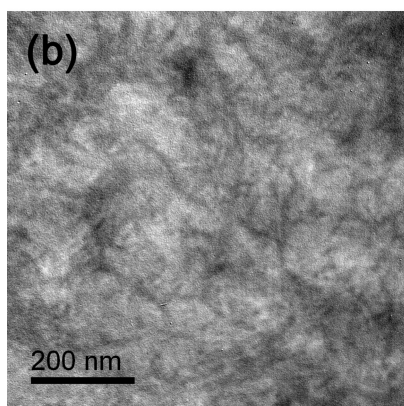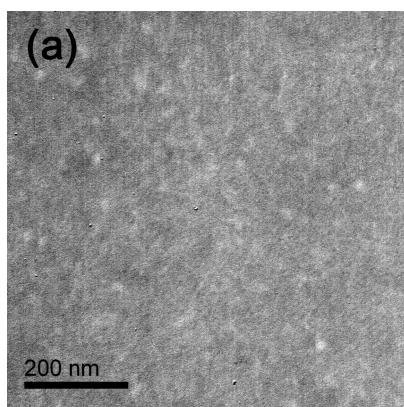
Figure 2.14. TEM images of (a) (TDPP)$_2$:PC$_{71}$BM (1:1 w/w), (b) T(TDPP)$_2$:PC$_{71}$BM (1:1 w/w), and (c) Ph(TDPP)$_2$:PC$_{71}$BM (1.25:1 w/w).

charge transport. Thus, the nanoscale phase separation with 20 nm domain size in BHJ materials is optimum for charge separation and transport because the exciton diffusion length is about 10 nm. When the morphologies of $(TDPP)_2:PC_{71}BM$, $T(TDPP)_2:PC_{71}BM$ and $Ph(TDPP)_2:PC_{71}BM$ blends after thermal annealing at 120 °C for 10 min are compared, as shown in Figure. 2.14 where bright and dark regions correspond to SM-rich phase and $PC_{71}BM$-rich domain, respectively. $Ph(TDPP)_2:PC_{71}BM$ exhibits bicontinuous two-phase nanostructure (<20 nm), which is essential for effective exciton dissociation and charge transport, whereas $(TDPP)_2:PC_{71}BM$ and $Ph(TDPP)_2:PC_{71}BM$ show homogeneous one-phase morphology and macro-phase separated morphology, respectively, both of which prevent exciton dissociation and charge transport. Considering the charge carrier mobility and phase morphology of blend films, it is reasonable that $Ph(TDPP)_2$ exhibits higher J_{SC} than $(TDPP)_2$ and $T(TDPP)_2$, although it has rather higher bandgap than other two SMs.

2.3.6 Charge carrier mobility of active layer

When the charge carrier mobilities of $SM:PC_{71}BM$ are determined from the space-charge limited current $J–V$ curves as obtained in the dark using the Mott–Gurney law (Figure. 2.15), the hole mobilities of $Ph(TDPP)_2:PC_{71}BM$ (8.8×10^{-5} cm^2/V s) is higher than those of $(TDPP)_2:PC_{71}BM$ (6.0×10^{-5} cm^2 V^{-1} s^{-1}) and $T(TDPP)_2:PC_{71}BM$ (2.5×10^{-5} cm^2 V^{-1} s^{-1}), whereas the electron mobilities of $(TDPP)_2:PC_{71}BM$ (2.2×10^{-4} cm^2 V^{-1} s^{-1}), $T(TDPP)_2:PC_{71}BM$
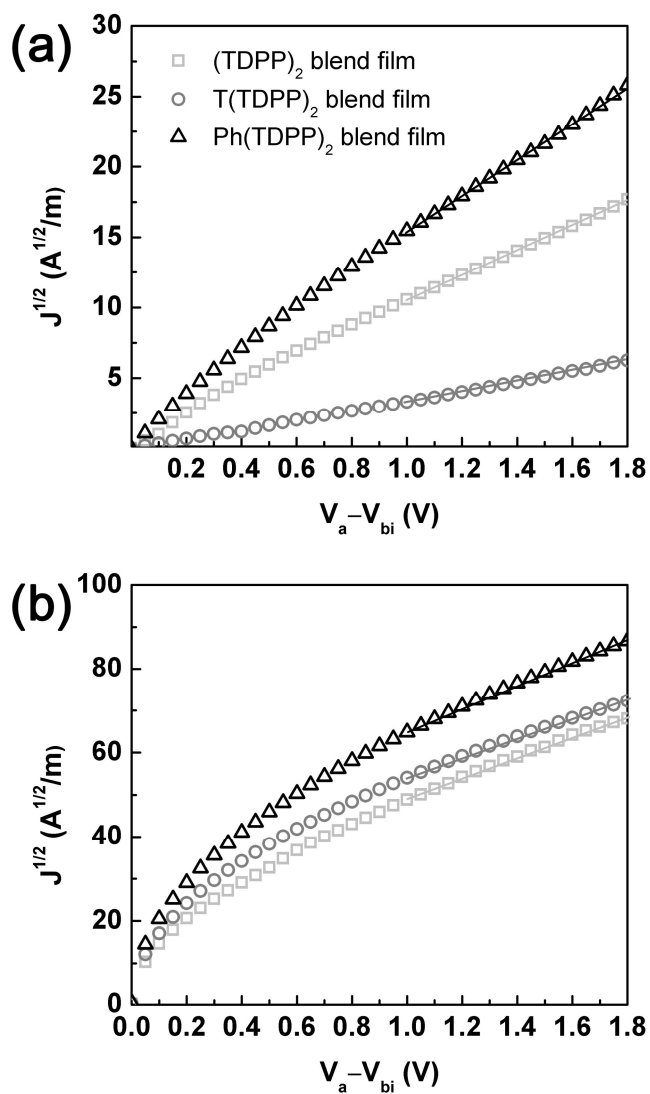
Figure 2.15. Dark *J–V* characteristics of DPP-based SM/PC$_{71}$BM blends with (a) hole-only and (b) electron-only device, where the solid lines represent the best linear fit of the data points.

$(2.0 \times 10^{-4}$ cm^2 V^{-1} s$^{-1})$ and Ph(TDPP)$_2$:PC$_{71}$BM $(2.4 \times 10^{-4}$ cm^2 V^{-1} s$^{-1})$ are almost the same. These results are consistent with morphological characteristics of SMs:PC$_{71}$BM film which are observed by TEM images. The (TDPP)$_2$:PC$_{71}$BM blend exhibits homogeneous one-phase morphology and thus cannot form interpenetrating network, while T(TDPP)$_2$:PC$_{71}$BM blending film shows a phase separation with large and discontinuous domains, which prevents effective charge transport. However, the Ph(TDPP)$_2$:PC$_{71}$BM blend exhibits a percolated two phase nanostructure with the domain size of less than 20 nm, which is an optimum for effective charge transport. Since Ph(TDPP)$_2$:PC$_{71}$BM exhibits higher hole mobility
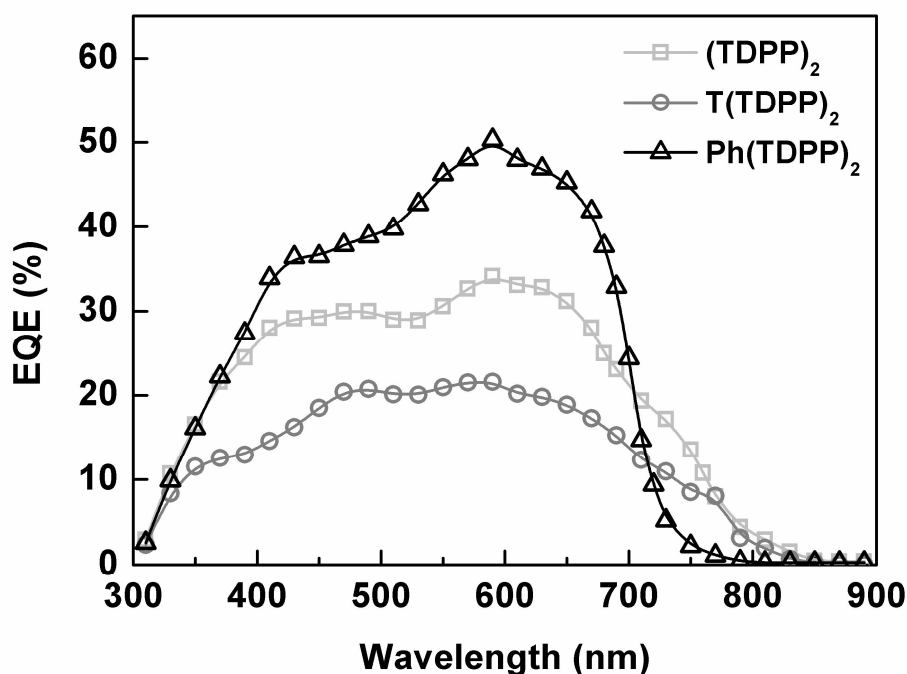
Figure 2.16. EQE spectra of DPP-based SM/PC$_{71}$BM solar cells.

and better balance between electron and hole mobility, the device from Ph(TDPP)$_2$:PC$_{71}$BM shows higher J_{SC} and better FF than others.

To further confirm higher J_{SC} of Ph(TDPP)$_2$, the external quantum efficiencies (EQEs) of (TDPP)$_2$, T(TDPP)$_2$, and Ph(TDPP)$_2$ blended with PC$_{71}$BM are measured and compared, as shown in Figure. 2.16. Ph(TDPP)$_2$ shows higher EQE in the range of 400–700 nm and a maximum EQE of 50.3% at 590 nm. Integration of EQE spectrum of Ph(TDPP)$_2$:PC$_{71}$BM yields J_{SC} = 8.82 mA/cm^2, which is well consistent with the J_{SC} value (9.09 mA/cm^2) obtained from J–V measurement.

2.4 Summary

Conjugated SMs with a simple A–D–A structure based on TDPP were successfully synthesized and characterized. The LUMO energy levels of three SMs ((TDPP)$_2$, T(TDPP)$_2$ and Ph(TDPP)$_2$) were almost the same (−3.70 eV) because all three SMs have the same electron accepting unit in the molecules. However, since the electron-donating power of phenylene between DPP units is weaker than that of thiophene, Ph(TDPP)$_2$ has deeper HOMO energy level, which consequently leads to a high V_{OC} of 0.93 V. Since Ph(TDPP)$_2$ shows higher hole mobility than other two molecules with well-developed nanoscale phase-separated morphology, it exhibits higher J_{SC} than others, yielding a PCE of 4.01%, although the bandgap of Ph(TDPP)$_2$ is higher than those of (TDPP)$_2$ and T(TDPP)$_2$.

Chapter 3. A strategy to enhance both V_{OC} and J_{SC} of A–D–A type small molecules based on diketopyrrolopyrrole

3.1 Introduction

Owing to intensive studies on the ideal donor material in BHJ-OSCs for the past decade, some requirements for high performance OSCs have been established: (1) broad and strong light absorption in the visible region, (2) high hole mobility for fast charge carrier transport to yield high J_{SC}, and (3) suitable energy levels to ensure high V_{OC} and efficient exciton dissociation. Broad absorption is requisite for efficient solar cells. One of effective strategies to broaden light absorption is to synthesize organic molecules with low optical bandgap through combination of electron-donating and electron-accepting units in alternative sequence, where the HOMO and LUMO energy levels of D–A type molecules become higher and lower than those of D and A molecules, respectively. Considering that the LUMO energy level of a typical acceptor, $PC_{61}BM$ is about -4.3 eV, the LUMO energy level of donor molecule should be higher than -3.9 eV, which limits lowering the bandgap, because the LUMO level offset between donor and acceptor should be larger than 0.3 eV for efficient exciton dissociation. On the other hand, raising the HOMO energy level for lowering the gap leads to decrease in V_{OC}, because
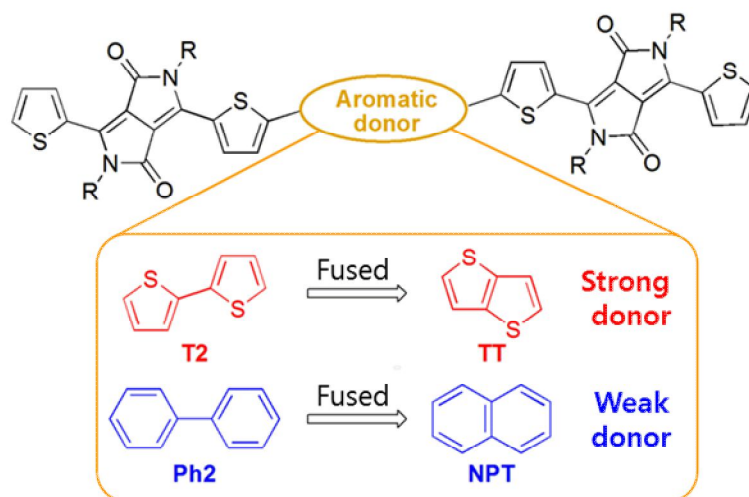
Scheme 3.1. Chemical structure of DPP-based small molecules.

the V_{OC} is proportional to the difference between the HOMO energy level of donor and the LUMO energy level of acceptor. Hence, the lowering of bandgap may sacrifice the V_{OC}. As a consequence, a new strategy to overcome this trade-off behavior should be developed for high performance solar cells.

Another method to improve J_{SC} is to incorporate planar molecular structure, [131,132] because the molecules with planar structure are efficiently packed for crystallization which enhances the charge carrier mobility. For this purpose, fused aromatic units have been incorporated in π-extended molecular backbone.[133–136] Recently, conjugated alternating copolymers based on fused aromatic ring such as thieno[3,2-b]thiophene (TT)[137,138] and naphthalene (NPT)[86] have exhibited high charge carrier mobility in FET device up to 0.79 cm^2/V s and 0.98 cm^2/V s, respectively.

In this work, to overcome the trade-off between J_{SC} and V_{OC}, we designed four different SMs with A–D–A type structure, where acceptor is TDPP and donor is electron-donating unit such as bithiophene (T2), biphenylene (Ph2), thienothiophene (TT) and naphthalene (NPT), as shown in Scheme. 3.1, where TT and NPT are the corresponding fused aromatic rings of T2 and Ph2, respectively. Here, it is expected that the use of weak donor increases V_{OC} while the introduction of fused aromatic ring increases J_{SC} as well. Since the electron-donating capability of Ph2 and NPT are weaker than T2 and TT, respectively, Ph2(TDPP)$_2$ and NPT(TDPP)$_2$ exhibit deeper HOMO energy levels than T2(TDPP)$_2$ and TT(TDPP)$_2$ and thus larger V_{OC}, while the introduction of fused aromatic rings (TT and NPT) instead of T2 and Ph2 increases J_{SC} due to planarity of SMs.

3.2 Experimental section

3.2.1 Synthesis

3.2.1.1 Small molecules composed of diketopyrrolopyrrole and bithiophene, biphenylene and corresponding fused donor units.

5,5'-Bis(trimethylstannyl)-2,2'-bithiophene (6): To 5,5'-dibromo-2,2'-bithiophene (1 g, 3.09 mmol) in anhydrous THF (15 mL), 2.5 M of n-BuLi in hexane (2.8 mL, 7.0 mmol) was added dropwise at –78 °C. After stirring for 30 min, the solution was further stirred for 30 min at room temperature. The
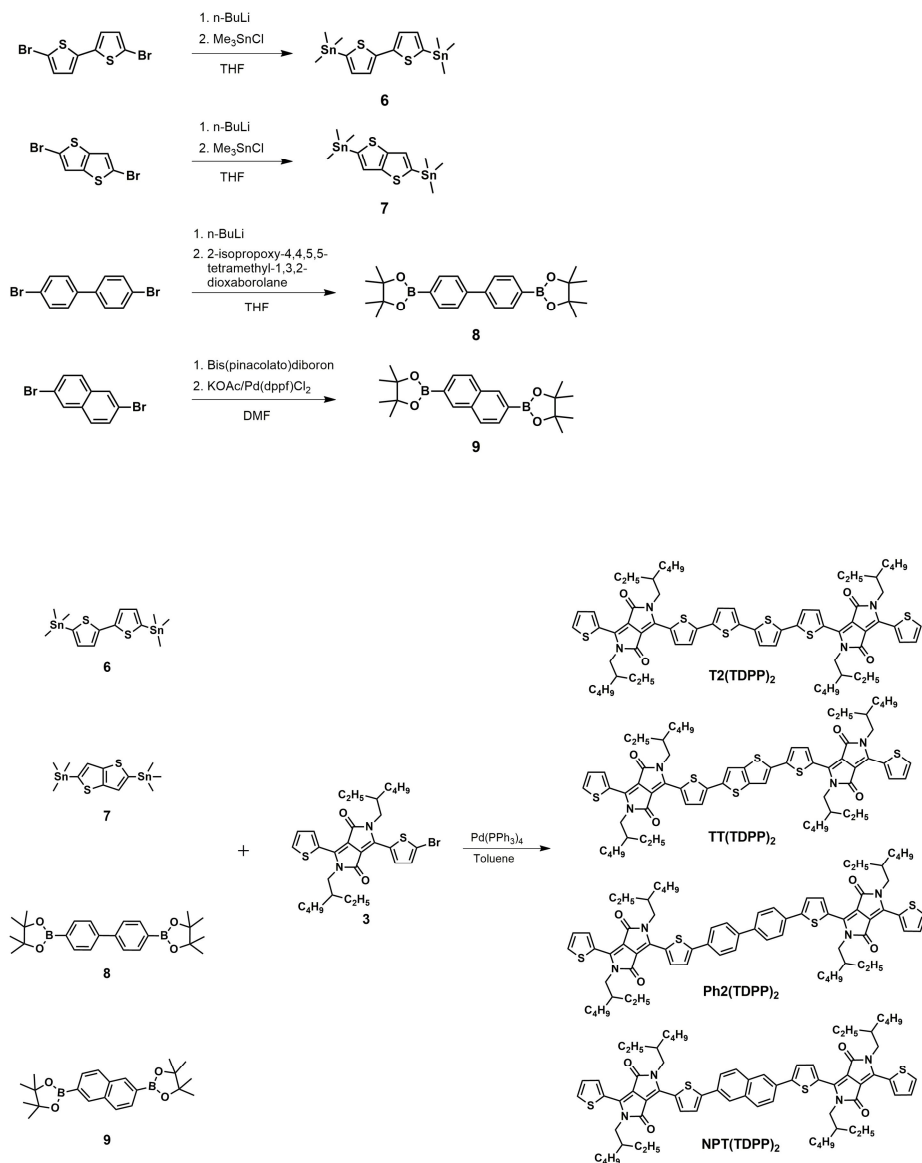
Scheme 3.2. Synthetic scheme of DPP-based small molecules with simple donors and corresponding fused donor units.

solution was then cooled to –78 °C again before 1 M of trimethyltin chloride in hexane (7.7 mL, 7.7 mmol) was added. After warming up to room temperature and stirring overnight, the resulting mixture was poured into water and extracted with diethyl ether. The organic phase was collected and dried over MgSO$_4$. Recrystallization from methanol yielded the compound **6** (0.97 g, 64%). ^{1}H NMR (300 MHz, CDCl$_3$): δ (ppm) 7.28 (d, 2H), 7.09 (d, 2H), 0.38 (m, 18H).

2,5-bis(trimethylstannyl)thieno[3,2-b]thiophene (7): To thieno [3,2-b]thiophene (0.5 g, 3.56 mmol) in anhydrous THF (15 mL), 2.5 M of *n*-BuLi in hexane (3.0 mL, 7.5 mmol) was added dropwise at –78 °C. After stirring for 30 min, the solution was further stirred for 30 min at room temperature. The solution was then cooled to –78 °C again before 1 M of trimethyltin chloride in hexane (7.8 mL, 7.8 mmol) was added. After warming up to room temperature and stirring overnight, the resulting mixture was poured into water and extracted with diethyl ether. The organic phase was collected and dried over MgSO$_4$. Recrystallization from methanol yielded the compound **7** (1.17g, 72%). ^{1}H NMR (300 MHz, CDCl$_3$): δ (ppm) 7.25 (t, 2H) 0.38 (s, 18H).

4,4'-bis(4,4,5,5-tetramethyl-1,3,2-dioxaborolan-2-yl)-1,1'-biphenyl (8): To 4,4'-dibromobiphenyl (1.0 g, 3.2 mmol) in anhydrous THF (15 mL), 2.5 M of *n*-BuLi in hexane (2.7 mL, 6.7 mmol) was added dropwise at –78 °C. After stirring for 30 min, the solution was further stirred for 30 min at room temperature. The solution was then cooled to –78 °C again before 2-

isopropoxy-4,4,5,5-tetramethyl-1,3,2-dioxaborolane (1.31 g, 7.05 mmol) was added. After warming up to room temperature and stirring overnight, the resulting mixture was poured into water and extracted with diethyl ether. The organic phase was collected and dried over MgSO$_4$. Recrystallization from methanol yielded the compound **8** (1.12g, 86%). ^{1}H NMR (300 MHz, CDCl$_3$): δ (ppm) 7.88 (d, 4H), 7.63 (d, 4H), 1.36 (s, 24H).

2,6-bis(4,4,5,5-tetramethyl-1,3,2-dioxaborolan-2-yl)naphthalene (9): To 2,6-dibromonaphthalene (1g, 3.50 mmol) in DMF, bis(pinacolato)diboron (1.95 g, 7.70 mmol), KOAc (1.51 g, 15.4 mmol), Pd(dppf)Cl$_2$ (51 mg, 0.07 mmol) was added under N$_2$. After stirring at 150 °C for 2h, the resulting mixture was poured into water and extracted with chloroform. The organic phase was collected and dried over MgSO$_4$. The residue was purified by flash column chromatography, and then, recrystallized from methanol to yield compound **9** (1.01g, 76%). ^{1}H NMR (300 MHz, CDCl$_3$): δ (ppm) 8.35 (s, 2H), 7.84 (m, 4H), 1.38 (s, 24H).

Synthesis of T2(TDPP)$_2$: T2(TDPP)$_2$ was synthesized by the Stille coupling. After the compound **3** (200 mg, 0.33 mmol), **6** (81 mg, 0.17 mmol) and Pd(PPh$_3$)$_4$ (19 mg, 0.02 mmol) were dissolved in toluene (10 mL) under N$_2$ atmosphere, the reaction mixture was stirred at 110 °C for 24 h and then cooled down to room temperature. The reaction mixture was poured into acidic methanol (200 mL methanol and 10 mL HCl) and stirred for 1 h to

remove the metal catalyst. The crude product was obtained by vacuum filtration and purified by column chromatography on silica gel (100% CHCl$_3$ as eluent) to yield T2(TDPP)$_2$ as a deep blue solid (160 mg, 80% yield). ^{1}H NMR (300 MHz, CDCl$_3$): δ (ppm) 8.94 (d, 2H), 8.89 (d, 2H), 7.62 (d, 2H), 7.30–7.22 (m, 6H), 7.15 (d, 2H), 4.10 (m, 8H), 1.90 (m, 4H), 1.38–1.20 (m, 32H), 0.95–0.86 (m, 24H).

Synthesis of TT(TDPP)$_2$: The same procedure as for T2(TDPP)$_2$ was performed. After the compound **3** (200 mg, 0.33 mmol), **7** (80 mg, 0.17 mmol) and Pd(PPh$_3$)$_4$ (19 mg, 0.02 mmol) were dissolved in toluene (10 mL) under N$_2$ atmosphere, the reaction mixture was stirred at 110 °C for 24 h and then cooled down to room temperature. The reaction mixture was poured into acidic methanol (200 mL methanol and 10 mL HCl) and stirred for 1 h to remove the metal catalyst. The crude product was obtained by vacuum filtration and purified by column chromatography on silica gel (100% CHCl$_3$ as eluent) to yield TT(TDPP)$_2$ as a deep blue solid (170 mg, 86% yield). ^{1}H NMR (300 MHz, CDCl$_3$): δ (ppm) 8.93 (d, 2H), 8.90 (d, 2H), 7.62 (d, 2H), 7.45 (d, 2H), 7.35 (d, 2H), 7.28 (s, 2H), 4.04–4.00 (m, 8H), 1.91–1.88 (m, 4H), 1.39–1.25 (m, 32H), 0.94–0.83 (m, 24H).

Synthesis of Ph2(TDPP)$_2$: Ph2(TDPP)$_2$ was synthesized by the Suzuki coupling. The compound **3** (200 mg, 0.33 mmol), **8** (67 mg, 0.17 mmol), and Pd(PPh$_3$)$_4$ (19 mg, 0.02 mmol) were dissolved in a mixture of aqueous K$_2$CO$_3$

solution (2 M, 3 mL) and toluene (10 mL). After the solution was purged with N_2 for 20 min, 3 drops of Aliguat 336 were added. The reaction mixture was stirred at 110 ºC for 24 h and then cooled down to room temperature. The reaction mixture was poured into acidic methanol (200 mL methanol and 10 mL HCl) and stirred for 1 h to remove the metal catalyst. The crude product was purified by column chromatography on silica gel (100% CHCl$_3$ as eluent). The product Ph2(TDPP)$_2$ was obtained as a reddish blue solid (120 mg, 60% yield). ^{1}H NMR (300 MHz, CDCl$_3$): δ (ppm) 8.98 (d, 2H), 8.90 (d, 2H), 7.78 (d, 4H), 7.70 (d, 4H), 7.62 (d, 2H), 7.53 (d, 2H), 7.28 (d, 2H), 4.09–4.04 (m, 8H), 1.95–1.88 (m, 4H), 1.42–1.28 (m, 32H), 0.95–0.88 (m, 24H).

Synthesis of NPT(TDPP)$_2$: The same procedure as for Ph2(TDPP)$_2$ was performed. The compound **3** (200 mg, 0.33 mmol), **8** (67 mg, 0.17 mmol), and Pd(PPh$_3$)$_4$ (19 mg, 0.02 mmol) were dissolved in a mixture of aqueous K$_2$CO$_3$ solution (2 M, 3 mL) and toluene (10 mL). After the solution was purged with N_2 for 20 min, 3 drops of Aliguat 336 were added. The reaction mixture was stirred at 110 ºC for 24 h and then cooled down to room temperature. The reaction mixture was poured into acidic methanol (200 mL methanol and 10 mL HCl) and stirred for 1 h to remove the metal catalyst. The crude product was purified by column chromatography on silica gel (100% CHCl$_3$ as eluent). The product NPT(TDPP)$_2$ was obtained as a deep blue solid (120 mg, 60% yield). ^{1}H NMR (300 MHz, CDCl$_3$): δ (ppm) 8.98 (d, 2H), 8.90 (d, 2H), 7.78 (d, 4H), 7.70 (d, 4H), 7.62 (d, 2H), 7.53 (d, 2H), 7.28 (d, 2H), 4.09–4.04 (m, 8H), 1.95–1.88 (m, 4H), 1.42–1.28 (m, 32H), 0.95–0.88 (m, 24H).

3.3 Results and discussion

3.3.1 Synthesis and characterization

Compound **6** and **7** were synthesized with n-butyl lithium and trimethyltin chloride at −78 °C under N_2. Compound **8** also was synthesized with n-butyl lithium and 2-isopropoxy-4,4,5,5-tetramethyl-1,3,2-dioxaborolane at −78 °C under N_2. Compound **9** was synthesized with bis(pinacolato)diboron in present of Pd(dppf)Cl$_2$. T2(TDPP)$_2$ and TT(TDPP)$_2$ were synthesized via Sille coupling and Ph2(TDPP)$_2$ and NPT(TDPP)$_2$ were synthesized via Suzuki coupling. The products in each step were assigned by ^{1}H NMR.

3.3.2 Optical and electrochemical properties

The UV–vis absorption spectra of four SMs in CHCl$_3$ solution and thin film state are shown in Figure. 3.9, and the spectroscopic data are summarized in Table 3.1. All of SMs show a strong and broad absorption peak at longer wavelength originated from the intramolecular charge transfer between donor and acceptor units in SMs and a weak absorption peak at shorter wavelength attributed to π-π transition. Such absorption spectra are the typical feature of D–A type conjugated molecules.[139] The λ_{onset} of T2(TDPP)$_2$ and TT(TDPP)$_2$ in solution is red-shifted by ~50 nm as compared to Ph2(TDPP)$_2$ and NPT(TDPP)$_2$ due to longer effective conjugation length afforded by thiophene derivatives in SMs as compared to phenylene derivatives. The absorption
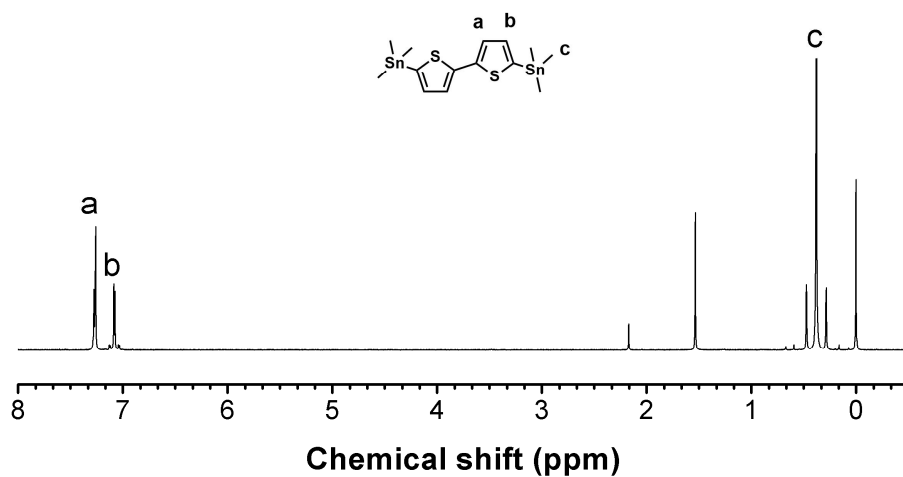
Figure 3.1. ^{1}H NMR spectrum of compound **6** in Scheme 3.2.
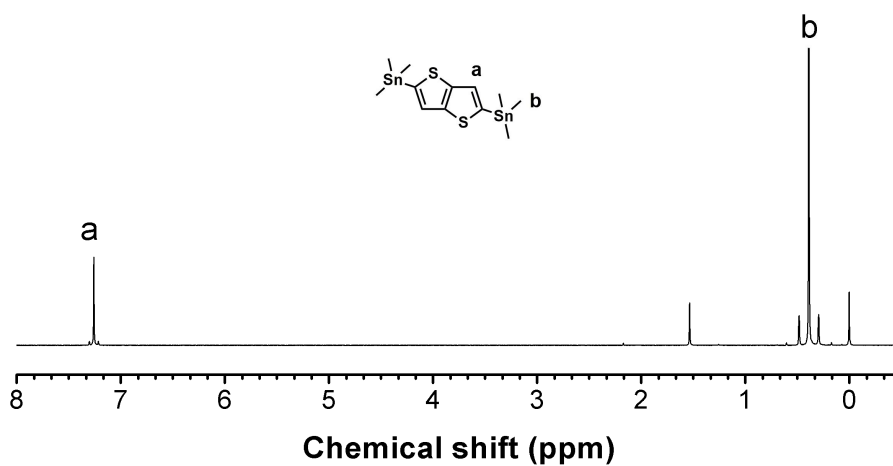
Figure 3.2. ^{1}H NMR spectrum of compound **7** in Scheme 3.2.

65
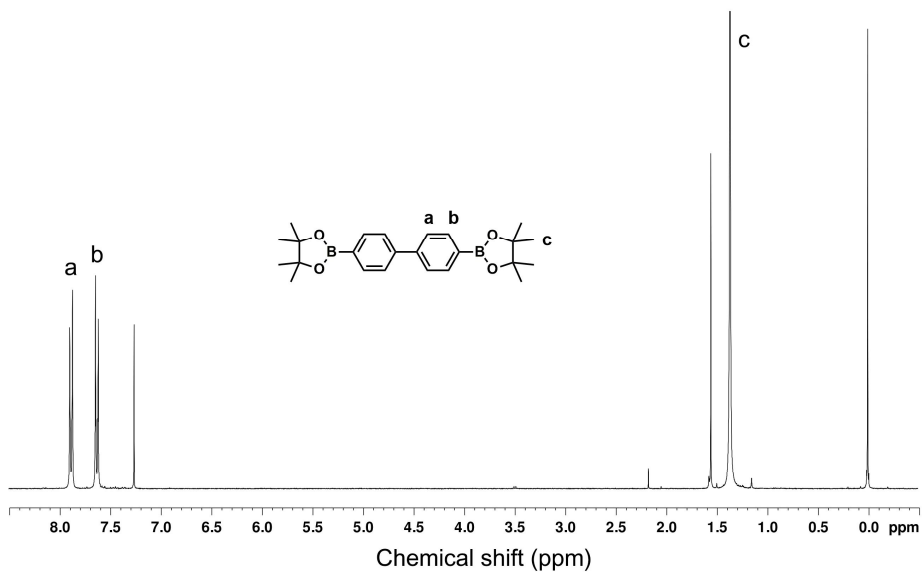
Figure 3.3. ^{1}H NMR spectrum of compound **8** in Scheme 3.2.
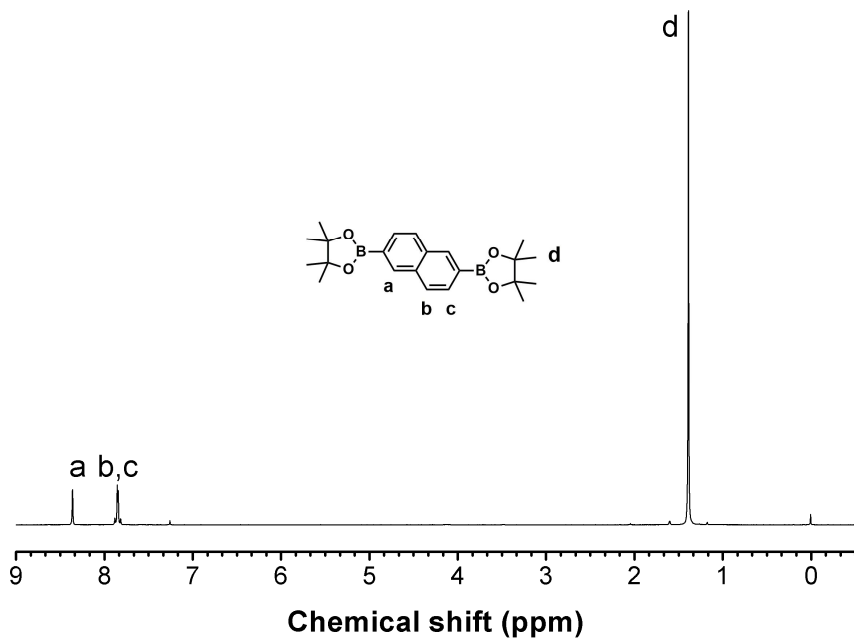
Figure 3.4. ^{1}H NMR spectrum of compound **9** in Scheme 3.2.

66
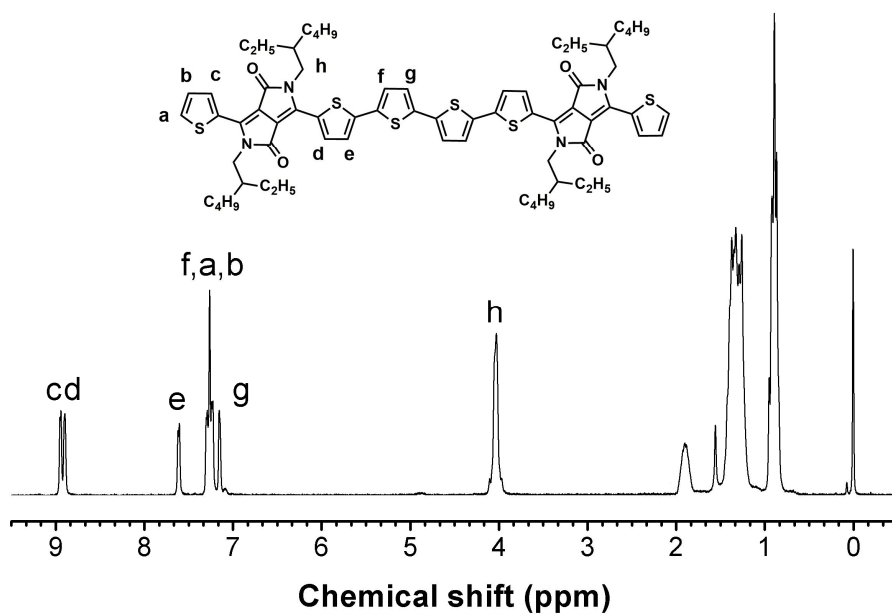
Figure 3.5. ^{1}H NMR spectrum of compound **T2(TDPP)₂** in Scheme 3.2.
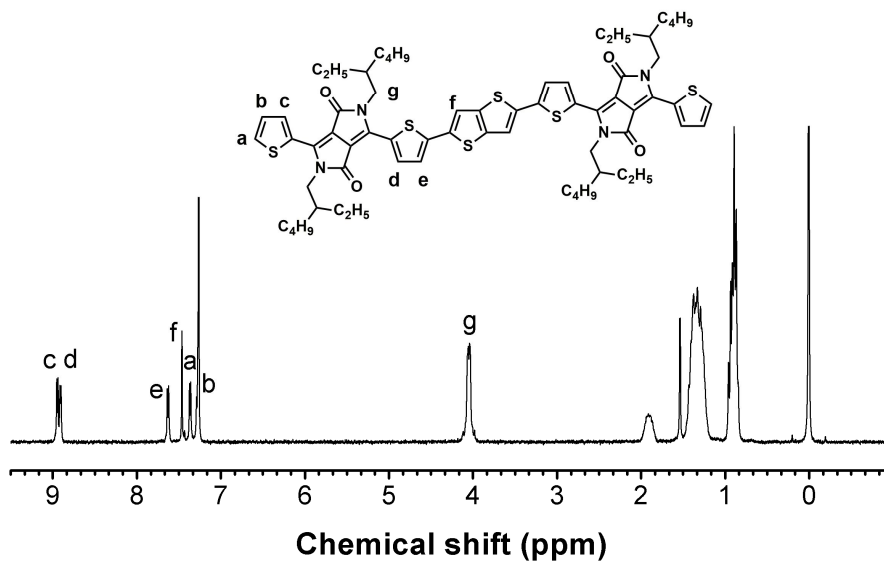
Figure 3.6. ^{1}H NMR spectrum of compound **TT(TDPP)₂** in Scheme 3.2.
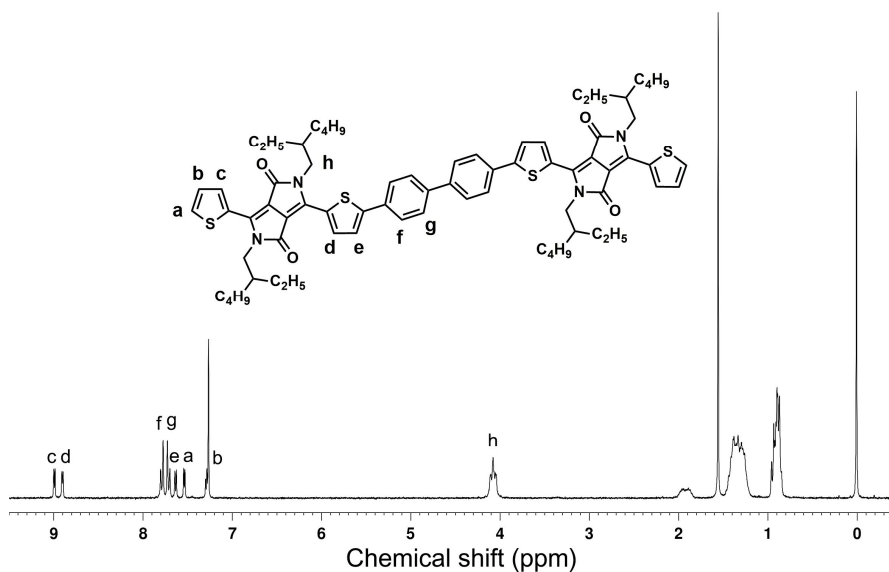
Figure 3.7. ^{1}H NMR spectrum of compound **Ph2(TDPP)₂** in Scheme 3.2.
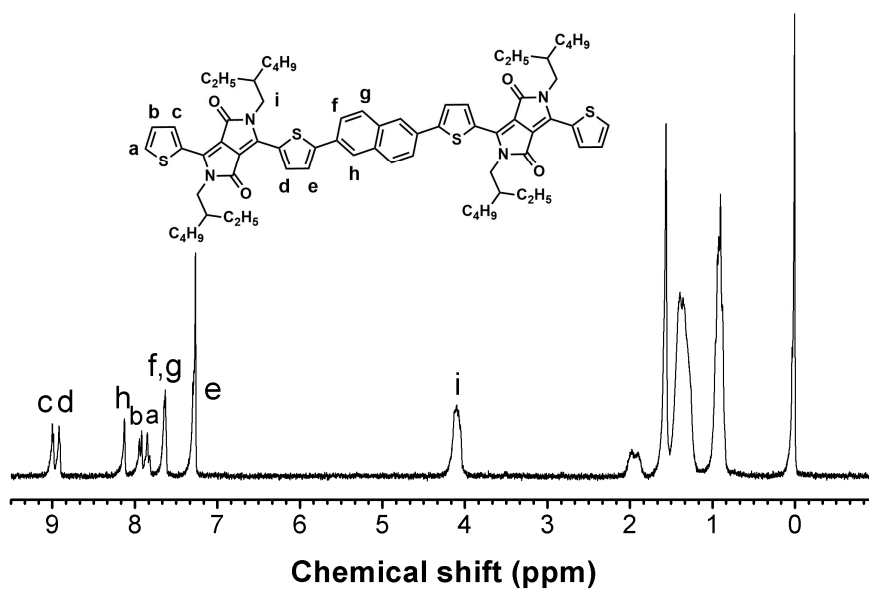
Figure 3.8. ^{1}H NMR spectrum of compound **NPT((TDPP)₂)** in Scheme 3.2.

spectra in solid state exhibit the red-shift of the λ_{max} and the λ_{onset} relative to the solution state. Particularly, TT(TDPP)$_2$ and NPT(TDPP)$_2$ exhibit a discernible vibronic shoulder peak, indicating that TT(TDPP)$_2$ and NPT(TDPP)$_2$ are more effectively packed in solid state due to more planar structure of fused aromatic ring. When the E_g^{opt} is estimated from λ_{onset}, the E_g^{opt} of the T2(TDPP)$_2$ (1.65 eV) is lower than that of Ph2(TDPP)$_2$ (1.80 eV), as listed in Table 3.1. This is because the torsional angle between the two thiophene units in T2(TDPP)$_2$ is smaller than that between the two phenylene units in Ph2(TDPP)$_2$ and thereby T2(TDPP)$_2$ has more extended delocalization of electrons.

The HOMO and LUMO energy levels are also measured by CV, as shown in Figure. 3.10, and the results are summarized in Table 3.1. It has generally been accepted that the HOMO and the LUMO energy levels of D–A type conjugated molecules are mainly governed by those of donor and acceptor units, respectively. In other words, the weak donating unit in D–A molecule lowers the HOMO energy level while the weak accepting unit raises the LUMO energy level, and vice versa. Since the electron-donating power of phenylene is weaker than that of thiophene, the HOMO energy levels of Ph2(TDPP)$_2$ (−5.21 eV) and NPT(TDPP)$_2$ (−5.18 eV) are lower than those of T2(TDPP)$_2$ (−5.14 eV) and TT(TDPP)$_2$ (−5.11 eV), respectively. As a result, the V_{OC}s of Ph2(TDPP)$_2$ and NPT(TDPP)$_2$ are higher than those of T2(TDPP)$_2$ and TT(TDPP)$_2$, as listed in Table 3.2, because the V_{OC} is proportional to the energy difference between the HOMO of electron donor and the LUMO of electron acceptor in active layer of BHJ solar cells. It is noted that the LUMO

69
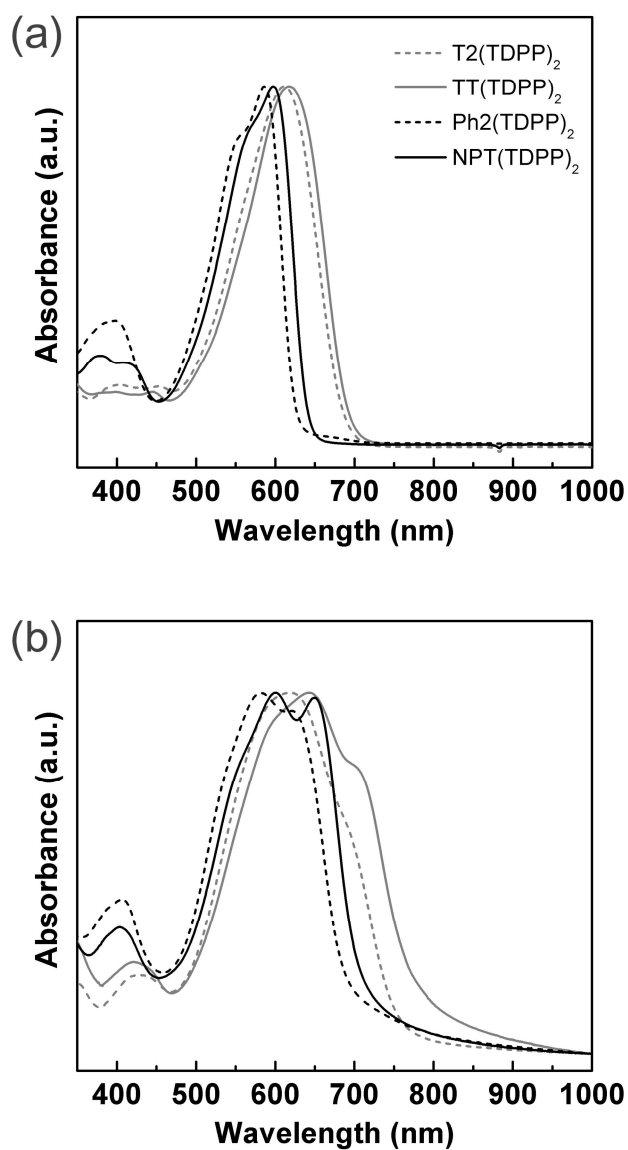
Figure 3.9. UV−vis absorption spectra of DPP-based SMs in (a) CHCl₃ solution and (b) film state.

70
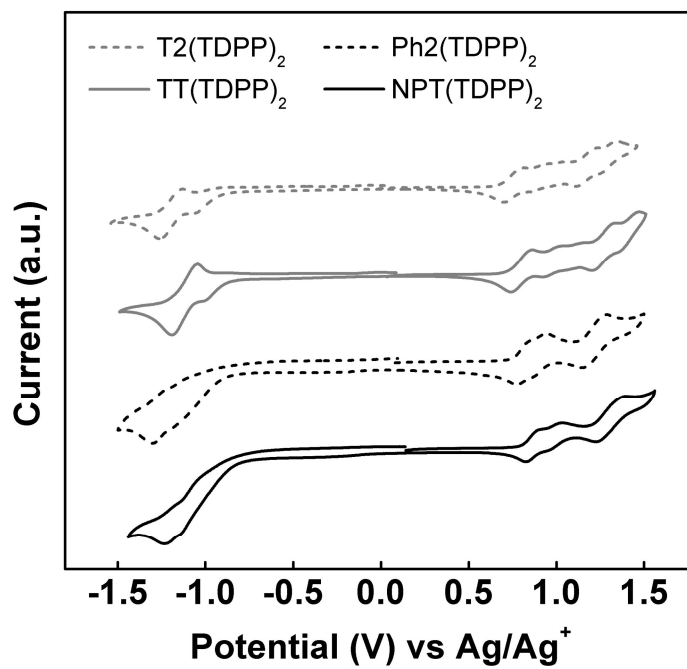
Figure 3.10. Cyclic voltammograms of DPP-based SMs.

Table 3.1. Optical and electrochemical properties of DPP-based small molecules.

SMs	UV–vis absorption		$E_{g,}^{opt}$ (eV)[a]	HOMO (eV)	LUMO (eV)	E_g^{el} (eV)	μ_h (cm^2 V^{-1} s^{-1})
	λ_{max},sol (nm)	λ_{max},film (nm)					
T2(TDPP)$_2$	612	620, 686	1.65	−5.14	−3.55	1.59	5.1×10^{-4}
TT(TDPP)$_2$	618	643, 702	1.60	−5.11	−3.58	1.54	7.7×10^{-4}
Ph2(TDPP)$_2$	586	583, 620	1.80	−5.21	−3.57	1.64	6.1×10^{-4}
NPT(TDPP)$_2$	597	600, 650	1.75	−5.18	−3.58	1.60	1.1×10^{-3}

[a] Determined from the onset of UV–vis absorption spectra.

energy levels of four SMs are nearly the same (-3.55 to -3.57 eV), because all SMs have the identical electron-accepting unit (DPP).

3.3.3 Crystallinity

When the crystallinity of SMs was examined by X-ray diffraction (XRD), as shown in Figure. 3.11, all SMs except for T2(TDPP)$_2$ showed a sharp diffraction peak at $2\theta = 6.6°$ corresponding to the interlayer d-spacing. Furthermore, TT(TDPP)$_2$ and NPT(TDPP)$_2$ with fused aromatic ring showed discernibly the second XRD peak at $2\theta = 13.2°$, indicating that these two SMs have higher crystallinity, which is primarily due to planarity of fused aromatic ring.
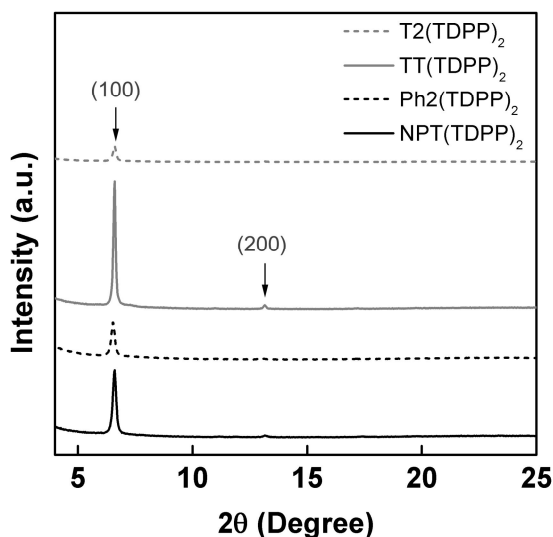
Figure 3.11. X-ray diffractograms of DPP-based SMs in thin film.
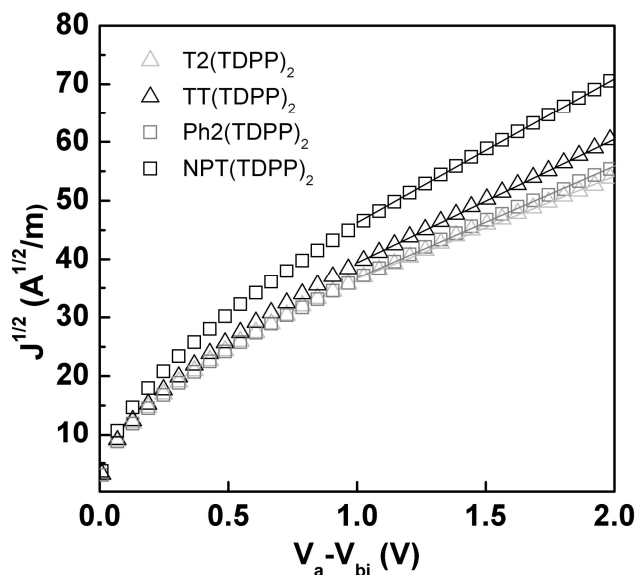
Figure 3.12. Dark *J−V* characteristics of DPP-based SM/PC$_{71}$BM blends with hole-only device, where the solid lines represent the best linear fit of the data points.

3.3.4 Charge charrier mobility of active layer

SCLC *J–V* curves were obtained in the dark condition using hole-only device fabricated under the identical condition with optimized photovoltaic cells (Figure. 12). When the hole mobility was estimated from the SCLC *J–V* curve using the Mott–Gurney law, the hole mobilities of TT(TDPP)$_2$ and NPT(TDPP)$_2$ are higher than those of T2(TDPP)$_2$ and Ph2(TDPP)$_2$, as listed in Table 3.2. These higher hole mobilities of TT(TDPP)$_2$ and NPT(TDPP)$_2$

may arise mainly from higher crystallinity due to more planar structure of fused aromatic units in the SMs.

3.3.5 Photovoltaic properties

The $J–V$ curves of photovoltaic devices fabricated from the blends of SMs and PC$_{71}$BM are shown in Figure 3.13, and their photovoltaic properties are summarized in Table 3.2. The J_{SC}s of TT(TDPP)$_2$ and NPT(TDPP)$_2$ are higher than those of T2(TDPP)$_2$ and Ph2(TDPP)$_2$ primarily due to their higher hole mobility, while the V_{OC}s of Ph2(TDPP)$_2$ and NPT(TDPP)$_2$ are higher than those of T2(TDPP)$_2$ and TT(TDPP)$_2$ owing to weaker electron-donating power of phenylenes. As a result, NPT(TDPP)$_2$ exhibits the highest PCE of 4.4% with a J_{SC} of 9.5 mA cm^{-2}, a V_{OC} of 0.87 V, and a FF of 0.53. The external quantum efficiency (EQE) spectra (Figure. 3.13) of optimized devices are nearly consistent with the absorption spectra (Figure. 3.9). When the J_{SC} of NPT(TDPP)$_2$ was calculated from integration of EQE spectrum, the value of J_{SC} was 9.3 mA cm^{-2}, which is well consistent with J_{SC} measured from $J–V$ curve.

3.3.6 Morphology of active layer

When the morphologies of SM/PC$_{71}$BM blend films prepared from CHCl$_3$/DIO solution are examined by TEM, as shown in Figure.3.14, the blend films of TT(TDPP)$_2$ and NPT(TDPP)$_2$ with fused aromatic rings exhibit
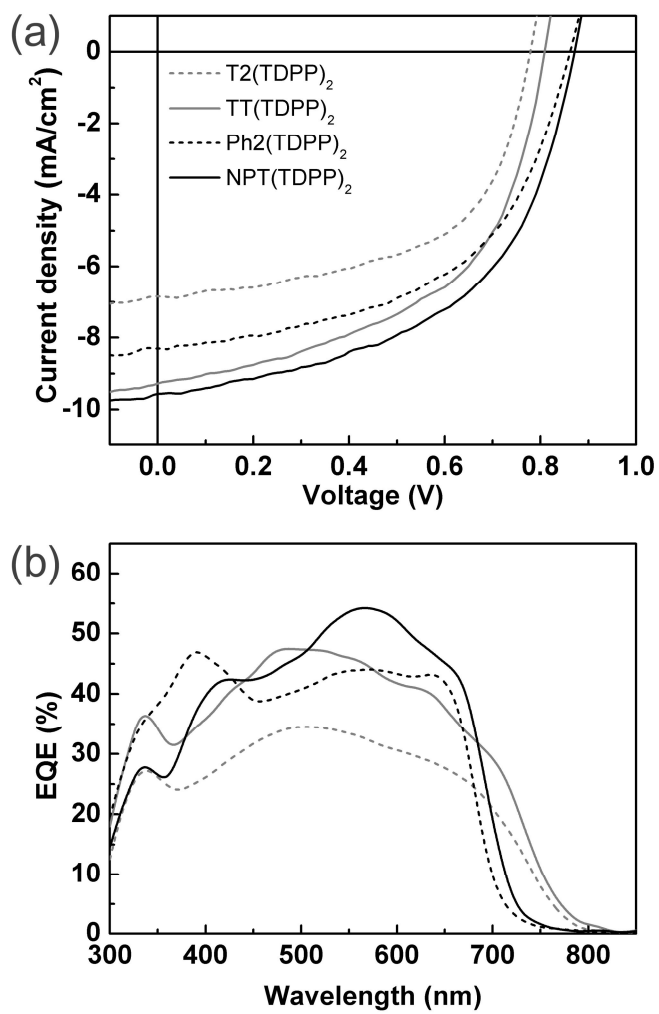
Figure 3.13. (a) *J−V* curves and (b) EQE spectra of DPP-based SM/PC$_{71}$BM solar cells.

Table 3.2. Photovoltaic properties of devices with DPP-based small molecules under standard AM 1.5G illumination.

Small molecules	SM: PC$_{71}$BM (w/w)	μ_h (cm^2 V^{-1} s^{-1})	V_{OC} (V)	J_{SC} (mA/cm^2)	FF (%)	PCE (%)
T2(TDPP)$_2$	1:1	5.1×10^{-4}	0.78	6.8	0.57	3.0
TT(TDPP)$_2$	1:1	7.7×10^{-4}	0.81	9.3	0.53	4.0
Ph2(TDPP)$_2$	1.5:1	6.1×10^{-4}	0.86	8.3	0.53	3.8
NPT(TDPP)$_2$	1:1	1.1×10^{-3}	0.87	9.5	0.53	4.4

needle-like nanoscale phase separation, which is beneficial for charge carrier transport, while the blends of T2(TDPP)$_2$ and Ph2(TDPP)$_2$ show sphere-like nanoscale domain. However, when the blend films prepared from CHCl$_3$ without addition of DIO, the morphologies of T2(TDPP)2 and Ph2(TDPP)2 blends show homogeneous morphology, while TT(TDPP)2 and NPT(TDPP)2 blends show largely aggregated domains, both of which do not form the pathway for charge carrier transport. Hence, it is realized that the addition of solvent additive (DIO) largely affects the blend morphology.

3.4 Summary

For enhancement of both J_{SC} and V_{OC} of DPP-based SMs, a series of SMs with A–D–A type structure, where acceptor is DPP and donor is different electron-donating units, are synthesized and their photovoltaic properties are compared. Ph2(TDPP)$_2$ and NPT(TDPP)$_2$ with weak electron-donating unit show deeper HOMO levels than T2(TDPP)$_2$ and TT(TDPP)$_2$ with strong electron-donating unit. As a consequence, the photovoltaic cells based on Ph2(TDPP)$_2$ and NPT(TDPP)$_2$ exhibit higher V_{OC} than T2(TDPP)$_2$ and TT(TDPP)$_2$ cells. The introduction of fused aromatic ring (TT and NPT) in SMs lowers the bandgap and enhances hole mobility mainly due to high crystallinity derived from planar structure of fused aromatic ring. As a result, TT(TDPP)$_2$ and NPT(TDPP)$_2$ exhibit higher J_{SC}s than T2(TDPP)$_2$ and Ph2(TDPP)$_2$. As a consequence, the introduction of NPT, which lowers the HOMO energy level and enhances hole mobility, affords the highest PCE of

4.4% with a V_{OC} of 0.87 V, a J_{SC} of 9.5 mA cm^{-2}, and a FF of 0.53. This successful result provides a guideline for rational design of conjugated SMs for enhancement of both V_{OC} and J_{SC}.
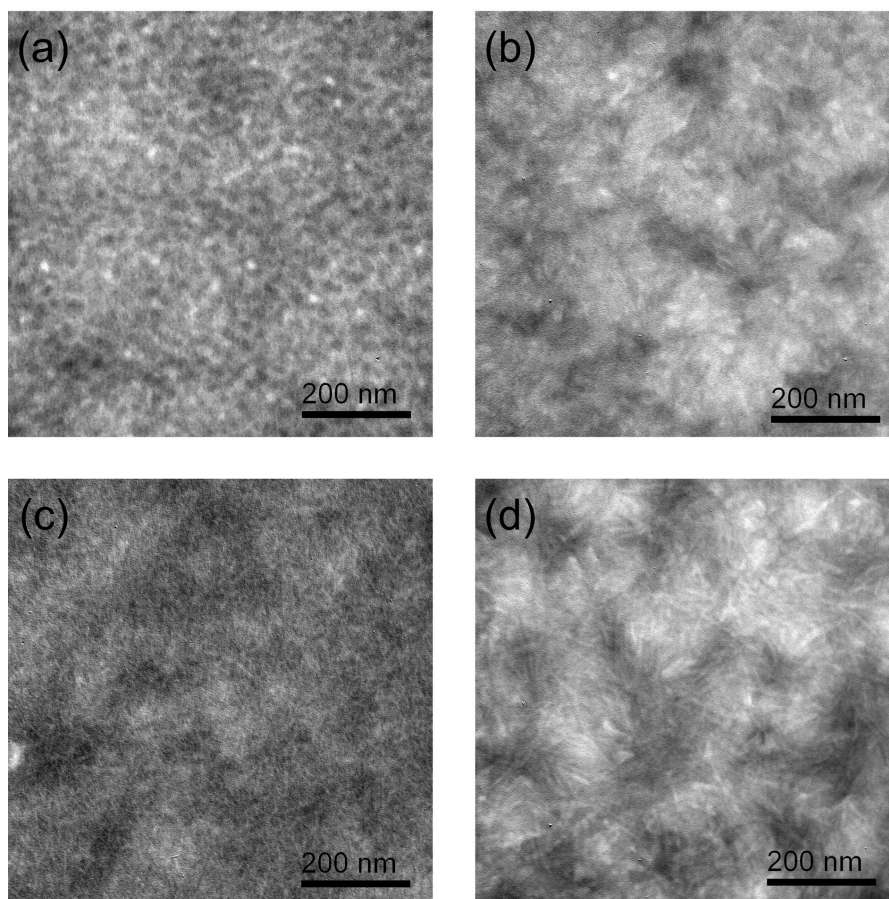
Figure 3.14. TEM images of (a) T2(TDPP)$_2$:PC$_{71}$BM (1:1 w/w), (b) TT(TDPP)$_2$:PC$_{71}$BM (1:1 w/w), (c) Ph2(TDPP)$_2$:PC$_{71}$BM (1.5:1 w/w), and (d) NPT(TDPP)$_2$:PC$_{71}$BM (1:1 w/w) blend.

Chapter 4. Small molecules based on thienopyrroledione for high V_{OC} organic photovoltaics

4.1 Introduction

Thieno[3,4-c]pyrrole-4,6-dione (TPD) has been a promising moiety as an acceptor unit[140–144] in D–A-type conjugated polymers, because its relatively strong electron accepting power leads to low frontier orbital energy levels of corresponding conjugated polymers, which is required for high V_{OC} in BHJ-OSCs. Although it is generally accepted that the HOMO and LUMO energy level of D–A-type conjugated molecules are governed mainly by the electronic properties of donor and acceptor units, respectively, exceptional but interesting results have been reported when a TPD unit is used as an acceptor unit in D–A type conjugated backbone: Both HOMO and LUMO levels are lowered when TPD is used as an acceptor unit in D–A-type conjugated molecules. For instance, it has been reported that a low-bandgap polymer (PTB7), composed of benzoditihophene (BDT) and thieno[3,4-b]thiophene (TT) as the D and A units, respectively, exhibits HOMO and LUMO energy levels of -5.15 and -3.31 eV, respectively. When the TT unit in PTB7 is replaced by a stronger electron accepting unit (TPD), the polymer (PBDTTPD) exhibits lower-lying HOMO and LUMO energy levels of -5.56

and -3.75 eV, respectively. Another polymer (PDTSTPD) composed of dithieno[3,2-b:2',3'-d]silole (DTS) as the D unit and TPD as the A unit also exhibits deep HOMO and LUMO energy levels of -5.57 and -3.88 eV, respectively. It should be mentioned here that TPD-based molecules exhibit deeper HOMO energy levels, which are beneficial for high V_{OC} without causing bandgap widening. In short, TPD moiety as an acceptor unit in a D–A type conjugated backbone effectively lowers their HOMO energy levels without the sacrifice of bandgap widening, leading to high V_{OC} without any loss of J_{SC}. This inspired us to design new TPD-based SMs to achieve high V_{OC} without significant sacrifice of J_{SC}. TPD-based SMs have rarely been reported, compared to corresponding polymer counterparts, probably because of limited synthetic procedures.[145–147] However, Leclerc and his co-workers reported a useful method to synthesize mono-brominated TPD unit with various alkyl chains, leading to facile synthetic route of TPD-based SMs for OSC application.[148–150]

In this work, we designed and synthesized two SMs with a D_1–A–D_2–A–D_1 structure, where D_2 is DTS as a center and donating unit, A is TPD as an accepting unit, and D_1 is end-capping bithiophene (2T) as π-conjugation extender. The chemical structures of two SMs differ only by the position of alkyl (hexyl) group substitution.

4.2 Experimental section

4.2.1 Synthesis

4.2.1.1 Small molecules composed of dithienosilole and thienopyroledione.

Thieno[3,4-c]furan-1,3-dione (11): 3,4-thiophenedicarboxylic acid (5.0 g, 29.0 mmol) was heated to 140 °C with acetic anhydride for 6 hours. The reaction was then cooled to room temperature and the solvent was removed under reduced pressure to yield a dark brown solid. The crude product was used for the next step without any purification.

5-hexyl-4H-thieno[3,4-c]pyrrole-4,6(5H)-dione (12): The brown solid (assuming 29.0 mmol) was dissolved in toluene (320 mL) then n-hexylamine (4.4 g, 43.5 mmol) was added and the mixture was refluxed for 24 h. The reaction mixture was cooled down to room temperature and the solvent was removed under reduced pressure. The crude solid was dissolved in thionyl chloride (100 mL) and the mixture was refluxed for 4 h. The reaction mixture was cooled to room temperature, and then slowly precipitated into water to yield off-white solid. (4.96 g, 72%) ^{1}H NMR (300 MHz, CDCl$_3$) δ (ppm): 7.81 (s, 2H), 3.61 (t, 2H), 1.85 (t, 2H), 1.31 (m, 6H), 0.88 (t, 3H).

5-methyl-4H-thieno[3,4-c]pyrrole-4,6(5H)-dione (13): The brown solid (assuming 29.0 mmol) was dissolved in toluene (320 mL) then methylamine (33 wt% solution in absolute ethanol) (5.4 ml, 43.5 mmol) was added and the
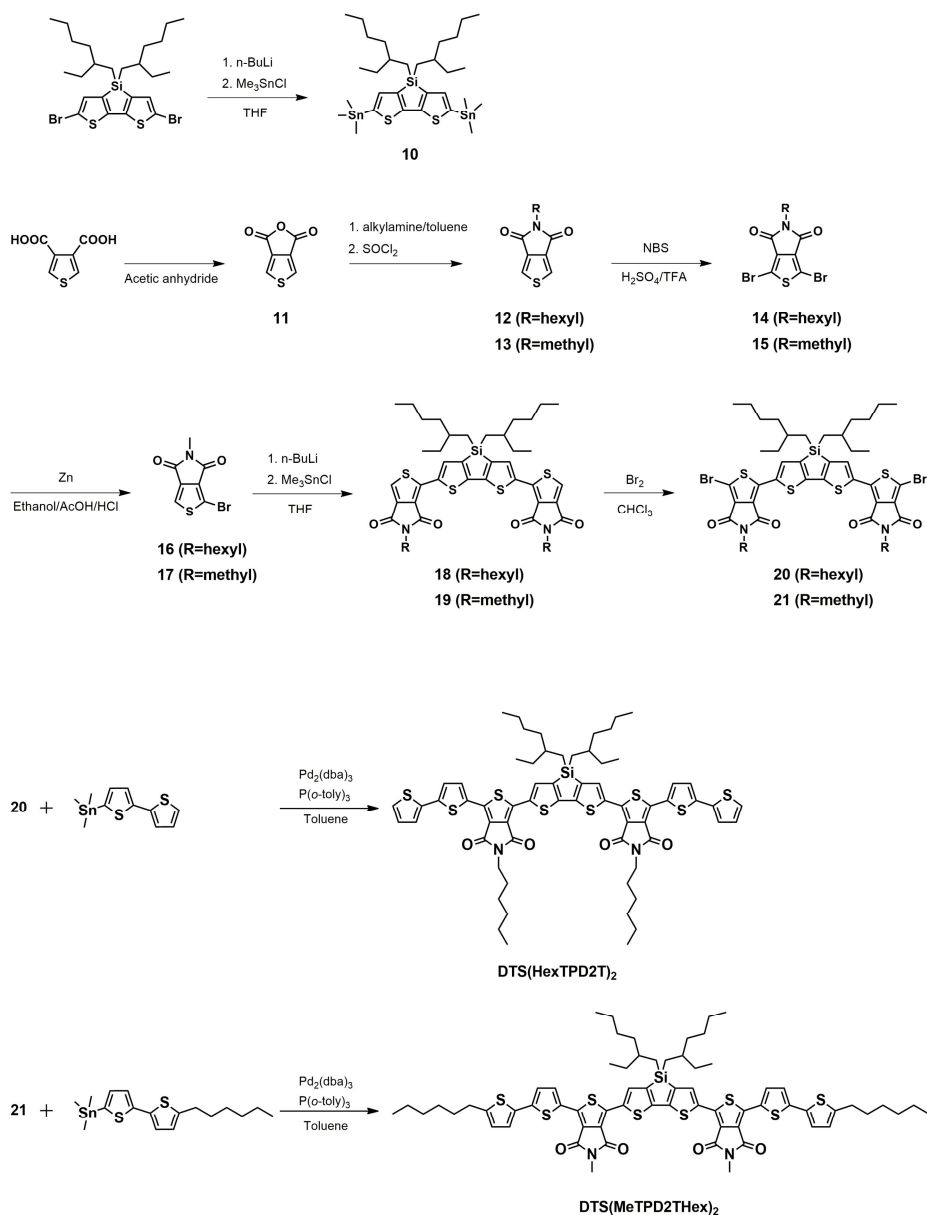
Scheme 4.1. Synthetic scheme of TPD-based small molecules.

mixture was refluxed for 24 h. The reaction mixture was cooled down to room temperature and the solvent was removed under reduced pressure. The crude solid was dissolved in thionyl chloride (100 mL) and the mixture was refluxed for 4 h. The reaction mixture was cooled to room temperature, and then slowly precipitated into water to yield off-white solid. (3.84 g, 79%) ^{1}H NMR (300 MHz, CDCl$_3$): δ (ppm) 7.81 (s, 2H), 3.12 (s, 3H).

1,3-dibromo-5-hexyl-4H-thieno[3,4-c]pyrrole-4,6(5H)-dione   (14): Compound **12** (3.0 g, 12.6 mmol) was dissolved in a mixture of sulfuric acid (15.0 mL) and trifluoroacetic acid (50.0 mL). While stirring, NBS (6.75 g, 37.9 mmol) was added in five portions to the solution and the reaction mixture was stirred at room temperature overnight. The brown-red solution was diluted with water (500 mL). The mixture was extracted with dichloromethane. The organic phase was dried over anhydrous magnesium sulfate and the solvent was evaporated under reduced pressure. The crude product was purified by column chromatography using dichloromethane/hexanes (1:1 ratio) to afford the title product as white needles (4.0 g, 81%). ^{1}H NMR (300 MHz, CDCl$_3$): δ (ppm) 3.95 (t, 2H), 1.60 (t, 2H), 1.29 (m, 6H), 0.88 (t, 3H).

1,3-dibromo-5-methyl-4H-thieno[3,4-c]pyrrole-4,6(5H)-dione   (15): Compound **13** (2.0 g, 11.9 mmol) was dissolved in a mixture of sulfuric acid (15.0 mL) and trifluoroacetic acid (50.0 mL). While stirring, NBS (6.38 g,

35.9 mmol) was added in five portions to the solution and the reaction mixture was stirred at room temperature overnight. The brown-red solution was diluted with water (500 mL). The mixture was extracted with dichloromethane. The organic phase was dried over anhydrous magnesium sulfate and the solvent was evaporated under reduced pressure. The crude product was purified by column chromatography using dichloromethane/ hexanes (2:1 ratio) to afford the title product as white needles (3.0 g, 77%). ^{1}H NMR (300 MHz, CDCl$_3$): δ (ppm) 3.12 (s, 3H).

1-bromo-5-hexyl-4H-thieno[3,4-c]pyrrole-4,6(5H)-dione   (16):
Compound **14** (1.5 g, 3.79 mmol) was placed in a 25 mL three-necked flask with a condenser. A solution of ethanol (40 mL), acetic acid (10 mL), and 3 drop of HCl was added and then heated until dissolution of the solid. Zinc powder (124 mg, 1.9 mmol) was then added, and the mixture was refluxed for 1 h. The mixture was then filtered through celite, and the solvent was evaporated under vacuum. The crude product was purified by column chromatography on silica gel to yield white solid. (0.56 g, 47%). ^{1}H NMR (300 MHz, CDCl$_3$): δ (ppm) 7.71 (s, 1H), 3.59 (t, 2H), 1.62 (t, 2H), 1.34 (m, 6H), 0.87 (t, 3H).

1-bromo-5-methyl-4H-thieno[3,4-c]pyrrole-4,6(5H)-dione   (17):
Compound **15** (1.5 g, 4.61 mmol) was placed in a 25 mL three-necked flask with a condenser. A solution of ethanol (40 mL), acetic acid (40 mL), and 3

drop of HCl was added and then heated until dissolution of the solid. Zinc powder (150 mg, 2.3 mmol) was then added, and the mixture was refluxed for 1 h. The mixture was then filtered through celite, and the solvent was evaporated under vacuum. The crude product was purified by column chromatography on silica gel to yield white solid. (0.56 g, 50%). ^{1}H NMR (300 MHz, CDCl$_3$):δ (ppm) 7.74 (s, 1H), 3.13 (s, 3H).

1,1'-(4,4-bis(2-ethylhexyl)-4H-silolo[3,2-b:4,5-b']dithiophene-2,6-diyl) bis(5-hexyl-4H-thieno[3,4-c]pyrrole-4,6(5H)-dione) (18): Compound **10** (650 mg, 0.87 mmol), 16 (580 mg, 1.8 mmol), tris(dibenzylideneacetone) dipalladium(0) (Pd$_2$(dba)$_3$) (31 mg, 0.03 mmol) in anhydrous toluene (10 mL) were placed in a flask and stirred at 110 °C for 24 h under N$_2$ atmosphere. The reaction mixture was poured into 200 mL of water and extracted with chloroform. Organic phase was collected and dried over MgSO$_4$. The crude product was purified by column chromatography to yield the compound **18** (626 mg, 81% yield): ^{1}H NMR (300 MHz, CDCl$_3$): δ (ppm) 8.01 (t, 2H), 7.59 (s, 2H), 3.65 (t, 4H), 1.65 (d, 4H), 1.44–1.01 (m, 34H), 0.90–0.84 (t, 6H), 0.77 (t, 12H).

1,1'-(4,4-bis(2-ethylhexyl)-4H-silolo[3,2-b:4,5-b']dithiophene-2,6-diyl) bis(5-methyl-4H-thieno[3,4-c]pyrrole-4,6(5H)-dione) (19): Compound **10** (650 mg, 0.87 mmol), 17 (517 mg, 1.8 mmol), tris(dibenzylideneacetone) dipalladium(0) (Pd$_2$(dba)$_3$) (31 mg, 0.03 mmol) in anhydrous toluene (10 mL)

were placed in a flask and stirred at 110 °C for 24 h under N_2 atmosphere. The reaction mixture was poured into 200 mL of water and extracted with chloroform. Organic phase was collected and dried over $MgSO_4$. The crude product was purified by column chromatography to yield the compound **19** (475 mg, 73% yield): ^{1}H NMR (300 MHz, $CDCl_3$): δ (ppm) 8.02 (t, 2H), 7.60 (s, 2H), 3.16 (s, 6H), 1.44–1.01 (m, 22H), 0.78 (t, 12H).

3,3'-(4,4-bis(2-ethylhexyl)-4H-silolo[3,2-b:4,5-b']dithiophene-2,6-diyl)bis(1-bromo-5-hexyl-4H-thieno[3,4-c]pyrrole-4,6(5H)-dione)   (20): After the compound **18** (550 mg, 0.53 mmol) was dissolved in chloroform (20 mL), bromine (0.06 ml, 1.15 mmol) was dropped into the solution. The reaction mixture stirred for 30 min and then poured into 200 mL of water and extracted with chloroform. Organic phase was collected and dried over $MgSO_4$. The crude product was purified by column chromatography to yield the compound **20**. (427 mg, 77% yield): ^{1}H NMR (300 MHz, $CDCl_3$): δ (ppm) 7.92 (t, 2H), 3.64 (t, 4H), 1.65 (d, 4H), 1.44–1.01 (m, 34H), 0.90–0.84 (t, 6H), 0.77 (t, 12H).

3,3'-(4,4-bis(2-ethylhexyl)-4H-silolo[3,2-b:4,5-b']dithiophene-2,6-diyl)bis(1-bromo-5-methyl-4H-thieno[3,4-c]pyrrole-4,6(5H)-dione)   (21): After the compound **19** (480 mg, 0.53 mmol) was dissolved in chloroform (20 mL), bromine (0.06 ml, 1.15 mmol) was dropped into the solution. The reaction mixture stirred for 30 min and then poured into 200 mL of water and

extracted with chloroform. Organic phase was collected and dried over MgSO$_4$. The crude product was purified by column chromatography to yield the compound **21**. (475 mg, 73% yield): ^{1}H NMR (300 MHz, CDCl$_3$): δ (ppm) 7.92 (t, 2H), 3.15 (s, 6H), 1.42–1.00 (m, 22H), 0.78 (t, 12H).

Synthesis of DTS(HexTPD2T)$_2$: Compound **20** (400 mg, 0.38 mmol), [2,2'-bithiophen]-5-yltrimethylstannane (314 mg, 0.95 mmol), and P(*o*-toly)$_3$ (9.3 mg, 0.03 mmol) and Pd$_2$(dba)$_3$ (14.0 mg, 0.02 mmol) in anhydrous toluene (10 mL) were placed in a flask and stirred at 110 °C for 24 h under N$_2$ atmosphere. The reaction mixture was poured into 200 ml of water and extracted with chloroform. Organic phase was collected and dried over MgSO$_4$. The crude product was purified by column chromatography and recrystallization with *n*-hexane to obtain the DTS(HexTPD2T)$_2$ (374 mg, 81% yield). ^{1}H NMR (300 MHz, CDCl$_3$): δ (ppm) 8.09 (t, 2H), 7.87 (d, 2H), 7.27 (d, 2H), 7.24 (d, 2H), 7.13 (d, 2H), 7.03 (q, 2H), 3.58 (t, 4H), 1.64 (m, 4H), 1.51 (m, 2H), 1.44–1.20 (m, 32H), 0.86 (m, 18H).

Synthesis of DTS(MeTPD2THex)$_2$: The same procedure as for DTS(HexTPD2T)$_2$ was performed. The compound **7** (200 mg, 0.220 mmol) was reacted with (5'-hexyl-[2,2'-bithiophen]-5-yl)trimethylstannane (200 mg, 0.485 mmol) in presence of Pd$_2$(dba)$_3$ (8.0 mg, 0.008 mmol) and tri(o-tolyl)phosphine (5.3 mg, 0.016 mmol) in toluene (10 mL), to afford the product DTS(MeTPD2THex)$_2$ (183 mg, 67% yield). ^{1}H NMR (300 MHz,

CDCl$_3$): δ (ppm) 8.07 (d, 2H), 7.91 (d, 2H), 7.08 (d, 4H), 6.71 (d, 2H), 3.14 (s, 6H), 2.81 (t, 4H), 1.70 (m, 4H), 1.44–1.20 (m, 34H), 0.88 (t, 6H), 0.83 (t, 12H).

4.3 Results and discussion

4.3.1 Synthesis

The compound **16** and **17** were synthesized by following the same procedure of Leclerc's group,[151] and then reacted with the compound **10** to afford the compounds **18** and **19** in 87 and 81% yield, respectively. The compounds **20** and **21** were prepared from the bromination of compounds **18** and **19** in chloroform and finally reacted with corresponding stannylated 2T to obtain the two SMs. The two SMs have good solubility in common solvents such as toluene, chlorobenzene, and chloroform. The products in each step were assigned by ^{1}H NMR.

4.3.2 Computational simulation.

When the density functional theory calculation at B3LYP/6-31G(d,p) basis set was performed to examine the electronic properties of the frontier orbital and optimized geometrical properties of the SMs, it reveals that the distributions of HOMO and LUMO energy levels of both SMs are similar, as shown in Figure 4.13. Both HOMO and LUMO wave functions delocalize over the
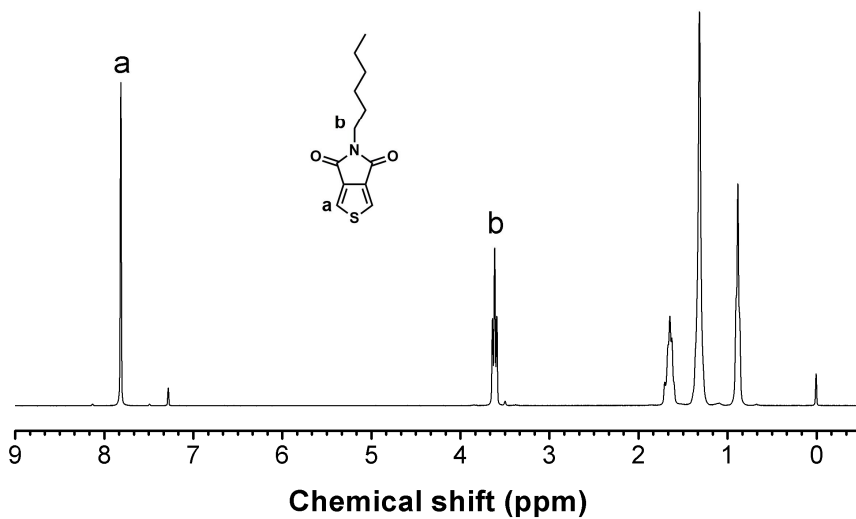
Figure 4.1. ^{1}H NMR spectrum of compound **12** in Scheme 4.1.
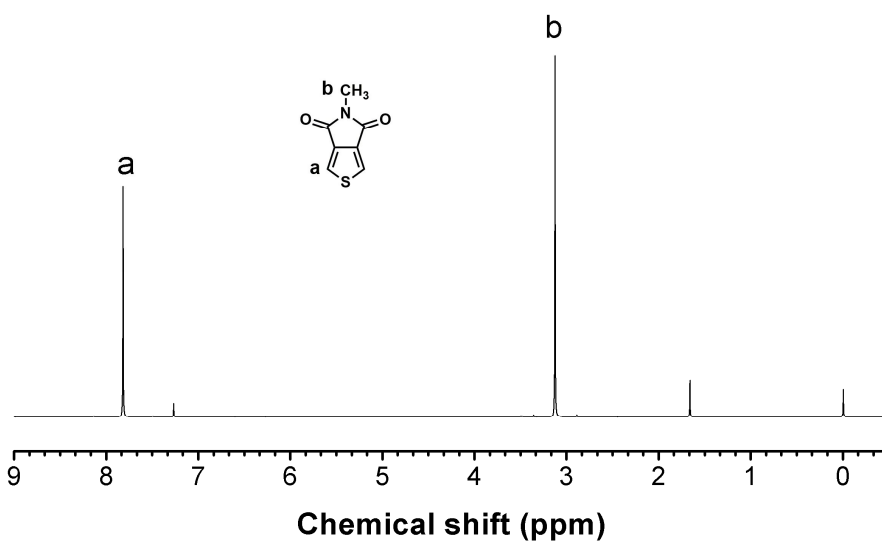
Figure 4.2. ^{1}H NMR spectrum of compound **13** in Scheme 4.1.
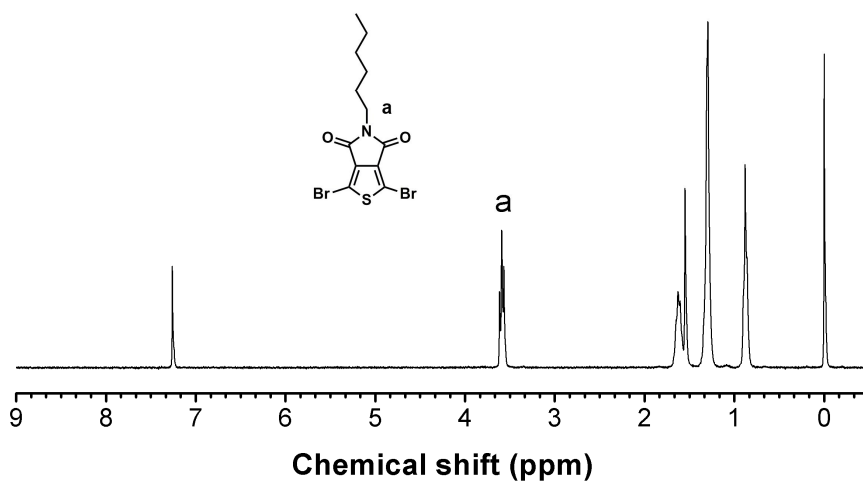
Figure 4.3. ^{1}H NMR spectrum of compound **14** in Scheme 4.1.
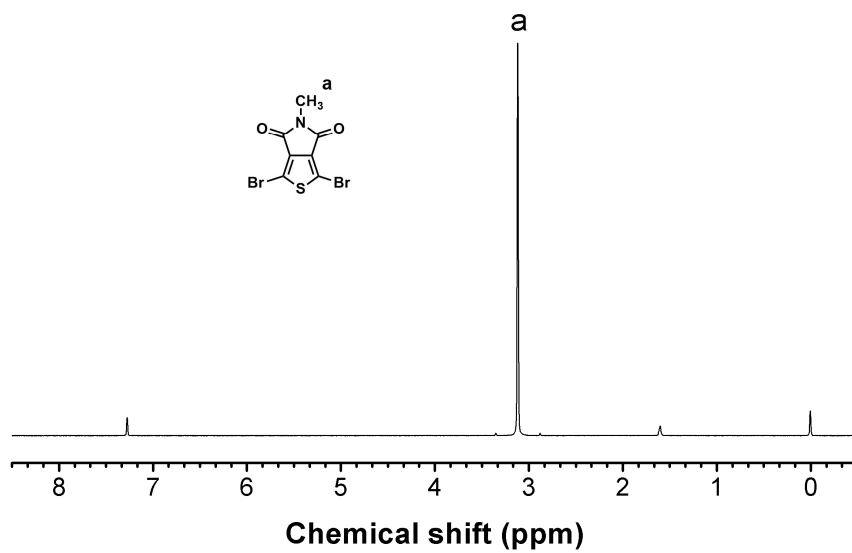
Figure 4.4. ^{1}H NMR spectrum of compound **15** in Scheme 4.1.

91
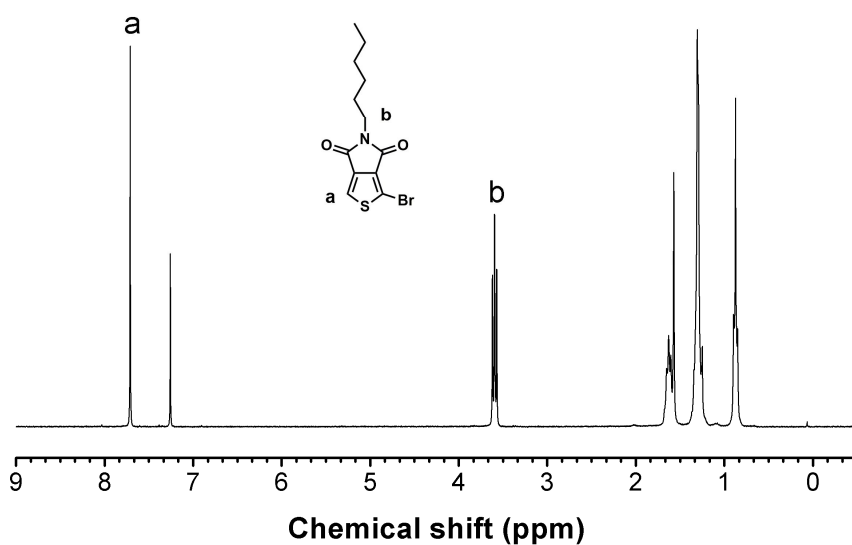
Figure 4.5. ^{1}H NMR spectrum of compound **16** in Scheme 4.1.
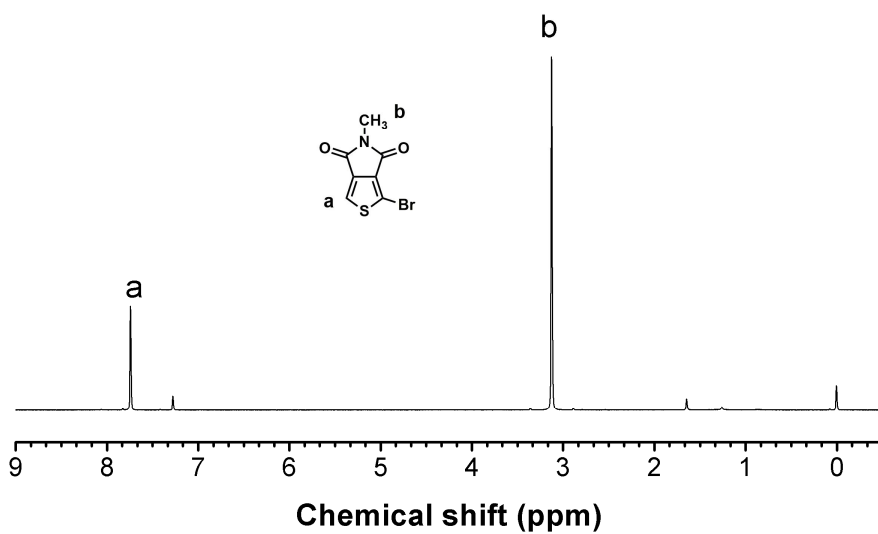
Figure 4.6. ^{1}H NMR spectrum of compound **17** in Scheme 4.1.

92
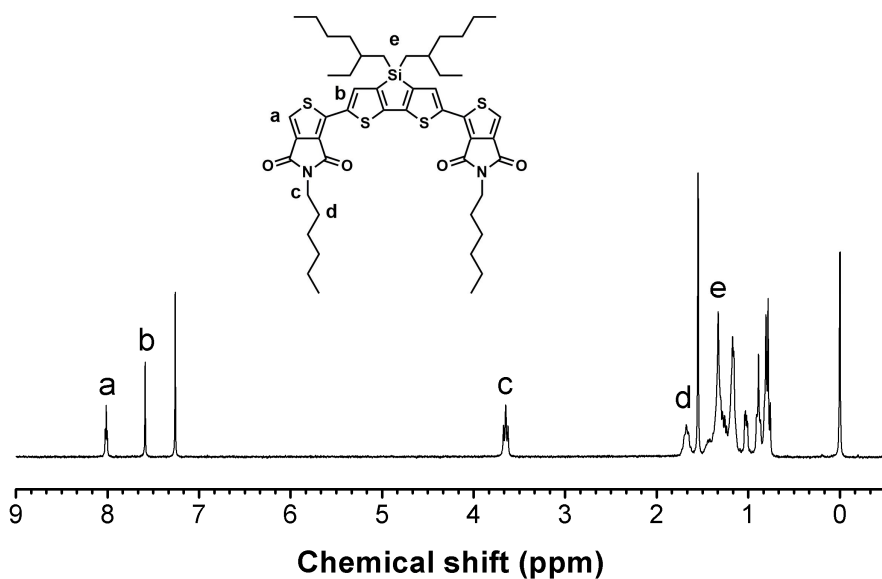
Figure 4.7. ^{1}H NMR spectrum of compound **18** in Scheme 4.1.
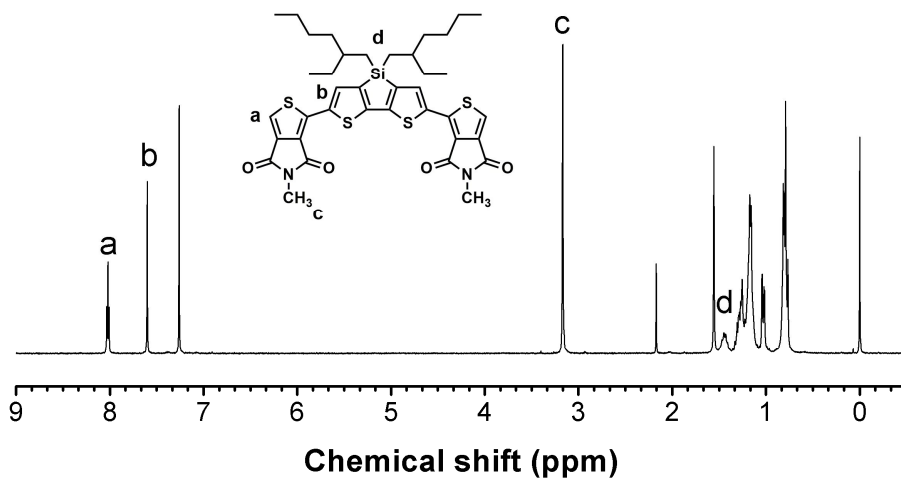
Figure 4.8. ^{1}H NMR spectrum of compound **19** in Scheme 4.1.
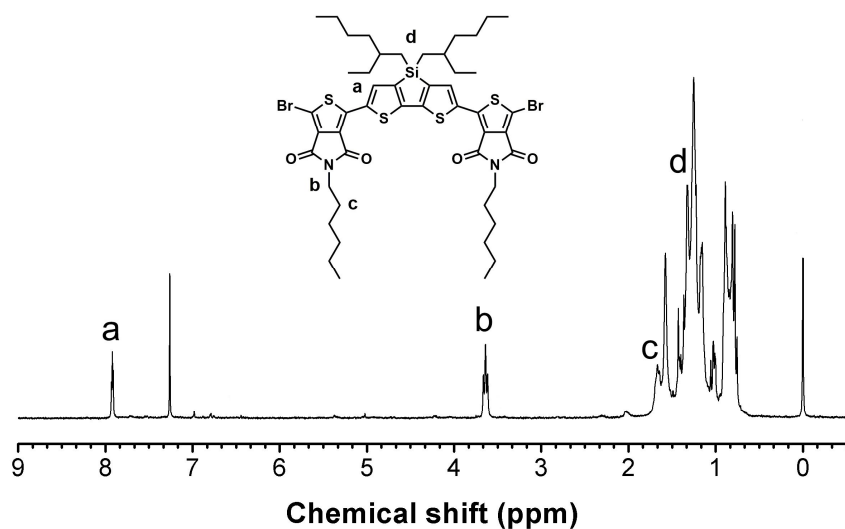
Figure 4.9. ^{1}H NMR spectrum of compound **20** in Scheme 4.1.
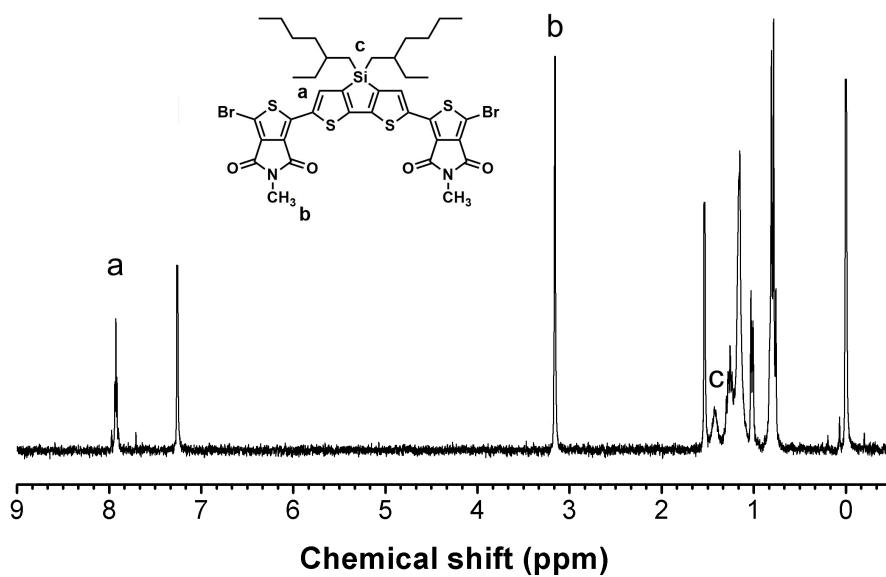
Figure 4.10. ^{1}H NMR spectrum of compound **21** in Scheme 4.1.

94
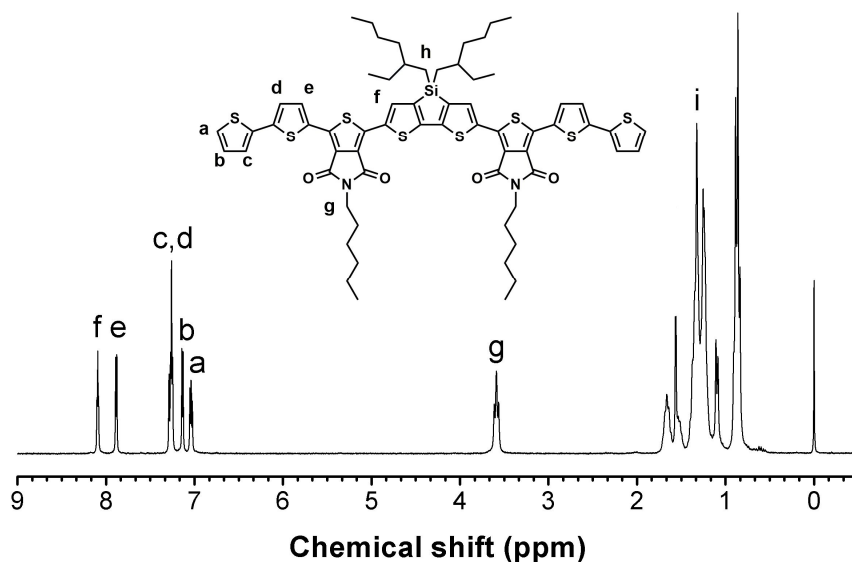
Figure 4.11. ^{1}H NMR spectrum of compound **DTS(HexTDP2T)₂** in Scheme 4.1.
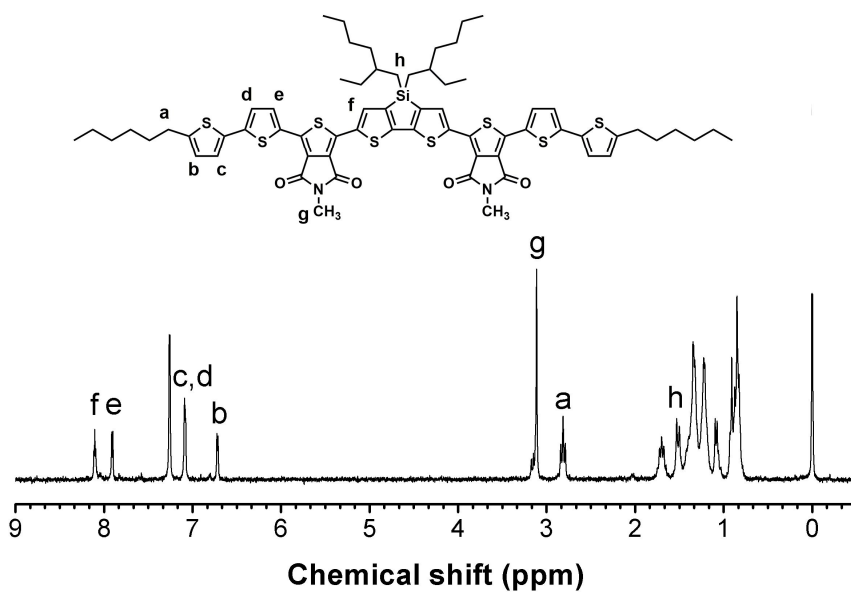
Figure 4.12. ^{1}H NMR spectrum of compound **DTS(MeTPD2THex)₂** in Scheme 4.1.
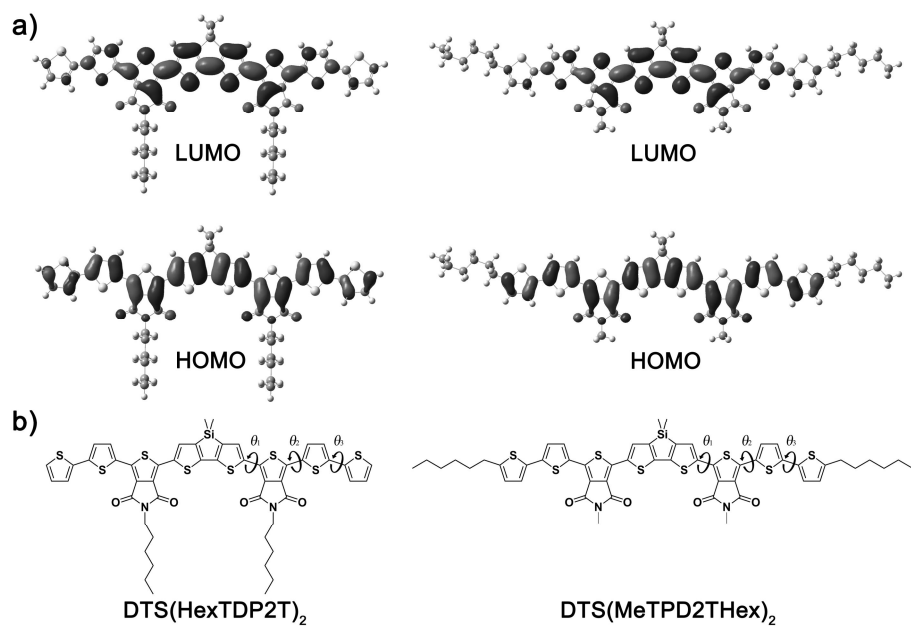
Figure 4.13. (a) HOMO and LUMO energy levels and (b) dihedral angles of small molecules calculated using DFT with a basis set of B3LYP/6-31G(d,p).

Table 4.1 Calculated HOMO and LUMO levels and dihedral angles of TPD-based small molecules.

SMs	HOMO (eV)	LUMO (eV)	θ_1 [Deg]	θ_2 [Deg]	θ_3 [Deg]
DTS(HexTPD2T)$_2$	−5.0	−2.6	0.6	0.9	13.2
DTS(MeTPD2THex)$_2$	−4.9	−2.6	0.2	0.1	10.0

entire π-conjugated backbone, indicating that strong intramolecular interaction takes place. When the dihedral angles between DTS, TPD, and T units as defined by θ_1, θ_2, and θ_3 in Table 4.1 are calculated, it reveals that the angles are very small, which is beneficial for chain ordering/packing in the film state.

4.3.3 Optical and electrochemical properties

The UV–vis absorption spectra of two SMs in CF solution and film state are represented in Figure 4.14 and the optical properties are summarized in Table 4.2. The molar extinction coefficients of two SMs at the λ_{max} of 530 nm are nearly equal (ca. 5.5×10^4 M^{-1} cm^{-1}) in solution, while the molar absorptivity of DTS(HexTPD2T)$_2$ is slightly higher than that of DTS(MeTPD2THex)$_2$ in solid film. The λ_{max} and the λ_{onset} of two SMs in film state are redshifted by ca. 35 and 60 nm, respectively, as compared to those in solution state. The E_g^{opt} of DTS (HexTPD2T)$_2$ and DTS(MeTPD2THex)$_2$, as estimated from the corresponding λ_{onset}, are 1.86 and 1.85 eV, respectively. Particularly, two SMs show a strong vibronic shoulder in both solution and the solid film state, indicating that the two SMs are aggregated in both states.

   The HOMO energy levels of two SMs are the same (−5.50 eV), while the LUMO energy level of DTS(HexTPD2T)$_2$ is slightly higher than that of DTS(MeTPD2THex)$_2$ (Figure 4.15) Particularly, the TPD unit lowers both the HOMO and LUMO energy level in D–A type conjugated SMs, leading to enhancement of V_{OC}. It is also noted here that the low-lying LUMO energy
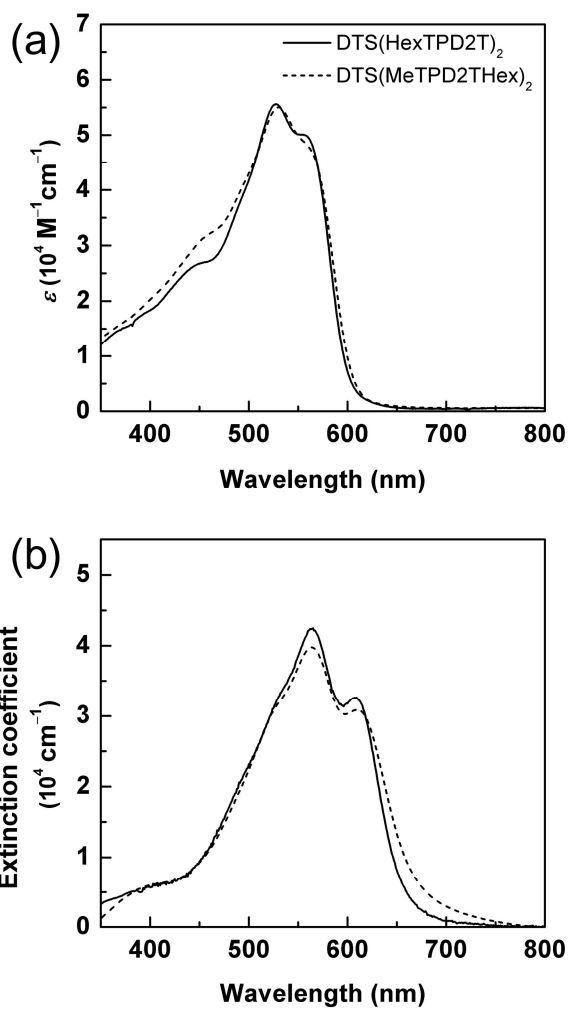
Figure 4.14. UV−vis absorption spectra of TPD-based SMs in (a) CHCl₃ solution and (b) film state.
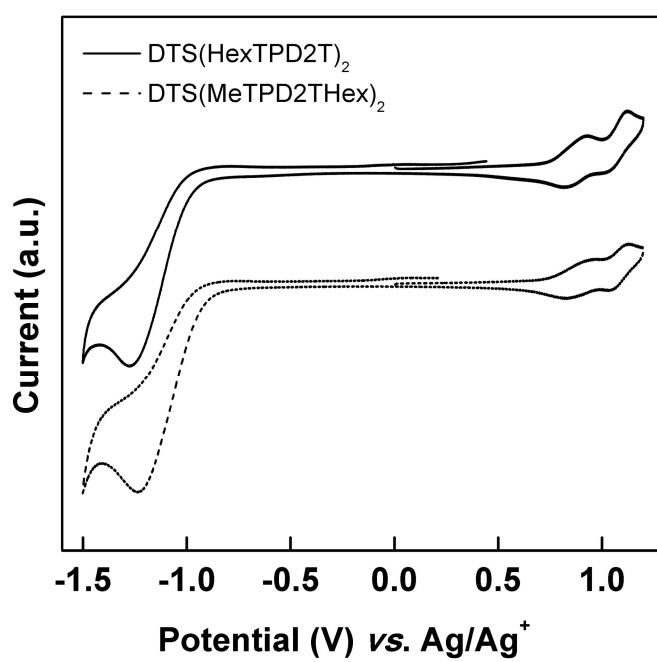
Figure 4.15. Cyclic voltammograms of TPD-based SMs.

Table 4.2 Optical and electrochemical properties of TPD-based small molecules.

Small molecules	UV–vis absorption		E_g^{opt} (eV)[a]	HOMO (eV)	LUMO (eV)	E_g^{el} (eV)[b]
	λ_{max} (solution) (nm)	λ_{max} (film) (nm)				
DTS(HexTPD2T)$_2$	528	564	1.86	−5.50	−3.78	1.72
DTS(MeTPD2THex)$_2$	530	565	1.85	−5.50	−3.83	1.67

[a] Determined from the onset of UV–vis absorption spectra.

[b] Determined from the cyclic voltammetry.

levels of the SMs are still sufficiently higher than the LUMO energy level of $PC_{71}BM$ for efficient exciton dissociation.

4.3.4 Photovoltaic properties

Photovoltaic performances of TPD-based SMs were measured with the conventional device structure, as shown in Figure 4.16, and the data are summarized in Table 4.3. The $PC_{71}BM$ was used as an acceptor, because its absorptivity is higher than that of $PC_{61}BM$. The devices were optimized by varying processing conditions, such as the blend ratio and addition of solvent additives. The PCEs of DTS(HexTPD2T)$_2$ are always higher than that of DTS(MeTPD2THex)$_2$, regardless of the solvent, when the same solvent and additive are used. After the device optimization, the DTS(HexTPD2T)$_2$-based cell shows a promising PCE of 6.0% with V_{OC} = 0.94 V, J_{SC} = 11.8 mA cm^{-2}, and a FF of 0.54, while DTS(MeTPD2THex)$_2$ exhibits a moderate PCE of 3.1% with V_{OC} = 0.93 V, J_{SC} = 6.4 mA cm^{-2}, and FF = 0.52. It should be noted that all devices from two SMs exhibit high V_{OC} values of 0.93–0.94 V, which are originated from low-lying HOMO energy levels of the two SMs. The higher PCE of DTS(HexTPD2T)$_2$ arises primarily from higher J_{SC}, as confirmed by EQE spectra (Figure 4.16), where the DTS(HexTPD2T)$_2$-based device exhibits a stronger photoresponse in the range of 300–700 nm, which contributes to higher J_{SC} values in OSCs. The J_{SC} values calculated from integration of EQE curves of DTS(HexTPD2T)$_2$ and DTS(MeTPD2THex)$_2$ are 11.3 and 6.3 mA cm^{-2}, respectively, which are consistent with the values
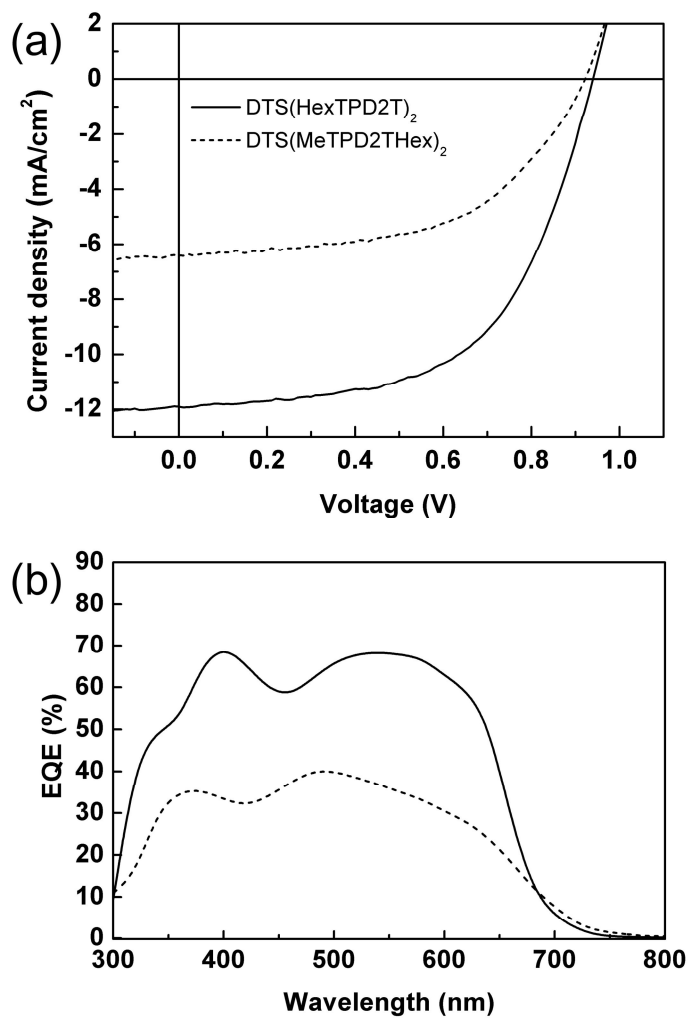
Figure 4.16. (a) *J–V* curves and (b) EQE spectra of SMs/PC$_{71}$BM solar cells.

Table 4.3. Photovoltaic properties of OSCs processed with 0.5 vol% DIO under standard AM 1.5G illumination.

Small molecules	SM: PC$_{71}$BM (w/w)	μ_h (cm^2 V^{-1} s^{-1})	V_{OC} (V)	J_{SC} (mA cm^{-2})	FF (%)	PCE (%)
DTS(HexTPD2T)$_2$[a]	1.5:1	9.26×10^{-4}	0.94	11.8	0.54	6.0
DTS(MeTPD2THex)$_2$[b]	1.5:1	7.04×10^{-4}	0.93	6.4	0.52	3.1

[a] Processed in chloroform (CF) solution

[b] Processed in chlorobenzene (CB) solution.

determined from the *J–V* curve.

4.3.5 Molecular orientation

While the optical and electrochemical properties of two SMs are nearly the same, regardless of the positon of alkyl chain substitution, photovoltaic properties of two SMs are largely different. To identify the reason for this large difference of photovoltaic properties, we compare the crystalline nature and molecular orientation of two SMs in film state. The grazing incidence X-ray diffraction (GIXD) patterns of both DTS(HexTPD2T)$_2$ and DTS(MeTPD2THex)$_2$ show characteristic diffraction peaks (100), (200), (300), and (400) in the q_z-direction and (010) in the q_{xy}-direction, indicating that the SMs exhibit crystalline nature (Figure. 4.17a and b). However, it should be noted that DTS(HexTPD2T)$_2$ molecules in the blend clearly exhibit a (010) peak at q = 1.78 Å^{-1} along the q_z-direction while the DTS(MeTPD2THex)$_2$ blend does not show a discernible peak at q = 1.78 Å^{-1}, as shown in Figures 4.17c and d, indicating that DTS (HexTPD2T)$_2$ molecules take partially face-on orientation while DTS(MeTPD2THex)^2 molecules do not clearly show face-on orientation. The out-of plane and in-plane scans also reveal that DTS(HexTPD2T)$_2$ in the blend shows a (010) peak at q = 1.78 Å^{-1} along the q_z- and q_{xy}-directions, as shown in Figures 4.17e and f, indicative of the existence of face-on orientation, which is advantageous for charge carrier transport in OSCs. It is interesting to observe that DTS(HexTPD2T)$_2$ has an interchain distance of 17.9 Å in the blend film,
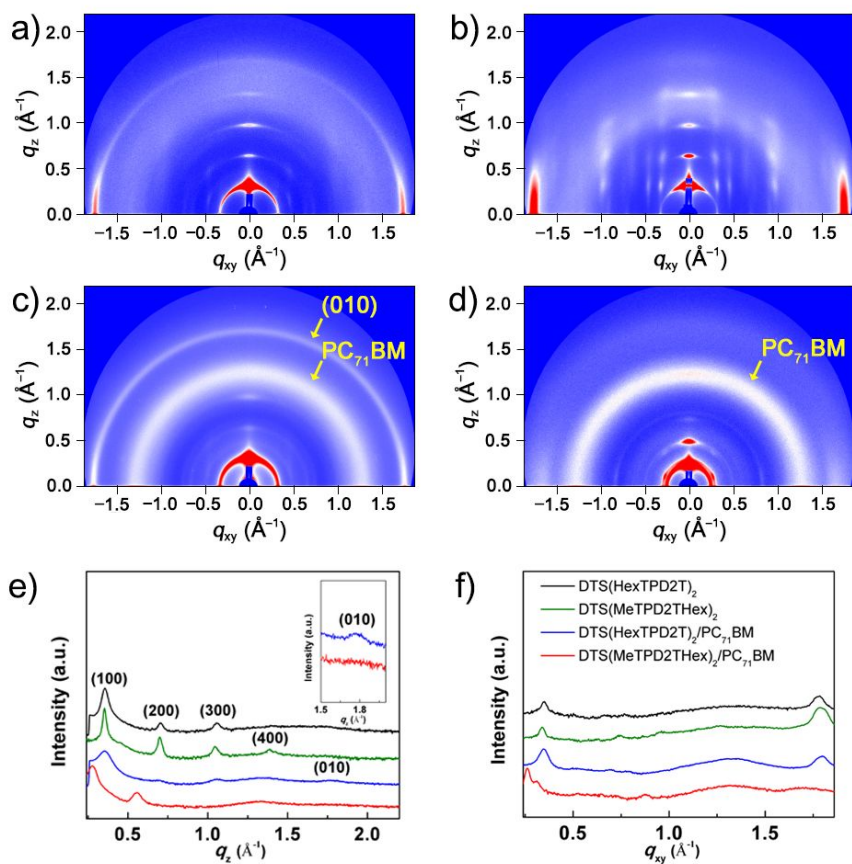
Figure 4.17. Two-dimensional grazing-incidence X-ray diffraction (2D–GIXD) images of (a) pristine DTS(HexTPD2T)$_2$, (b) pristine DTS(MeTPD2THex)$_2$, (c) DTS(HexTPD2T)$_2$:PC$_{71}$BM (1.5:1 w/w) and (d) DTS(MeTPD2THex)$_2$:PC$_{71}$BM (1.5:1 w/w) blends. Panels (e) and (f) show out-of-plane and in-plane scans of pristine and blends, respectively.

while DTS(MeTPD2THex)$_2$ shows an interchain distance of 23.3 Å, indicating that the number of DTS(HexTPD2T)$_2$ molecules per unit volume is larger than that of DTS(MeTPD2THex)$_2$, assuming that the two molecules have the same unit lengths along the (010) and (001) directions. In other words, the number of light-harvesting molecules of DTS(HexTPD2T)$_2$ per unit volume is larger than that of DTS(MeTPD2THex)$_2$. It is noteworthy to mention here that the interchain distance of DTS(HexTPD2T)$_2$ does not change, whereas that of DTS(MeTPD2THex)$_2$ increases from 17.9 Å to 23.3 Å when they are blended with PC$_{71}$BM. Although we do not provide an exact reason for that, it is speculative that PCBM is more miscible with DTS(MeTPD2THex)$_2$ than with DTS(HexTPD2T)$_2$, so that some of the PCBM molecules are intercalated between DTS(MeTPD2THex)$_2$ molecules, which may increase the interchain distance. Considering that the PCE difference between the two SMs arises mainly from the J_{SC} difference, it is concluded that the more-preferential face-on orientation and larger number of light-harvesting molecules of DTS(HexTPD2T)$_2$ crystal per unit volume, compared to those of DTS(MeTPD2THex)$_2$, contribute to the larger J_{SC} values.

4.3.6 Charge carrier mobility and photoluminescence

When the hole mobilities of two SMs are measured by the SCLC method under the identical condition for optimized photovoltaic cell (Figure 4.18) and are compared, the hole mobility of DTS(HexTPD2T)$_2$ (9.26×10^{-4} cm^2 V^{-1}
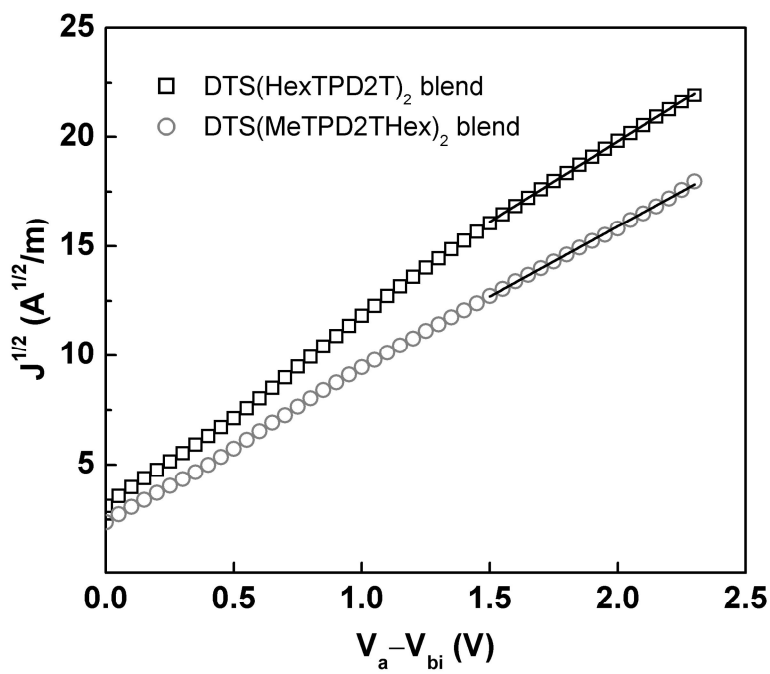
Figure 4.18. Dark *J–V* characteristics of TPD-based SMs/PC$_{71}$BM blends with hole-only device, where the solid lines represent the best linear fit of the data points.
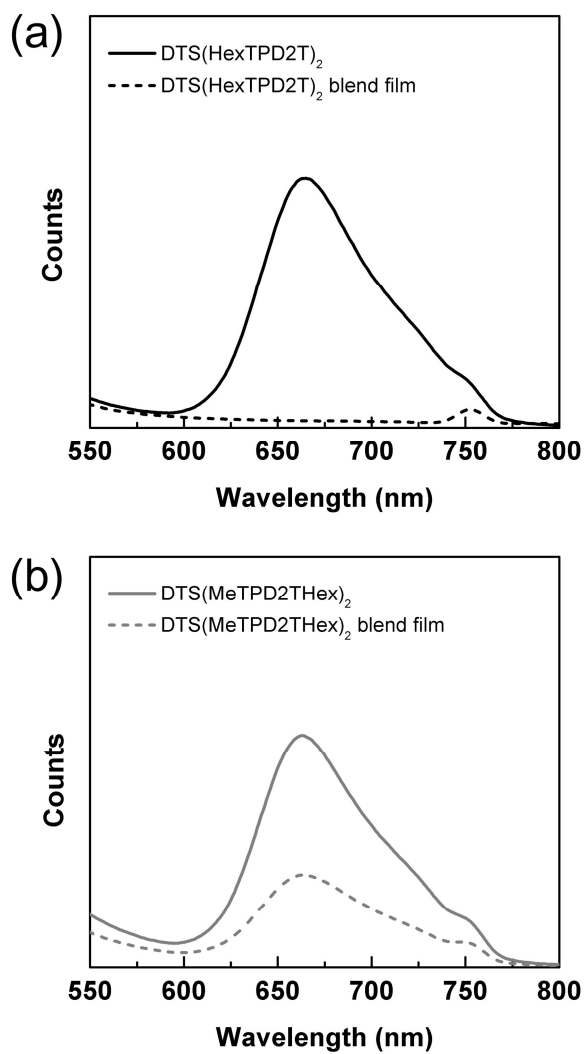
Figure 4.19. Photoluminescence spectra (excitation wavelength: 500 nm) measured from SMs and blend films of (a) DTS(HexTPD2T)$_2$ and (b) DTS (MeTPD2THex)$_2$..

s^{-1}) is higher than that of DTS-(MeTPD2THex)$_2$ (7.04×10^{-4} cm^2 V^{-1} s^{-1}). More preferential face-on orientation of DTS(HexTPD2T)$_2$ in the blend as compared to DTS(MeTPD2THex)$_2$ in the blend facilitates effective charge carrier transport, leading to a higher hole mobility in SCLC and, thus, higher J_{SC} values in OSCs.

To further investigate the J_{SC} difference between two SMs, we examined the photoluminescence (PL) quenching of blend film (Figure 4.19). The PL of DTS(HexTPD2T)$_2$ in the blend is almost completely quenched while that of DTS(MeTPD2THex)$_2$ is quenched by 67%, indicating that the charge dissociation of excitons in DTS(HexTPD2T)$_2$ occurs more efficiently than that of DTS(MeTPD2THex)$_2$, which also contributes to higher J_{SC} values of DTS(HexTPD2T)$_2$.

4.3.7 Morphologies of active layers

The J_{SC} values of OSCs are also dependent on the morphology of blend film. When TEM images of two SMs blended with PC$_{71}$BM were compared, as shown in Figure 4.20, the DTS(HexTPD2T)$_2$ blend reveals distinctly nanophase separated network while the DTS(MeTPD2THex)$_2$ blend does show blurred phase, indicating that the morphology of DTS(HexTPD2T)$_2$ blend is more beneficial for charge transport than that of DTS(MeTPD2THex)$_2$. The above results of GIXD, the SCLC hole mobility, and TEM lead us to conclude that DTS(HexTPD2T)$_2$ exhibits better photovoltaic performance than DTS(MeTPD2THex)$_2$.
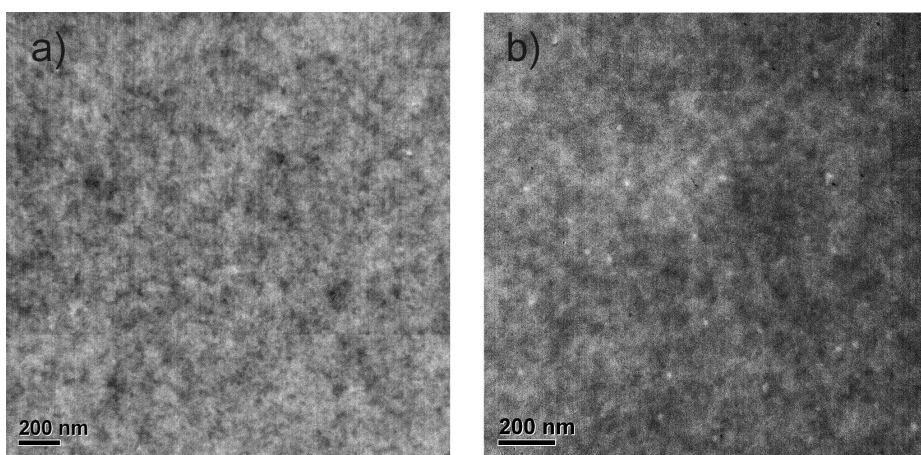
Figure 4.20. TEM images of (a) DTS(HexTPD2T)$_2$:PC$_{71}$BM (1.5:1 w/w) and (b) DTS(MeTPD2THex)$_2$:PC$_{71}$BM (1.5:1 w/w) blend films. The scale bar denotes 200 nm.

4.4 Summary

Two SMs based on TPD unit with the same alkyl length but different substitution position are synthesized, and the effect of alkyl substitution position on their optical, electrochemical, and photovoltaic properties are examined. Since TPD, as an electron-accepting unit, lowers both HOMO and LUMO energy levels of D−A type conjugated polymers, we have introduced TPD unit into conjugated SMs for achieving high V_{OC} of OSCs without any significant loss of J_{SC}. As expected, two SMs exhibited low-lying HOMO (−5.50 eV) and LUMO (−3.83 eV) energy level, and thereby high V_{OC} of 0.93–0.94 V in OSCs. Although the optical and electrochemical properties of the two SMs are almost the same, regardless of alkyl substitution position, photovoltaic performances of two SM:PC$_{71}$BM-based OSC devices are largely different. The DTS(HexTPD2T)$_2$-based OSC device exhibited a promising PCE of 6.0% with V_{OC} = 0.94 V, J_{SC} = 11.8 mA cm^{-2}, and FF = 0.54, while the DTS(MeTPD2THex)$_2$-based one showed a moderate PCE of 3.1% with V_{OC} = 0.93 V, J_{SC} = 6.4 mA cm^{-2}, and FF = 0.52. The larger J_{SC} value of DTS(HexTPD2T)$_2$ is mainly attributed to the face-on orientation of crystallites, high SCLC hole mobility and nanoscale phase separation observed in the blend.

Chapter 5. Conclusions

In this study, we designed and synthesized DPP- and TPD-based SMs to enhance the photovoltaic parameter of V_{OC} and J_{SC} for high performance OSCs, and investigated their photovoltaic performance in terms of molecular structure and energy levels.

Fundamentally, trade-off relationship exists between V_{OC} and J_{SC} in OSCs. In donor-acceptor type conjugated materials, low-lying HOMO energy levels are highly required for high V_{OC} in OSCs. However, considering that the LUMO energy level of $PC_{61}BM$ is -4.2 eV, the LUMO energy level of donor molecules should be higher than -3.9 eV, which leads to trade-off relationship between V_{OC} and J_{SC}. In short, lowering the HOMO energy level results in the optical bandgap widening. To overcome the relationship, we designed the small molecules including low-lying HOMO level and molecular planarity. Generally, close ordering/packing of conjugated materials leads to efficient charge carrier transport. First, the HOMO energy level are finely tuned by introducing donor units with different electron donating power such as thiophene and phenylene ring in A–D–A type small molecules, where DPP moiety are used as acceptor building block. As a result, SM with week electron donating unit, $Ph(TDPP)_2$, affords high V_{OC} of 0.94 eV. And further, naphthalene, weak and fused donor unit, are used as donor unit in the identical A–D–A type SM ($NPT(TDPP)_2$), which leads to higher J_{SC} value than that of $Ph(TDPP)_2$ and thus improved PCE of 4.4%. As a consequence, both of deep

HOMO energy level derived from weak electron donating units and high charge mobility resulted from molecular planarity are contributed to enhanced photovoltaic properties.

Furthermore, we have found that the TPD units as an acceptor unit in D–A conjugated backbone effectively lower the HOMO energy level without the sacrifice of bandgap widening and S–O interaction involving imide C=O groups of TPD and adjacent thienyl S atoms can serve as conformational locks to preserve molecular planarity. When the TPD is incorporated in D1–A–D2–A–D1 type conjugated SMs, low-lying HOMO level and high V_{OC} of 0.94 eV are demonstrated. Among the TPD-based SMs, DTS(HexTPD2T)$_2$ with n-hexyl group substituted at TPD units exhibits high J_{SC} of 11.8 cm^2 V^{-1} s^{-1} in OCS$_S$.

When design the small molecule for OSCs, we focused on the small molecules with deep HOMO energy levels and their planarity to overcome the trade-off relationship between V_{OC} and J_{SC}. It is evident that frontier orbital energy level and crystallinity are important for device performance. In particular, selection of donor or acceptor building block determines optical, electrochemical property and crystalline nature. In addition, the position of side substituents also influences solubility and molecular orientation in blend film. From these results, we can further consider the concept of quinoid structure or S-F interaction, which afford the molecular planarity. While much research has concentrated on the polymer solar cells, clear understand of structure-property relationship from small molecular solar cell provide the guideline for high performance OSCs

Bibliography

(1)   Turner, J. A. *Science* **1999**, *285*, 687.

(2)   Chow, J.; Kopp, R. J.; Portney, P. R. *Science* **2003**, *302*, 1528.

(3)   Smalley, R. E. *MRS Bull.* **2005**, *30*, 412.

(4)   Chu, S.; MaJumdar, A. *Nature* **2012**, *488*, 294.

(5)   Green, M. A. *Sol. Energy* **2004**, *76*, 3.

(6)   Bauhuis, G. J.; Mulder, P.; Haverkamp, E. J.; Huijben, J. C. C. M.;
        Schermer, J. J.; *Sol. Energy Mater. Sol. Cells* **2009**, *93*, 1488.

(7)   Contreras, M. Am; Egaas, B.; Ramanathan, K.; Hiltner, J.;
        Swartzlander, A.; Hasson, F.; Noufi, R. *Prog. Photovoltaics* **1999**, *7*,
        311.

(8)   Romeo, A.; Terheggen, A.; Abou-Ras, D.; Bätzner, D. L., Haug, F.-
        J.; Kälin, M.; Rudmann, D.; Tiwari, A. N. *Prog. Photovoltaics* **2004**,
        12, 93

(9)   Hoppe, H.; Sariciftci, N. S.; Meissner, D. *Mol. Cryst. Liq. Cryst.*
        2002, *385*, 113.

(10)   Roncali, J. *Chem. Rev.* **1997**, *97*, 173.

(11)   Dimitrakopoulos, C. D.; Malenfant, P. R. L. *Adv. Mater.* **2002**, *14*,
        99.

(12)   Singh, B.; Sariciftci, N. S. *Ann. Rev. Mater. Res.* **2006**, *36*, 199.

(13)   Lane, P. A.; Rostalski, J.; Giebeler, C.; Martin, S. I.; Bradley, D. D. C.; Meissner, D. *Sol. Energy Mater. Sol. Cells* **2000**, *63*, 3.

(14)   Günes, S.; Neugebauer, H.; Sariciftci, N. S. *Chem. Rev.* **2007**, *107*, 1324.

(15)   Thompson, B. C.; Fréchet, M. J. *Angew. Chem., Int. Ed.* **2008**, *47*, 58.

(16)   Helgesen, M.; Sondergaard, R.; Krebs, F. C. *J. Mater. Chem.* **2010**, *20*, 36.

(17)   Krebs, F. C.; Fyenbo, J.; Jorgensen, M. *J. Mater. Chem.* **2010**, *20*, 8994.

(18)   Brabec, C. J.; Gowrisanker, S.; Halls, J. J. M.; Laird, D.; Jia, S. J.; Williams, S. P. *Adv. Mater.* **2010**, *22*, 3839.

(19)   Dennler, G.; Scharber, M. C.; Bracbec, C. J. *Adv. Mater.* **2009**, *21*, 1323.

(20)   Tang, C. W. *Appl. Phys. Lett.* **1986**, *48*, 183.

(21)   Sariciftci, N. S.; Smilowitz, L.; Heeger, A. J.; Wudl, F. *Science* **1992**, *258*, 1474.

(22)   Kraabel, B.; Lee, C. H.; McBranch, D.; Moses, D.; Sariciftci, N. S.; Heeger, A. J. *Chem. Phys. Lett.* **1993**, *213*, 389.

(23)   Halls, J. J. M.; Walsh, C. A.; Greenham, N. C.; Marseglia, E. A.; Friend, R. H.; Moratti, S. C.; Holmes, A. B. *Nature* **1995**, *376*, 498.

(24)   Yu, G.; Gao, J.; Hummelen, J. C.; Wudl, F.; Heeger, A. J. *Science* **1995**, *270*, 1789.

(25)   Vohra, V.; Kawashima, K.; Kakara, T.; Koganezawa, T.; Osaka, I.; Takimiya, K.; Murata, H. *Nature Photon.* **2015**, *9*, 403.

(26)   Kan, B.; Li, M.; Zhang, Q.; Liu, F.; Wan, X.; Wang, Y.; Ni, W.; Long, G.; Yang, X.; Feng, H.; Zuo, Y.; Zhang, M.; Huang, F.; Cao, Y.; Russell, T. P.; Chen, Y. *J. Am. Chem. Soc.* **2015**, *137*, 3886.

(27)   Brabec, C. J.; Shaheen, S. E.; Winder, C.; Sariiftci, N. S.; Denk, P. *Appl. Phys. Lett.* **2002**, *80*, 1288.

(28)   Kim, J. Y.; Kim, S. H.; Lee, H.-H.; Lee, K.; Ma, W.; Gong, X.; Heeger, A. J.; *Adv. Mater.* **2006**, *18*, 572.

(29)   Ma, H.; Yip, H.-L.; Huang, F.; Jen, A. K.-Y. *Adv. Funct. Mater.* **2010**, *20*, 1371.

(30)   Oh, S.-H.; Na, S.-I.; Jo, J.; Lim, B.; Vak, D.; Kim, D.-Y. *Adv. Funct. Mater.* **2010**, *20*, 1977.

(31)   He, Z.; Zhong, C.; Huang, X.; Wong, W.-Y.; Wu, H.; Chen, L.; Su, S.; Cao, Y. *Adv. Mater.* **2011**, *23*, 4636.

(32)   Peumans, P.; Yakimov, A.; Forrest, S. R. *J. Appl. Phys.* **2003**, *93*, 3693.

(33)   Brabec, C. J.; Cravino, A.; Meissner, D.; Sariciftci, N. S.; Fromherz, T.; Rispens, M. T.; Sanchez, L.; Hummelen, J. C. *Adv. Funct. Mater.* **2001**, *11*, 374.

(34)   Lenes, M.; Wetzelaer, G. A. H.; Kooistra, F. B.; Veenstra, S. C.; Hummelen, J. C.; Blom, P. W. M *Adv. Mater.* **2008**, *20*, 2116.

(35)   Kooistra, F. B.; Knol, J.; Kastenberg, F.; Popescu, L. M.; Verhees, W. J. H.; Kroon, J. M.; Hummelen, J. C. *Org. Lett.* **2007**, *9*, 551

(36)   Dennler, G.; Schaber, M. C.; Brabec, C. J. *Adv. Mater.* **2009**, *21*, 1323.

(37)   Rostalski, J.; Meissner, D. *Sol. Energy Mater. Sol. Cells* **2000**, *61*, 87.

(38)   Wienk, M. M.; Kroon, J. M.; Verhees, W. J. H.; Knol, J.; Hummelen, J. C.; van Hal, P. A.; Janssen, R. A. J. *Angew. Chem., Int. Ed.* **2003**, *42*, 3371

(39)   Sirringhaus, H.; Brown, P. J.; Friend, R. H.; Nielsen, M. M.; Bechgaard, K.; Langeveld-Voss, B. M. W.; Spiering, A. J. H.; Janssen, R. A. J.; Meijer, E. W.; Herwig P.; de Leeuw, D. M. *Nature* **1999**, *401*, 685.

(40)   Bao, Z.; Dodabalapur A.; Lovinger, A. J. *Appl. Phys. Lett.* **1995**, *69*, 4108.

(41)   Hoffert, M. I.; Caldeira, K.; Benford, G.; Criswell, D. R.; Green, C.; Herzog, H.; Jain, A. K.; Kheshgi, H. S.; Lackner, K. S.; Lewis, J. S.; Lightfoot, H. D.; Manheimer, W.; Mankins, J. C.; Mauel, M. E.; Perkins, L. J.; Schlesinger, M. E.; Volk T.; Wigley, T. M. L. *Science* **2002**, *298*, 981.

(42)   Sirringhaus, H.; Tessler N.; Friend, R. H. *Science* **1998**, *280*, 1741.

(43)   Kim, Y.; Choulis, S.A.; Nelson, J; Bradley, D.D.C. *Appl. Phys. Lett.* **2005**, *86*, 063502.

(44)   Yang, X.; Loos, J.; Veenstra, S.C.; Verhees, W.J.H.; Wien, M.M.; Kroon, J.M.; Michels, M.A.J.; Janssen, R.A.J. *Nano Lett.* **2005**, *5*, 579.

(45)   Lu, L.; Yu, L. *Adv. Mater.* **2014**, *26*, 4413.

(46)   Liu, T.; Zhao, J.; Li, Z.; Mu, C.; Ma, W.; Hu, H.; Jiang, K.; Lin, H.; Ade, H.; Yan, H. *Nat. Commun.* **2014**, *5*, 5293.

(47)   Chamberlain, G. A. *Sol. Cells* **1983**, *8*, 47.

(48)   Schulze, K.; Uhrich, C.; Schüppel, R.; Leo, K.; Pfeiffer, M.; Brier, E.; Reinold, E.; Bäuerle, *Adv. Mater.* **2006**, *18*, 2872

(49)   Li, Z.; He, G.; Wan, X.; Liu, Y.; Long, G; Zuo, Y.; Zang, M.; Chen, Y. *Adv. Energy Mater.* **2012**, *2*, 74.

(50)   Zhang, Q.; Kan, B.; Liu, F.; Long, G.; Wan, X.; Chen, X.; Zuo, Y.; Ni, W.; Zhang, H.; Li, M.; Hu, Z.; Huang, F.; Cao, Y.; Liang, Z.; Zhang, M.; Russell, T. P.; Chen, Y. *Nature Photon.* **2015**, *9*, 35.

(51)   Sum, Y.; Welch, G. C.; Leong, W. L.; Takacs, C. J.; Bazan, G. C.; Heeger, A. J *Nat. Mater.* **2012**, *11*, 44.

(52)   Kyaw, A. K. K.; Wang, D. H.; Luo, C.; Cao, Y.; Nguyen, T.-Q.; Bazan, G. C.; Heeger, A. J. *Adv. Energy Mater.* **2014**, *4*, 1301469.

(53)   He, Y.; Li, Y *Phys. Chem. Chem. Phys.* **2011**, *13*, 1970.

(54)   Anthony, J. E.; Facchetti, A.; Heeney, M.; Marder, S. R.; Zhan, X. *Adv. Mater.* **2010**, *22*, 3876.

(55)   He, Y.; Chen, H.-Y.; Hou, J.; Li, Y *J. Am. Chem. Soc.* **2010**, *132*, 1377.

(56)   He, Y.; Chen, H.-Y.; Hou, J.; Li, Y *J. Am. Chem. Soc.* **2010**, *132*, 5532.

(57)   Lenes, M.; Shelton, S. W.; Sieval, A. B.; Kronholm, D. F.; Hummelen, J. C.; Blom, P. W. M *Adv. Funct. Mater.* **2009**, *19*, 3002.

(58)   He, F.; Yu, L. *J Phys. Chem. Lett.* **2011**, *2*, 3102.

(59)   Liang, Y.; Yu, L. *Acc. Chem. Res.* **2010**, *43*, 1227.

(60)   Zhou, H.; Yang, L.; You, W *Macromolecules*, **2012**, *45*, 607.

(61)   Dou, L.; You, J.; Hong, Z.; Li, G.; Street, R. A.; Yang, Y. *Adv. Mater.* **2013**, *25*, 6642.

(62)   Duan, C.; Huang, F.; Cao, Y. *J. Mater, Chem.* **2012**, *22*, 10416.

(63)   Stuart, A. C.; Tumbleston, J. R.; Zhou, H.; Li, W.; Liu, S.; Ade, H,; You, W. *J. Am. Chem. Soc.* **2013**, *135*, 1806.

(64)   He, Z.; Zhong, C.; Su, S.; Xu, M.; Wu, H.; Cao, Y *Nature Photon.* **2012**, *6*, 591.

(65)   Liao, S.-H.; Jhuo, H.-J.; Cheng, Y.-S.; Chen, S.-A. *Adv. Mater.* **2013**, *25*, 4766.

(66)   Guo, X.; Zhang, M.; Ma, W.; Ye, L.; Zhang, S.; Liu, S.; Ade, H.; Huang, F.; Hou, J. *Adv. Mater.* **2014**, *26*, 4043.

(67)   Zhang, W.; Wu, Y,; Bao, Q.; Gao, F.; Fang, J. *Adv. Energy Mater.* **2014**, *4*, 100359.

(68)   Chen, C.-C.; Chang, W.-H.; Yoshimura, K.; Ohya, K.; You, J.; Gao, J.; Hong, Z.; Yang, Y. *Adv. Mater.* **2014**, *26*, 5670.

(69)   Mohd Yusoff, A. R. B.; Kim, D.; Kim. H. P.; Shneider, F. K.; da Silva, W. J.; Jang, J. *Energy Environ. Sci.* **2015**, *8*, 303.

(70)   Chen. Y.; Wan, X.; Long, G. *Acc. Chem. Res.* **2013**, *46*, 2645.

(71)   Coughlin, J. E.; Henson, Z. B.; Welch G. C.; Bazan, G. C. *Acc. Chem. Res.* **2013**, *47*, 257.

(72)   Lin, H.-Y. Hwang, W.-C., Chen, H.-H.; Hsu, C.-Y. Lin, J. T.; Lin, H.-W. *Chem. Commun.* **2012**, *48*, 8913.

(73)   Tamayo, A. B.; Dang, X.-D.; Walker, B.; Seo, J.; Kent, T.; Nguyen, T.-Q. *Appl. Phys. Lett.* **2009**, *94*, 103301.

(74)   Liu, X.; Sun, Y.; Perez, L. A.; Wen, W.; Toney, M. F.; Heeger, A. J.; Bazan, G. C. *J. Am. Chem. Soc.* **2012**, *134*, 20609.

(75)   Wu, Y.; Zhu, W. *Chem. Soc. Rev.* **2013**, *42*, 2039.

(76)   Chochos, C. L.; Choulis,S. A. *Prog, Polym. Sci.* **2011**, *36*, 1326.

(77)   Zhang, Z.-G.; Wang, J. *J. Mater. Chem.* **2005**, *15*, 1123.

(78)   Nunzi, J.-M. *C. R. Phys.* **2002**, *3*, 523.

(79)   Scharber, M. C.; Mühlbacher, D.; Koppe, M.; Denk, P.; Waldauf, C.; Heeger, A. J.; Brabec, C. J. *Adv. Mater.* **2006**, *18*, 789.

(80)   Son, H. J.; He, F.; Carsten, B.; Yu, L. *J. Mater. Chem.* **2011**, *21*, 18934.

(81)   Svensson, M.; Zhang, F.; Veenstra, S. C.; Verhees, W. J. H.; Hummelem, J. C.; Kroon, J.M.; O. Inganäs, O.; Andersson, M.R. *Adv. Mater.* **2003**, *15*, 988.

(82)   Slooff, L. H.; Veenstra, S. C.; Kroon, J. M.; Moet, D. J. D.; Sweelssen, J.; Koetse, M. M. *Appl. Phys, Lett.* **2007**, *90*, 143506.

(83)   Wang, E.; Wang, L.; Lan, L.; Luo, C.; Zhuang, W.; Peng, J.; Cao, Y. *Appl. Phys. Lett.* **2008**, *92*, 033307.

(84)   Bloun, N.; Michaud, A.; Leclerc, M. *Adv. Mater.* **2007**, *19*, 2295.

(85)   Bloun, N.; Michaud, A.; Gendron, D.; Wakim, S.; Blair, E.; Plesu, R. N.; Belletête, M.; Durocher, G.; Tao, Y.; Leclerc, M. *J. Am. Chem. Soc.* **2008**, *130*, 732.

(86)   Sonar, P.; Singh, S. P.; Li, Y.; Ooi, Z.-E.; Ha, T.-J.; Wong, I.; Soh, M. S.; Dodabalapur, A. *Energy Environ. Sci.* **2011**, *4*, 2288.

(87)   Ha, T.-J.; Sonar, P.; Dodabalapur, A. *Appl. Phys. Lett.* **2011**, *98*, 253305.

(88)   Mühlbacher, D.; Scharber, M.; Morana, M.; Zhu, Z.; Waller, D.; Gaudiana, R.; Brabec, C *Adv. Mater.* **2006**, *18*, 2884.

(89)   Peet, J.; Kim, J. Y.; Coates, N. E.; Ma, W. L.; Moses, D.; Heeger, A.

J.; Bazan, G. C. *Nat. Mater.* **2007**, *6*, 497.

(90) Chu, T.-Y.; Lu, J.; Beaupré, S.; Zhang, Y.; Pouliot, J.-R.; Wakim, S.; Zhou, J.; Leclerc, M.; Li, Z.; Ding, J.; Tao, Y. *J. Am. Chem. Soc.* **2011**, *133*, 4250.

(91) Scharber, M. C.; Koppe, M.; Gao, J.; Cordella, F.; Loi, M. A.; Denk, P.; Morana, M.; Egelhaaf, H.-J.; Forberich, K.; Dennler, G.; Gaudiana, R.; Waller, D.; Zhu, Z.; Shi, X.; Brabec, C. J. *Adv. Mater.* **2010**, *22*, 367.

(92) Blouin, N.; Michaud, A.; Leclerc, M. *Adv. Mater.* **2007**, *19*, 2295.

(93) Seo, J. H.; Gutacker, A.; Sun, Y.; Wu, H.; Huang, F.; Cao, Y.; Scherf, U.; Heeger, A. J.; Bazan, G. C *J. Am. Chem. Soc.* **2011**, *133*, 8416.

(94) Zhang, X.-R.; Richter, L. J.; DeLongchamp, D. M.; Kline, R. J.; Hammond, M. R.; McCulloch, I.; Heeney, M.; Ashraf, R. S.; Smith, J. N.; Anthopoulos, T. D.; Schroeder, B.; Geerts, Y. H.; Fischer, D. A.; Toney, M. F. *J. Am. Chem. Soc.* **2011**, *133*, 15073.

(95) Li, Y.; Singh, S. P.; Sonar, P. *Adv. Mater.* **2010**, *22*, 4862.

(96) Ong, K.-H.; Lim, S.-L.; Tan, H.-S.; Wong, H.-K.; Li, J.; Ma, Z.; Noh, L. C. H.; Lim, S.-H.; de Mello, J. C.; Chen, Z.-K. *Adv. Mater.* **2011**, *23*, 1407.

(97) Zhou, H.; Yang, L.; Price, S. C.; Knight, K. J.; You, W. *Angew. Chem., Int. Ed.* **2010**, *49*, 7992.

(98)   Zhang, S.; Guo, Y.; Fan, H.; Liu, Y.; Chen, H.-Y; Yang, G.; Zhan, X.; Liu, Y.; Li, Y.; Yang, Y. *J. Polym. Sci., Part A: Polym. Chem.* **2009**, *47*, 5498.

(99)   Wang, E.; Hou, L.; Wang, Z.; Hellström, S.; Zhang, F.; Inganäs, O.; Andersson, M. R. *Adv. Mater.* **2010**, *22*, 5240.

(100) Zhang, J.; Cai, W.; Huang, F.; Wang, E.; Zhong, C.; Liu, S.; Wang, M.; Daun, C.; Yang, T.; Cao, Y. *Macromolecules* **2011**, *44*, 894.

(101) Zhou, E.; Wei, Q.; Yamakawa, S.; Zhang, Y.; Tajima, K.; Yang, C.; Hashimoto, K. *Macromolecules* **2009**, *42*, 821.

(102) Wienk, M. M.; Turbiez, M.; Gilot, J.; Janssen, R. A. J *Adv. Mater.* **2008**, *20*, 2556.

(103) Wang, E.; Ma, Z.; Zhang, Z.; Vandewal, K.; Henriksson, P.; Inganäs, O.; Zhang, F.; Andersson, M. R. *J. Am. Chem. Soc.* **2011**, *133*, 14244.

(104) Stalder, R.; Grand, C.; Subbiah, J.; So, F.; Reynolds, J. R. *Polym.Chem.* **2012**, *3*, 89.

(105) Liu, B.; Zou, Y.; Peng, B.; Zhao, B.; Huang, K.; He, Y.; Pan, C. *Polym. Chem.* **2011**, *2*, 1156.

(106) Piliego, C.; Holcombe, T. W.; Douglas, J. D.; Woo, C. H.; Beaujuge, P. M.; Frèchet, J. M. J. *J. Am. Chem. Soc.* **2010**, *132*, 7595.

(107) Zou, Y.; Najari, A.; Berrouard, P.; Beauprè, S.; Aïch, B. R.; Tao, Y.; Leclerc, M. *J. Am. Chem. Soc.* **2010**, *132*, 5330.

(108) Zhang, G.; Fu, Y.; Zhang, Q.; Xie, Z. *Chem. Commun.* **2010**, *46*, 4997.

(109) Guo, X.; Xin, H.; Kim, F. S.; Liyanage, A. D. T.; Jenekhe, S. A.; Watson, M. D. *Macromolecules* **2011**, *44*, 269.

(110) Yuan, M.-C.; Chiu, M.-Y.; Liu, S.-P.; Chen, C.-M.; Wei, K.-H. Macromolecules **2010**, *43*, 6936.

(111) Guo, X.; Zhou, N.; Lou, S. J.; Hennek, J. W.; Ortiz, R. P.; Butler, M. R.; Boudreault, P.-L. T.; Strzalka, J.; Morin, P.-O.; Leclerc, M.; Navarrete, J. T. L.; Ratner, M. A.; Chen, L. X.; Chang, R. P. H.; Facchetti, A.; Marks, T. J. *J. Am. Chem. Soc.* **2012**, *134*, 18427.

(112) Pomerantz, M. *Tetrahedron Lett.* **2003**, *44*, 1563.

(113) Pomerantz, M.; Amarasekara, A. S.; Dias, H. V. R. *J. Org. Chem.* **2002**, *67*, 6931.

(114) Guo, X.; Ortiz, R. P.; Zheng, Y.; Kim, M.-G, Zhang, S.; Hu, Y.; Lu, G..; Facchetti, A.; Marks, T. J. *J. Am. Chem. Soc.* **2011**, *133*, 13685.

(115) Shoaee, S.; Clarke, T. M.; Huang, C.; Barlow, S.; Marder, S. R.; Heeney, M.; McCulloch, I.; Durrant, J. R. *J. Am. Chem. Soc.* **2010**, *132*, 12919.

(116) Peuman, P.; Forrest, S. R.; *Chem. Phys. Lett.* **2004**, *398*, 27.

(117) Lee, Y.; Jo, W. H. *J. Phys. Chem. C* **2012**, *116*, 8379.

(118) Lin, Y.; Li Y.; Zhan, X. *Chem. Soc. Rev.* **2012**, *41*, 4245.

(119) Mishra, A.; Bäuerle, P. *Angew. Chem. Int. Ed.* **2012**, *51*, 2020.

(120) Roncali, J. *Acc. Chem. Res.* **2009**, *42*, 1719.

(121) Walker, B.; Kim, C.; Nguyen, T.-Q. *Chem. Mater.* **2010**, *23*, 470.

(122) Tamayo, A. B.; Walker, B.; Nguyen, T. Q. *J. Phys. Chem. C* **2008**, *112*, 11545

(123) Tamayo, A. B.; Dang, X. D.; Walker, B.; Seo, J.; Kent, T.; Nguyen, T. Q. *Adv. Funct. Mater.* **2009**, *19*, 3063

(124) Liu, Y.; Zhou, J.; Wan, X.; Chen, Y. *Tetrahedron* **2009**, *65*, 5209.

(125) Liu, Y.; Wan, X.; Wang, F.; Zhou, J.; Long, G.; Tian, J.; You, J.; Yang, Y.; Chen, Y. *Adv. Energy Mater.* **2011**, *1*, 771.

(126) Eisenmenger, N. D.; Su, G. M.; Welch, G. C.; TAkacs, C. J.; Bazan, G. C.; Kramer, E. J.; Chabinyc, M. L. *Chem. Mater.* **2013**, *25*, 1688.

(127) Gupta, V.; Kyaw, A. K. K.; Wang, D. H.; Chand, S.; Bazan, G. C.; Heeger, A. J. *Sci. Rep.* **2013**, *3*, 1965.

(128) Zhou, H.; Yang, L.; Stoneking, S.; You, W. *ACS appl. Mater. Interfaces* **2010**, *2*, 1377.

(129) Zhou, E.; Yamakawa, S.; Tajma, K.; Yang, C.; Hashimoto, K. *Chem. Mater.* **2009**, *21*, 4055.

(130) Loser, S.; Bruns, C. J.; Miyauchi, H,; Ortiz, R.P.; Faccetti, A.; Stupp, S. I.; Marks, T. J. *J. Am. Chem. Soc.* **2011**, *133*, 8142.

(131) Lee, O. P.; Yiu, A. T.; Beaujuge, P. M.; Woo, C. H.; Holcombe, T. W.; Millstone, J. E.; Douglas, J. D.; Chen, M. S.; Fréchet, J. M. J.

Adv. Mater. **2011**, *23*, 5359.

(132) Seo. J. H. *Syn. Metals* **2012**, *162*, 748.

(133) McCulloch, I.; Heeney, M.; Bailey, C.; Genevicius, K.; Macdonald, I.; Shkunov, M.; Sparrowe, D.; Tierney, S.; Wagner, R.; Zhang, W.; Chabinyc, M. L.; Kline, R. J.; McGehee, M. D.; Toney, M. F. *Nat. Mater.* **2006**, *5*, 328.

(134) Wu, J. S.; Cheng, Y. J.; Dubosc, M.; Hsieh, C. H.; Chang, C. Y.; Hsu, C. S. *Chem. Commun.* **2010**, *46*, 3259.

(135) Takimiya, K.; Shinamura, S.; Osaka, I.; Miyazaki, E. *Adv. Mater.* **2011**, *23*, 4347.

(136) Lee, Y.; Nam, Y. M.; Jo, W. H. *J. Mater. Chem.* **2011**, *21*, 8583.

(137) Lee, J. S.; Son, S. K.; Song, S.; Kim, H.; Lee, D. R.; Kim, K.; Ko, M. J.; Choi, D. H.; Kim, B.; Cho, J. H. *Chem. Mater.* **2012**, *24*, 1316.

(138) Bronstein, H.; Chem, Z.; Ashraf, R. S.; Zhang, W.; Du, J.; Durrant, J. R.; Tuladhar, P. S.; Song, K. Watkins, S. E.; Geerts, Y.; Wienk, M. M.; Jasssen, R. A. J.; Anthopoulos, T.; Sirringhaus, H.; Heenry, M.; McCulloch, I. *J. Am. Chem. Soc.* **2011**, *133*, 3272.

(139) Henson, Z. B.; Welch, G. C.; Poll, T.; Bazan, G. C. *J. Am. Chem. Soc.* **2011**, *134*, 3766.

(140) Su, M.-S.; Kuo, C.-Y.; Yuan, M.-Y.; Jeng, U.-S.; Su, C.-J.; Wei, K.-H. *Adv. Mater.* **2011**, *23*, 3315

(141) Zhang, Y.; Zou, J.; Yip, H.-L.; Sun, Y.; Davies, J. A.; Chen, K.-S.;

Acton, O.; Jen, A. K.-Y. *J. Mater. Chem.* **2011**, *21*, 3895.

(142)   Small, C. E.; Chen, S.; Subbiah, J.; Amb, C. M.; Tsang, S.-W.; Lai, T.-H.; Reynolds, J. R.; So, F. *Nat. Photonics* **2011**, *6*, 115.

(143)   Hong, Y.-R.; Wong, H.-K.; Moh, L. C. H.; Tan, H.-S.; Chen, Z.-K *Chem. Commun.* **2011**, *47*, 4920.

(144)   Jo, J.; Pron, A.; Berrouard, P.; Leong, W. L.; Yuen, J. D.; Moon, J. S.; Leclerc, M.; Heeger, A. J. *Adv. Energy Mater.* **2012**, *2*, 1397.

(145)   Ha, J.-J.; Kim, Y. J.; Park, J.-G.; An, T. K.; Kwon, S.-K.; Park, C. E.; Kim, Y.-H. *Chem. Asian J.* **2014**, *9*, 1045.

(146)   Kim, Y. J.; Park, K. H.; Ha, J.-J.; Chung, D. S.; Kim, Y.-H.; Park, C. E. *Phys. Chem. Chem. Phys.* **2014**, *16*, 19874.

(147)   Kim, Y. J.; Baek, J. Y.; Ha, J.-J.; Chung, D. S.; Kwon, S.-K.; Park, C. E.; Kim, Y.-H. *J. Mater. Chem. C* **2014**, *2*, 4937.

(148)   Berrouard, P.; Grenier, F.; Pouliot, J.-R.; Gagnon, E.; Tessier, C.; Leclerc, M. *Org. Lett.* **2011**, *13*, 38.

(149)   Berrouard, P.; Dufresne, S.; Pron, A.; Veilleux, J.; Leclerc, M. *J. Org. Chem.* **2012**, *77*, 8167.

(150)   Ottone, C.; Berrouard, P.; Louarn, G.; Beaupré, S.; Gendron, D.; Zagorska, M.; Rannou, P.; Najari, A.; Sadki, S.; Leclerc, M.; Pron, A. *Polym. Chem.* **2012**, *3*, 2355.

(151)   Pron, A.; Berrouard, P.; Leclerc, M. *Macromol. Chem. Phys.* **2013**, *214*, 7.

초   록

최근 저분자 유기태양전지에 대한 연구가 활발히 진행되고 있다. 저분자는 고분자에 비해 합성과 정제가 용이하고 분자 구조와 분자량이 명확하기 때문에 배치간 편차가 적고 분자구조와 태양전지 특성간의 관계에 대한 이해도를 높인다는 장점이 있다. 하지만 여전히 저분자 유기태양전지의 특성은 고분자에 비해 낮기 때문에 새로운 물질 개발이 필요하다.

지난 십여 년간 벌크 이종접합 유기태양전지에 대한 연구가 집중적으로 이루어진 결과, 고성능 유기태양전지를 구현하기 위해 광활성층 물질에 대한 필수 조건들이 제시되고 있다: (1) 태양광을 충분히 흡수하기 위해 가시광선 이상으로의 넓고 강한 흡수 영역이 필요하고, (2) 높은 단락 전류를 위해 높은 전공이동도가 요구된다. 또한, (3) 높은 개방전압과 효과적인 엑시톤 분리를 가능케 할 수 있는 적절한 에너지 레벨이 필요하며, (4) 전자받개 물질로 사용되는 플러렌유도체와 나노 스케일의 상분리를 위해 플러렌과의 적절한 용해도를 갖는 광활성층 물질이 요구된다. 이와 같은 특성은 높은 단락전류, 개방전압, 채움인자을 나타냄으로써 높은 광전효율을 나타낼 수 있다.

이와 같은 조건을 만족시키기 위해서는, 합성될 저분자의 에너지 레벨, 평면서, 용해도, 결정성 등을 고려하여 전자주개와 받개 단위체의 합리적인 선택이 이루어져야 한다.

먼저, diketopyrrolopyrrole(DPP)을 기반으로 하는 A–D–A 형태의

저분자 물질을 합성하였다. 이때 사용되는 전자주개 단위체의 전자주개 능력을 고려하였다. 상대적으로 강한 전자주개 능력을 갖는 thiophene과 약한 전전주개 능력을 갖는 phenylene을 도입하여 A–D–A 형태의 저분자의 에너지 준위를 조절하였다. 약한 전자주개인 phenylene을 갖는 Ph2(TDPP)$_2$ 는 –5.31 eV의 낮은 HOMO 에너지 준위를 나타냈고 PC$_{71}$BM과의 블랜드 필름에서 높은 전공이동도 및 나노 스케일의 상분리를 관찰할 수 있었다. 결과적으로, Ph2(TDPP)$_2$를 기반으로 하는 소자에서 0.93 V의 높은 개방전압과 4.01%의 효율은 나타냈다.

이 DPP를 기반으로 하는 저분자 물질은 높은 개방전압을 나타냈지만 낮은 단락전류로 인해 효율에 제한이 있었다. 일반적으로 분자간의 밀접한 패킹은 전하 운반체의 분자간 이동을 용이하게 하므로 전하 이동도를 높일 수 있다. 따라서 이번 연구에서는 앞선 연구 결과를 기반으로 각각 전자주개 능력이 서로 다른, 그리고 그에 상응하는 융합된 형태의 전자주개 단위체를 도입하였다. 즉, DPP 기반의 A–D–A 형태 저분자로, 전자주개 단위체로 bithiophene, theinothiophene, biphenylene, naphthalene을 도입하였다. 약한 전자주개 능력을 갖는 biphenylene과 naphthalene을 포함하는 저분자의 경우 낮은 HOMO 에너지 레벨을 나타내어 bithiophene과 thienothiophene (강한 전자주개)를 포함하는 저분자 보다 높은 개방전압을 나타냈다. 또한 융합된 형태의 thienothiophene과 naphthalene을 포함하는 저분자는 다른 저분자에 비해 높은 전공이동도 및 높은 단락전류 값을 나타냈다. 결과적으로 약한 전자주개 능력과 평면성을 함께 갖는 naphthalene이 도입된

NPT(TDPP)$_2$의 경우 높은 단락전류과 높은 개방전압을 동시에 달성함으로써 태양전지의 효율을 개선할 수 있었다.

마지막으로, 두 종류의 thienopyrroledione을 기반으로 하는 저분자 물질, DTS(HexTPD2T)$_2$와 DTS(MeTPD2THex)$_2$를 합성하였다. 일반적으로 D–A 형태 공액 저분자 물질의 HOMO와 LUMO는 각각 전자주개 단위체의 HOMO와 전자받개 단위체의 LUMO 에너지 레벨에 주된 영향을 받는다. 그러나 이례적으로 강한 전자받개 단위체인 TPD가 도입된 경우 합성된 고분자의 HOMO와 LUMO 에너지 레벨이 동시에 낮아지고 높은 개방전압을 나타내는 것을 확인 할 수 있었다. 이를 바탕으로 TPD를 포함하는 저분자 물질을 설계 및 합성하였다. 이때 알킬 체인의 위치에 따른 효율 변화를 관찰하고자 n-hexyl 체인의 위치를 달리한 두 종류의 저분자를 합성하였다. 예상했듯이, 두 종류의 저분자 모두 낮은 HOMO 에너지 레벨(–5.5 eV)을 가졌고 그에 상응할 만한 높은 개방전압(0.93–0.94 V)을 나타냈다. 하지만 단락전류의 값은 큰 차이를 보였다. 결정학적 분석과 모폴로지 분석을 통해 DTS(HexTPD2T)$_2$:PC$_{71}$M 블랜드 필름에서 전하 이동도에 유리한 face-on 배열과 나노 스케일의 상분리를 관찰하였다. 결과적으로 DTS(HexTPD2T)$_2$ 공액 저분자 물질을 이용하여 6.0%의 높은 효율을 달성할 수 있었다.

이와 같이 전자적 특성 및 평면성을 고려한 전자주개 및 전자받개 단위체의 선택은 합성된 저분자의 에너지 준위 및 평면성을 결정할 뿐만 아니라 유기태양전지의 광활성층 물질로써 개방전압과 단락전류를 개선시킬 수 있는 요인임을 확인하였다.

List of papers

1. <u>Choi, Y. S.</u>; Lee, J. W.; Jo, W. H. *Org. Electron.* **2012**, *13*, 3060.

2. <u>Choi, Y. S.</u>; Jo, W. H. *Org. Electron.* **2013**, *14*, 1621.

3. <u>Choi, Y. S.</u>; Sin, T. J.; Jo, W. H. *Appl. Mater. Interfaces* **2014**, *6*, 20035.